Characterization of T2R14 signaling mechanisms in extraoral tissues

By

Feroz Ahmed Shaik

A thesis submitted to the Faculty of Graduate Studies of

The University of Manitoba

in partial fulfilment of the requirements of the degree of

Doctor of Philosophy

Department of Oral Biology

Dr. Gerald Niznick College of Dentistry

University of Manitoba

Winnipeg, Manitoba, Canada

CONTRIBUTIONS OF AUTHORS

The modified sandwich thesis comprises of five multi-authored manuscripts (one review and four research articles), of which two are published in scientific journals and three are in peer-review. The author of this thesis has contributed to the majority of the work and is credited with the first authorship in four manuscripts and co-authorship in one manuscript. The manuscript wise author contribution details are as follows,

1. Bitter taste receptors: Extraoral roles in pathophysiology. Feroz Ahmed Shaik, Nisha Singh, Makoto Arakawa, Kangmin Duan, Rajinder Pal Bhullar, Prashen Chelikani. *Int J Biochem Cell Biol, 2016*. 77(Pt B): p. 197-204.
   Feroz Ahmed Shaik is the first author and along with Prashen Chelikani were responsible for design of the content and literature review. All the authors contributed to the writing of this review article.

2. Cholesterol modulates signaling of the chemosensory bitter taste receptor T2R14 in human airway cells. Feroz Ahmed Shaik, Manoj Reddy Medapati, Prashen Chelikani. *Am J Physiol Lung Cell Mol Physiol,* 2019 Jan 1;316(1): L45-L57.
   Feroz Ahmed Shaik is the first author of this research publication and along with Prashen Chelikani was responsible for designing the experiments and drafting the manuscript. Feroz Ahmed Shaik was responsible for experiments involving airway cells. Feroz Ahmed Shaik and Manoj Reddy Medapati worked on structure-function experiments and analysis.

3. Chemosensory Bitter Taste Receptors T2R4 and T2R14 Activation Attenuates Proliferation and Migration of Breast Cancer Cells. Nisha Singh, Feroz Ahmed Shaik, Yvonne Myal, Prashen Chelikani.
   Nisha Singh, Feroz Ahmed Shaik and Prashen Chelikani were responsible for designing the experiments. Feroz Ahmed Shaik is a second-author in this manuscript and was responsible for experiments involving T2R14. Nisha Singh was responsible for experiments involving T2R4. Both Nisha Singh and Feroz Ahmed Shaik were responsible for data analysis. Yvonne Myal contributed resources including breast tissue samples. All the authors were involved with drafting the manuscript.

4. The role of membrane sphingomyelin and cholesterol in bitter taste receptor T2R14 signaling. Feroz Ahmed Shaik, Prashen Chelikani.
   Feroz Ahmed Shaik is the first author of the manuscript and along Prashen Chelikani designed the experiments and prepared the manuscript. Feroz Ahmed Shaik performed the experiments and analyzed the data. Both the authors were involved with drafting the manuscript.

5. Intracellular H208 residue influences agonist selectivity in bitter taste receptor T2R14. Feroz Ahmed Shaik, Appalaraju Jaggupilli, Prashen Chelikani.
   Feroz Ahmed Shaik is the first author of this manuscript and along with Prashen Chelikani designed the experiments and prepared the manuscript. Feroz Ahmed shaik performed the wet lab experiments and analyzed the data. Appalaraju Jaggupilli performed computational molecular modeling. All the authors were involved with drafting the manuscript.

THESIS ABSTRACT

Bitter taste receptors (referred to as T2Rs) are integral cell membrane receptors that belong to G protein-coupled receptor family. In humans, 25 T2R subtypes have been discovered thus far, and are differentially expressed in various organs. Embracing the newly recognized extraoral and functional roles of T2Rs, I investigated the significance of select T2Rs in pathophysiological conditions. The function of T2Rs in breast cancer is not clearly understood. We characterized the expression and function of T2R4 and T2R14 in breast cancer clinical samples and analyzed their physiological role using highly metastatic breast cancer and non-cancerous cell lines. The results show that compared to normal breast epithelial cells, intrinsic activation of T2Rs in breast cancer cells elicited anti-proliferative, anti-migratory and pro-apoptotic responses. These findings demonstrate that the chemosensory T2R signaling network is involved in evoking beneficial physiological responses in breast cancer.

The second part of my thesis involved identifying intrinsic factors regulating T2R14 signaling in airways. The pathophysiological relevance of T2R14 in airway cells is well recognized. Using human airway smooth muscle cells and human bronchial epithelial cells, I studied the role of membrane lipids, cholesterol and sphingomyelin, in airway T2R14 signaling. The results reveal that membrane cholesterol regulates T2R14 signaling, however, T2R14 signaling was not dependent on the availability of sphingomyelin. Furthermore, this work identified the site on T2R14 that potentially binds cholesterol.

The final part of my thesis involved identification of a highly conserved histidine (H208) on the intracellular side of T2R14 in determining agonist selectivity. Structure-function analysis of H208 suggests its role in regulating T2R14 active conformation and consequentially agonist

promoted downstream signaling. Collectively, these studies provide novel insights into various factors governing the T2R14 signaling in extraoral tissues.

ACKNOWLEDGEMENTS

At the outset, I would like to express my gratitude to my academic advisor Dr. Prashen Chelikani for his mentorship, guidance and most importantly for his patience during my stay in the Chelikani Lab as a graduate student. I am also thankful to Dr. Prashen Chelikani for his encouragement and for having a positive influence on me throughout this past 5 years.

I would like to extend my thanks to my committee members Dr. Rajinder Pal Bhullar, Dr. Kangmin Duan and Dr. Gilbert Arthur for their guidance and valuable insights in my research projects. I am also appreciative of the support offered by the academic and administrative staff of the Dept. of Oral Biology.

I am grateful to my external examiner, Dr. John Hwa (Cardiovascular Medicine, Yale University) for reviewing my thesis and for his insightful comments.

I also acknowledge the funding agencies IGSES, UMGF, MITACS-Accelerate and CHRIM for providing me financial support during my graduate studies.

My heartiest thanks to my lab colleagues Manoj, Nisha, Raju, Kun, Anurag, Vivianne, Prem, Raja, Jasbir, Rohini and Ryan for their help and friendly advice with my experiments. Special thanks to Sai for his help and guidance throughout my graduate studies. I am also grateful to graduate students of the Dept. of Oral Biology namely Yanqi (Colin), Maryam, Crystal, Navneet, Laya, Abeer, Iris, Vikram and Nuwanthika for their support. I also acknowledge my friends in Winnipeg namely Harish, Amar and family, Mahmood, Omar, Kallesh, Ashfaque, and Ehsaan for their friendship.

Special thanks to my brother-in-law, Mohammad Jafurullah, for his continued encouragement and motivation. I am grateful to my father, Shaik Noor Ahmed; mother, Shaik

Mehrunisa; sister, Shaik Ruksana; brother, Shaik Fayaz Ahmed and nephews, Ameen and Anees for their love and unconditional support that has helped me to be at a stage in my life that I am in today.

TABLE OF CONTENTS Page

LIST OF FIGURES

LIST OF TABLES

LIST OF COPYRIGHT MATERIAL FOR WHICH PERMISSION WAS OBTAINED

CHAPTER 4

Figure 4.4.1 Reprinted with permission from Biochemical and Biophysical Research Communications; "Differential expression of bitter taste receptors in non-cancerous breast epithelial and breast cancer cells", 446(2): p. 499-503, 2014. License number-4566030987453 © by Elsevier.

Figure 4.4.2 Reprinted with permission from Molecular and cellular biochemistry; "Analysis of the expression of human bitter taste receptors in extraoral tissues", 426(1-2): p. 137-147, 2017. License number-4561460516967 © by Springer Nature.

LIST OF ABBREVIATIONS

API	Apigenin
AMPK	AMP activated protein kinase
AngII	Angiotensin II human
AT_1R	Angiotensin II type1 receptor
AHL	Acyl homoserine lactones
AMP	Antimicrobial peptides
ASMC	Airway smooth muscle cells
ATP	Adenosine triphosphate
AUDIT	Alcohol use disorders identification test
BSA	Bovine serum albumin
BC	Breast cancer
BK_{Ca}	Ca^{2+} activated K^+ channels
BEGM	Bronchial epithelial growth media
CAM	Constitutive active mutant
CRAC	Cholesterol recognition amino acid consensus
CARC	Mirror version of CRAC motif

CALHM1	Calcium homeostasis modulator1
cAMP	Cyclic adenosine monophosphate
CBF	Ciliary beat frequency
CFTR	Cystic fibrosis transmembrane conductance regulator
COPD	Chronic obstructive pulmonary disease
COase	Cholesterol oxidase
CRS	Chronic rhinosinusitis
C-terminus	Carboxy terminus
$[Ca^{2+}]_i$	Intracellular calcium
DPH	Diphenhydramine
DAG	Diacylglycerol
DB	Denatonium benzoate
DMEM	Dulbecco's modified eagle's media
EC_{50}	Half-maximal effective concentration
ECL	Extracellular loop
EDTA	Ethylenediaminetetraacetic acid
ER	Endoplasmic reticulum
FACS	Fluorescence-assisted cell cytometry

FBS	Fetal bovine serum
FFA	Flufenamic acid
FOXM1	Forkhead box M1
FESS	Functional endoscopic sinus surgery
GPCR	G protein-coupled receptor
GRM	Metabotropic glutamate receptor
G-protein	Guanine nucleotide-binding protein
GTEx	The genotype-tissue expresssion
HEK cells	Human embryonic kidney cells
hEGF	Human epidermal growth factor
HASM	Human airway smooth muscle
hGSMCs	Human gastric smooth muscle cells
hMSC	human bone marrow derived mesenchymal cells
HGNC	HUGO gene nomenclature committee
IC_{50}	Half-maximal inhibitory concentration
IgE	IgE immunoglobulin
IP_3	Inositol-1,4,5-triphosphate
IP_3R	IP_3 receptors

ICL	Intracellular loop
L-VDCC	L-type voltage sensitive Ca^{2+} channels
MCC	Mucociliary clearance
MßCD	Methyl-ß-cyclodextrin
MD	Molecular dynamics
MFI	Mean fluorescence intensity
NO	Nitric oxide
N-terminus	Amino terminus
NuLi-1	Normal lung bronchial epithelial cells
PPARα1	Peroxisome proliferator-activated receptor α1
QUI	Quinine
qPCR	Quantitative polymerase chain reaction
PIP_2	Phosphatidylinositol-4,5-bisphosphate
PKA	Protein kinase A
$PLC\beta_2$	Phospholipase C-β_2
PROP	6-n-propylthiouracil
PTC	phenylthiocarbamide
PDEs	Phosphodiesterases

PGD_2	Prostaglandin D_2
p-AMPK	phosphorylated AMP activated protein kinase
QSMs	quorum sensing molecules
RMSD	Root mean square deviation
RFU	Relative fluorescence units
SCC	Solitary chemosensory cells
SNPs	Single nucleotide polymorphisms
SBM	Sphingolipid binding motif
SMase	Sphingomyelinase
shRNA	short hairpin RNA
SEM	Standard error of the mean
TCGA	The cancer genome atlas
TNBC	Triple negative breast cancer
T1R	Sweet and umami taste receptors
T2R	Bitter taste receptors
TM	Transmembrane
TAS2R	Bitter taste receptor coding genes
TRC	Taste receptor cells

TRPM5	Transient receptor potential cation channel subfamily member 5
WT	Wild-type

CHAPTER 1

1.0 INTRODUCTION

Bitter taste receptors: Extraoral roles in pathophysiology

Feroz Ahmed Shaik, Nisha Singh, Makoto Arakawa, Kangmin Duan, Rajinder Pal Bhullar, Prashen Chelikani.

Int J Biochem Cell Biol, 2016. 77(Pt B): p. 197-204

1.0 INTRODUCTION

1.1 Overview

G protein-coupled receptors (GPCRs) constitute the largest family of cell surface receptors involved in signal transduction across cell membrane. GPCRs respond to a wide range of extracellular stimuli including photons, odorants, tastants and initiate an intracellular signalling cascade which ultimately leads to a physiological response (Pierce et al., 2002). Aberrations in the GPCR signaling leads to altered physiological responses. In addition to their crucial role in physiological processes, their involvement in various pathological states has been well established. The disease causing mutations in GPCRs are reviewed in great detail elsewhere (Schoneberg et al., 2004;Lania et al., 2006;Tao, 2006). GPCRs play a crucial role in regulating neuronal signalling. Impairment of this signalling contributes to the pathology of CNS disorders such as Alzheimer's, Schizophrenia and Parkinson's (Catapano and Manji, 2007;Thathiah and De Strooper, 2011;Navarro et al., 2015). Transcriptional gene expression profiling has shown that several genes encoding GPCRs are differentially expressed in different disease stages, especially in cancer (Durig et al., 2001;Sud et al., 2006;Singh et al., 2014). For example, the β_2-adrenergic receptor's dysfunction contributes to the pathophysiology of obstructive airway diseases and congestive heart failure (Green et al., 1995;Feldman et al., 2005). GPCRs are also implicated in various metabolic disorders such as obesity, Type II diabetes and osteoporosis (Heng et al., 2013). Recent reports have demonstrated the role of virally encoded GPCRs (vGPCRs) in the pathology of infectious diseases in humans (Vischer et al., 2014;Cheng et al., 2015). Due to their unequivocal involvement in the pathophysiology of diverse disease states, they are considered as potent drug targets. Close to 30-40% of pharmaceuticals used today target these receptors to elicit desired responses (Venkatakrishnan et al., 2013). The role of a sub-

family of GPCRs, bitter taste receptors (T2Rs), in various pathophysiological states has been an area of interest in recent times. T2Rs are implicated in the pathophysiology of airway diseases, various cancers and in metabolic and developmental disorders (Jeon et al., 2008;Ansoleaga et al., 2015;Clark et al., 2015;Shaik et al., 2016;Kim et al., 2018b).

1.2 Bitter Taste Receptors (T2Rs): Role in Pathophysiological states

1.2.1 Taste Receptors

Taste perception is one of the main sensory defence mechanisms in mammals preventing ingestion of toxic substances. Humans can distinguish between five taste modalities which are bitter, sweet, umami, sour and salty (Chandrashekar et al., 2006). The bitter taste is sensed by T2Rs which are predominantly expressed on type II taste receptor cells (TRCs) in the taste buds on the tongue (Chandrashekar et al., 2000;Chaudhari and Roper, 2010). The sweet and umami tastes are perceived by the T1R family of receptors. T1R2 and T1R3 combine to detect sweet taster whereas umami is detected by a dimer of T1R1 and T1R3 (Li et al., 2002). Due to this unique ligand recognition mechanism, sweet and umami taste receptors (T1Rs) are classified into class C of GPCR superfamily, whereas T2Rs are categorized into class T (Munk et al., 2016). Sour and salty taste perception is mediated by specialized membrane channels on the apical surface of the taste cells. Recently a sixth taste modality has been proposed, which is involved in the detection of dietary fat (Running et al., 2015;Besnard et al., 2016). Interestingly, the membrane protein target on the taste cells involved in the detection of dietary fat includes GPCRs (GPR40 and GPR120) and K^+ channels (DRK) (Besnard et al., 2016). In humans, 25 T2Rs have been identified thus far and the genes encoding for them are located on chromosomes 5p15, 7q31 and 12p13. The standard gene symbol assigned by the HUGO Gene Nomenclature Committee (HGNC) for T2R coding genes is TAS2R (Gray et al., 2015). The T2Rs recognize

and respond to a diverse array of bitter compounds (Adler et al., 2000). Mechanistic studies have provided insights into structure-function relationships and also the basis of activation of T2Rs by a diverse array of bitter ligands (Singh et al., 2011a;Pydi et al., 2012;Pydi et al., 2014c;Thomas et al., 2017;Nowak et al., 2018).

1.2.2 Bitter taste signal transduction

The canonical bitter signal transduction pathway in a TRC starts with the binding of a bitter tastant to its corresponding T2R. This induces a conformational change in T2R leading to activation of its cognate heterotrimeric G protein. The functional heterotrimeric G protein involved in taste transduction in TRC is composed predominantly of Gα gustducin, Gβ3 and Gγ13 subunits (Huang et al., 1999;Chandrashekar et al., 2000;Rossler et al., 2000;Caicedo et al., 2003). The T2R mediated activation of heterotrimeric G protein leads to its dissociation into Gα gustducin and Gβ3/Gγ13 subunits. The Gβ3/Gγ13 subunits activate downstream Phospholipase C-β2 (PLCβ2), which hydrolyses phosphatidylinositol-4,5-bisphosphate (PIP2) to inositol-1,4,5-triphosphate (IP_3) and diacylglycerol (DAG). IP_3 stimulates the release of Ca^{2+} from intracellular calcium stores by acting on IP_3 receptors (IP3R) on endoplasmic reticulum (Clapp et al., 2001;Zhang et al., 2003). Alternatively, the Gα subunit activates phosphodiesterases (PDEs) which leads to a reduction in protein kinase A (PKA) activity by decreasing cAMP levels. PKA acts as an inhibitor of IP3R mediated Ca^{2+} release by phosphorylating the receptor and rendering it unsuitable for activation by secondary messengers such as IP3 (Clapp et al., 2008). In the TRCs, the Ca^{2+} released activates TRPM5 channels (Perez et al., 2002;Damak et al., 2006). This leads to depolarization of cell membrane and activation of sodium channels. Subsequently, this results in the generation of an action potential that causes the release of ATP from CALHM1 ion channels (Taruno et al., 2013a;Taruno et al., 2013b). The ATP activates purinergic receptors on

afferent nerve fibers and transmits the chemosensory signals to CNS (Kinnamon, 2012;Workman et al., 2015). Several reports have shown that in airways, the bitter tastants, induce an increase in intracellular Ca^{2+} levels similar to the canonical bitter taste signaling cascade. However, the Ca^{2+} mediated responses and post bitter tastant stimulation have shown the involvement of other molecular components (Deshpande et al., 2010;Lee et al., 2012;Zhang et al., 2013;Upadhyaya et al., 2014;Howitt et al., 2016;Kim et al., 2018b).

1.2.3 Extraoral expression of T2Rs

T2Rs were first discovered in the taste buds of the oral cavity (Hoon et al., 1999). The function of the 25 T2Rs in humans was initially purported to only detect the taste of the ingested food and thereby perform a defensive role against ingesting toxic bitter tasting xenobiotics. However, in recent years, T2R expression has been uncovered in several extraoral regions of the human body **(Figure 1.2.1)** (Shaik et al., 2016;Lu et al., 2017). Among these extraoral regions, the expression and potential functional role of T2Rs in airways have attracted a lot of interest. Deshpande and Liggett first reported the bitter tastant induced bronchodilatory effect mediated by T2Rs in airway smooth muscle cells (Deshpande et al., 2010). The bronchial relaxant effect mediated by T2Rs was reported to be similar compared to the traditional β_2-adrenergic receptor agonists and hence T2Rs are considered as potential targets for a novel class of bronchodilators. Functional T2Rs are expressed in various cell types of the upper airways such as sinonasal ciliated epithelial cells and solitary chemosensory cells. T2Rs in upper airways have been shown to regulate airway immune responses in respiratory infections (Lee et al., 2014). T2Rs are also expressed in extra gustatory tissues such as gastrointestinal tract, heart, uterus, thyroid and brain and play a role in their physiology (Chen et al., 2006;Jang et al., 2007;Singh et al., 2011b;Foster et al., 2013;Clark et al., 2015;Zheng et al., 2017;Luo et al., 2019). However, their involvement in

pathophysiological states pertaining to these organs is not well understood. Furthermore, their activation was shown to result in physiological responses, which were comparable to the ones elicited by well-characterized GPCRs.

1.2.4 Role of T2Rs in upper airway diseases

1.2.4.1 Role of T2Rs in chronic rhinosinusitis

Previous studies have shown the expression of T2Rs in upper airway epithelium in humans and rodents. T2Rs are expressed in specialized epithelial cells of the sinonasal cavity such as ciliated epithelial cells and solitary chemosensory cells (SCC) (Tizzano et al., 2010;Tizzano et al., 2011;Lee et al., 2012;Saunders et al., 2014). T2Rs were shown to be involved in upper airway immune responses to microbial infections. They were proposed to mediate innate immune defense mechanisms in response to microbial infections from inhaled bacteria, virus and fungi. T2Rs were found to be one of the chemosensory molecules involved in recognizing these foreign microbes and initiate a signaling cascade as part of a defensive response. Activation of T2R by their ligands was shown to increase the motile ciliary beat frequency which speeds up the process of mucociliary clearance (MCC). Experiments carried out in sinonasal airway liquid interface (Sinonasal ALI) cultures reported that T2R38 localized on motile cilia were involved in recognizing acyl homoserine lactones (AHLs) secreted by gram-negative bacteria such as *Pseudomonas aeruginosa*. Post stimulation with AHLs, T2R38 triggered the release of nitric oxide (NO) through a Ca^{2+} dependent pathway. NO exerts its anti-microbial effects by penetrating into bacteria such as *P. aeruginosa* and causes cell death. Additionally, NO release can speed up the ciliary beat frequency by activating protein kinase G and guanylyl cyclase which in turn phosphorylate proteins in cilia. The involvement of the TRPM5 channel and PLCβ2, two integral components of bitter taste signaling cascade in T2R38

mediated NO secretion pathway was also reported. The specificity of T2R38 in mediating the anti-microbial responses was studied by stimulation with a very low potency agonist, sodium thiocyanate. Results suggested T2R38 dependent production of NO and these responses were not observed when T2R38 was stimulated with bitter ligands such as thujone and denatonium, which do not activate T2R38 (Lee et al., 2012). The differential ability to detect antimicrobial secretions between polymorphic variants of T2R38 and its implications in disease states have been discussed in section 1.2.4.2. In addition, these studies highlight a novel T2R38 mediated antimicrobial pathway that can be targeted for treatment of chronic sinonasal infections such as chronic rhinosinusitis (CRS).

Besides T2R38, T2R14 has been proposed to play a major role in sino-nasal ciliated epithelial cells. T2R14 co-localizes with T2R38 and activation of T2R14 with flavones elicited antimicrobial responses like nitric oxide production and increase in ciliary beat frequency (Hariri et al., 2017). Moreover, *P. aeruginosa* quinolone secretions activated T2R4, T2R14, T2R16, and T2R38 and resulted in calcium release, decreased cAMP levels and nitric oxide secretion in primary airway epithelial cells and sino-nasal cells (Freund et al., 2018). Recent studies suggest functional T2Rs and T1Rs to be expressed in rodent and human SCCs in the nasal cavity (Tizzano et al., 2010;Braun et al., 2011). Studies carried out in mouse models have shown that stimulation of SCCs with AHLs and bitter agonists induced pro-inflammatory responses via canonical bitter taste signaling pathway (Saunders et al., 2014). In human SCCs, denatonium benzoate induced Ca^{2+} responses lead to secretion of antimicrobial peptides (Braun et al., 2011;Lee et al., 2014). The studies have demonstrated a novel chemosensory role of T2Rs in regulating the antimicrobial responses in the upper respiratory tract. In addition, it was found that the antimicrobial responses mediated by T2Rs are regulated by T1Rs. Interestingly the

antagonistic role of T1Rs towards AMP secretions induced by T2Rs is confined to the upper respiratory tract. The antagonistic effects of these taste receptors were not observed in studies conducted in lower airway bronchial epithelial cultures (Lee et al., 2014). In the light of these findings, further studies are required to exploit the potential of T2Rs as novel targets in the management of upper airway infections such as CRS.

1.2.4.2 Role of T2R38 polymorphism in chronic rhinosinusitis

Polymorphism in TAS2R38 has been extensively investigated and T2R38 haplotypes with allelic variation at three amino acid sites result in distinct phenotypic variations. Two of the most common T2R38 haplotypes are tasters and non-tasters based on the ability to taste phenylthiocarbamide (PTC). Genotyping of taster haplotypes of TAS2R38 have shown the presence of Proline, Alanine and Valine at 49, 262 and 296 positions respectively and usually referred to as the PAV haplotype. The non-taster haplotypes are characterized by Alanine, Valine and Isoleucine at the above mentioned variant sites and referred to as AVI haplotype (Kim et al., 2003;Bufe et al., 2005). Recently, the association between T2R38 polymorphisms with a predisposition to upper respiratory tract infections was investigated (Lee et al., 2012). It was reported that, in human sinonasal cells from individuals with non-functional T2R38 haplotype (AVI/AVI) there was an increased susceptibility to airway infections compared to individuals with T2R38 functional haplotypes (PAV/PAV) (Lee et al., 2012). These observations were further confirmed by genotyping studies on patients undergoing functional endoscopic sinus surgery (FESS) for the treatment of CRS. Results suggest that non-functional TAS2R38

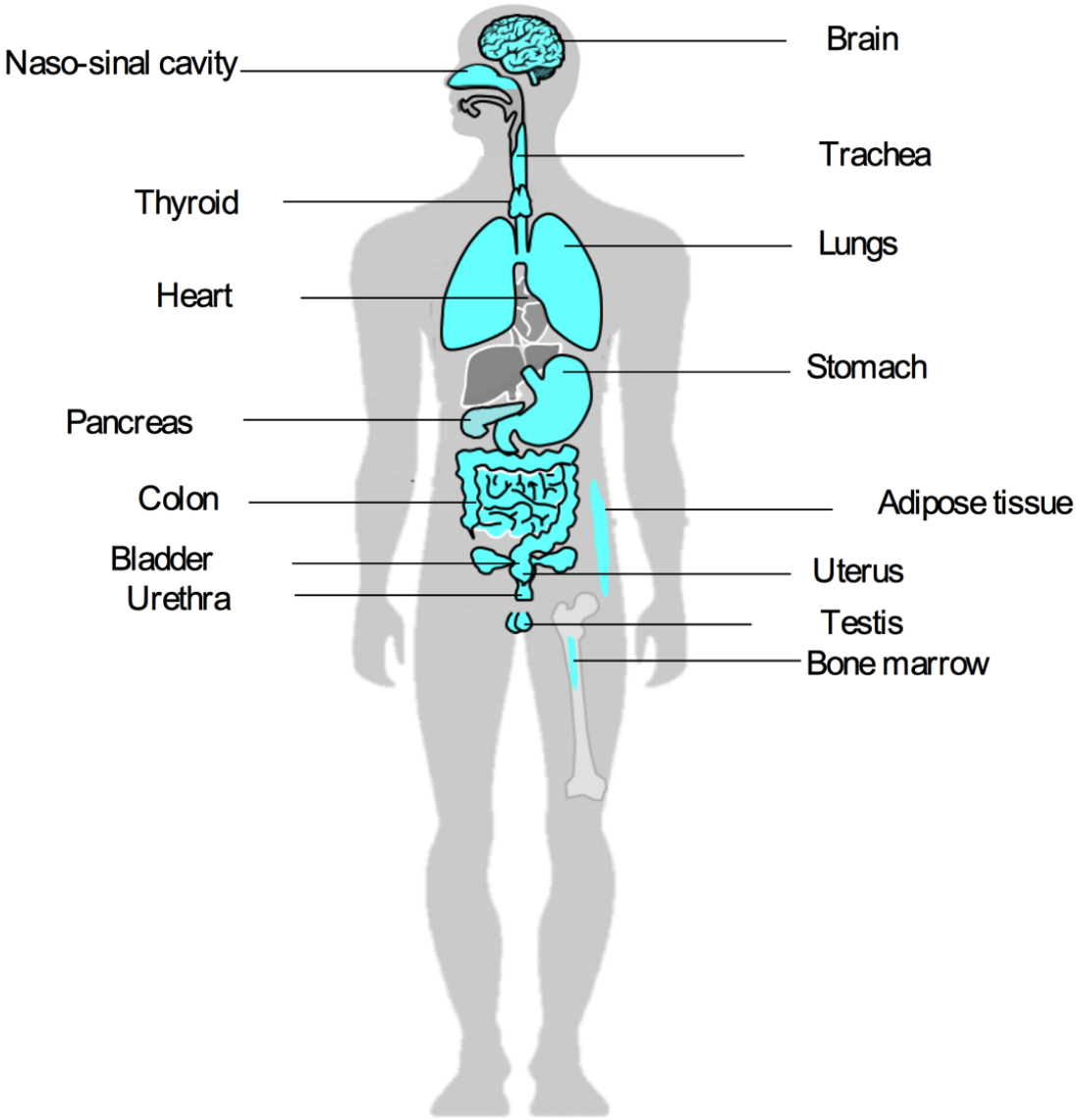

Figure 1.2.1 Extraoral expression of T2Rs. A human illustration highlighting the organs in which T2Rs expression has been discovered. Specifically, T2Rs potential in eliciting physiological responses has been shown in lungs, naso-sinal region, thyroid, stomach, intestinal regions, and uterus.

genotype was overrepresented in samples from patients undergoing FESS. This data suggests that T2R38 polymorphism does play a role in an individual's predispositions to resistant types of CRS. The non-taster T2R38 haplotype was reported to be an independent risk factor for chronic CRS (Adappa et al., 2014).

1.2.5 Role of T2Rs in lower airway diseases

1.2.5.1 Role of T2Rs in asthma

Asthma is a chronic obstructive airway disease characterized by inflammation of respiratory tract mediated by the release of various inflammatory proteins, abnormal smooth muscle contractility, and elevation in airway secretions (Fanta, 2009). The airway obstruction in asthmatic conditions is variable and reversible in some cases (Barnes, 2008). The traditional therapeutic management of asthma involves the administration of bronchodilators such as β2-adrenergic receptor agonists and anti-inflammatory corticosteroids. However, recently T2Rs have emerged as potential drug targets in the treatment of asthma.

In 2010, Deshpande et al., reported the expression and function of T2Rs in human airway smooth muscle (ASM) cells. It was found that bitter tastants cause relaxation of ASMs in a T2R dependent manner. The T2R mediated increase in Ca^{2+} results in the opening of Ca^{2+} activated K^+ (BK_{ca}) channels and subsequently leads to membrane hyperpolarization and ultimately produces relaxation of ASMs. In isolated mouse airways, it was found that bitter tastants elicited dose-dependent relaxation. Additionally, in a mouse model of asthma, bitter tastants produced a more potent bronchodilatory effect compared to β-agonists (Deshpande et al., 2010). The T2R mediated airway smooth muscle relaxation effect induced by bitter agonists was further confirmed by other groups who found a similar effect in human bronchi and mouse ASM cells

(Grassin-Delyle et al., 2013;Zhang et al., 2013). Interestingly, Zhang et al., in 2013 demonstrated that bitter tastant induced bronchodilatory effect in mouse ASM was independent of the increase in intracellular Ca^{2+} events by canonical bitter taste signaling cascade. It was shown that the mouse ASM relaxation is caused by reversing the increase in Ca^{2+} induced by bronchoconstrictors through inhibition of L-type voltage sensitive Ca channels (L-VDCCs) by G-protein βγ subunits of T2R signaling cascade (Zhang et al., 2013). In a study analyzing the bronchodilatory effects induced by selective and non-selective T2R agonists in isolated human bronchi, it was found that T2R5, T2R10, and T2R14 subtypes played a prominent role in bronchial relaxation (Grassin-Delyle et al., 2013).

Robinett et al., in 2014 have investigated the T2R mediated bronchodilatory effects in human ASM cells derived from asthmatic patients and normal patients. It was found that T2R expression and T2R mediated bronchodilatory effect was independent of disease state and IL-13 induced inflammatory environment. Interestingly, the relaxant effect induced by β-adrenergic receptor agonist (formoterol) was reduced, in the presence of IL-13 (Robinett et al., 2014). T2R agonists apart from their ASM cell relaxation effect, also inhibit the growth of ASM cells without causing cell death via inhibition of several mitogenic signaling pathways. This aspect of T2R agonists could be beneficial in countering the airway remodeling issues in asthma (Sharma et al., 2015). Moreover, recently T2R14 biased agonists, have been identified which could stabilize the T2R14 in specific conformations evoking growth inhibitory responses in human ASM cells to a different degree (Kim et al., 2018a). Several publications have reported the anti-inflammatory effects of T2R agonists such as caffeine, dapsone, colchicine, and erythromycin in obstructive lung diseases, however whether this effect is T2R mediated is a question that needs further investigation (Ghio et al., 2005;Sanz et al., 2005;Kanoh et al., 2011;Weichelt et al.,

2013). The recent discoveries of bitter agonists as potent bronchodilators in treatment of asthma are promising, however, more studies are required to unequivocally establish their higher efficacy as an alternative to currently available bronchodilators.

1.2.5.2 Role of T2Rs in airway inflammation

Airway inflammation is a characteristic feature of airway diseases such as asthma and chronic obstructive pulmonary disease (COPD). Inflammatory responses are characterized by an increase in expression of inflammatory proteins such as cytokines, chemokines, pulmonary macrophages and adhesion molecules (Caramori and Adcock, 2003). Gene expression analysis of white blood cells from patients with severe therapy resistant and controlled asthma has revealed an upregulation of T2Rs expression. Bitter agonist treatment in leucocytes from adult asthmatic patient resulted in the inhibition of LPS induced cytokine release (Orsmark-Pietras et al., 2013). TAS2R transcripts were also found to be expressed in lung parenchyma and pulmonary macrophages (Stanislas Grassin et al., 2014). T2Rs were found to be expressed in human primary mast cells and on stimulation with bitter agonists T2Rs inhibited the release of IgE dependent pro-inflammatory histamines and PGD2 from primary human mast cells (Ekoff et al., 2014). In allergen challenged mice, bitter agonist treatment attenuated the allergic airway inflammation (Sharma et al., 2017). Considering the central role of inflammatory mediators in the pathology of airway obstructive diseases, there is a need for a better understanding of their role in the pathophysiology of airway inflammation in disease states. On the clinical side, considering their expression in components of inflammatory machinery, T2Rs could be a novel target in modulating the inflammatory responses in pathological states. Nevertheless, more studies are required to elucidate the functional role of T2Rs in regulating the inflammatory responses.

1.2.5.3 Role of T2Rs in cystic fibrosis

Cystic fibrosis (CF) is an autosomal recessive disorder occurring in certain populations. At a genetic a level it is characterized by ΔF508 mutation in gene encoding cystic fibrosis transmembrane conductance regulator (CFTR) protein. CFTR is an epithelial Cl^- channel responsible for the transport of ions and water across epithelial barrier (Riordan et al., 1989). CF is characterized by chronic bacterial infection, bronchiectasis and excessive viscous mucous secretion in airways and pancreatic ducts. The abnormal secretion leads to obstruction and subsequent inflammation which adversely affects the normal physiology of these organ systems. Over the past two decades, several advances have been made in understanding the pathophysiology of the CF. However, several factors contributing toward this complex disease such as how mutated CFTR affects the mucosal immune responses or the connection between CFTR dysfunction and susceptibility to pulmonary infections are yet to be studied and understood (Cohen and Prince, 2012).

The emerging role of T2R38 in upper airway epithelial innate immune function has been described earlier (section 1.2.4). Recently, it was shown that individuals with PAV/PAV genotype were less susceptible to developing sinonasal infections such as CRS (Lee et al., 2012). Additionally, a cohort study involving ΔF508 homozygous CF patients of age group 18-32 years examined the CRS manifestations in CF patients. Subsequently, it was found that CF patients with T2R38 functional alleles (PAV/PAV) had a better rhinologic quality of life scores compared to CF patients with non-functional PAV/AVI and AVI/AVI genotypes (Adappa et al., 2015). In addition, differential expression of 25 T2Rs has been shown in immortalized bronchial epithelial cell lines isolated from normal and CF patients, NuLi-1 and CuFi-1 respectively have been shown and prototypical T2R agonist, quinine elicited dose-dependent calcium mobilization

in NuLi-1 and CuFi-1 (Jaggupilli et al., 2017). A recent report demonstrated that T2Rs were activated by broad-spectrum antibiotics generally used in the treatment of respiratory infections associated with CF (Jaggupilli et al., 2018a). In light of the proposed significance of T2Rs in airway infections, we speculate that in CF epithelial cells, T2Rs might mediate host responses to bacterial infection by recognizing quorum sensing molecules. A schematic of T2R mediated antimicrobial responses in CF epithelial cell is shown in **figure 1.2.2**. Moreover, controlled clinical trials have established the therapeutic benefits of targeting both pathological immune responses as well as infecting microbes. We suggest that investigating the potential role of T2Rs in the pathophysiology of CF could contribute towards developing novel therapeutic strategies targeting infectious organism in CF therapy.

1.2.6 Polymorphism in bitter taste receptor genes – Disease risk factors

Genomic analysis for identification of polymorphic sites has uncovered 151 T2R coding haplotypes. The majority of single nucleotide polymorphisms (SNPs) were found to be non-synonymous which results in altered amino acid sequences. Two-thirds of the SNPs had a frequency of 1-50%, which is significant considering it only requires a section of the polymorphic allele with high frequency to give rise to functionally diverse polymorphic variants of T2Rs (Kim et al., 2005;Behrens and Meyerhof, 2006). The significance of TAS2R polymorphism extends beyond mere differential sensitivity in tasting bitter compounds. Numerous studies have shown the influence of genetic polymorphism in T2Rs towards a predisposition to disease risk factors such as cancer, alcohol dependence and food preferences.

According to the World Health Organization, harmful use of alcohol results in 3.3 million deaths per year (Alcohol) (http://www.who.int/substance_abuse/facts/alcohol/en/). Alcohol dependence is characterized by addiction to alcohol which is associated with life-threatening

psychiatric, psychological, cardiovascular and cancer related complications (Cargiulo, 2007). In a study conducted to understand the relationship between TAS2R38 genotype and alcohol intake, it was found that non-taster phenotypes which are characterized by homozygous AVI/AVI diplotypes predicted higher alcohol intake compared to individuals with heterozygous PAV/AVI and homozygous PAV/PAV diplotypes (Duffy et al., 2004). A coding SNP in TAS2R16 (rs846664) has been associated with increased alcohol dependence. The naturally occurring K172 allele in TAS2R16 is associated with decreased bitter sensitivity to β-glucopyranosides and increased alcohol dependence. Individuals with the K172N variant showed increased bitter sensitivity to β-glucopyranosides and decreased alcohol dependence (Hinrichs et al., 2006). Studies from cohorts comprising different ethnicities have shown an association between K172 allele of TAS2R16 with decreased bitter sensitivity and increased alcohol dependence (Hinrichs et al., 2006;Wang et al., 2007). In addition, a genomic study on head and neck cancer patient cohorts has demonstrated an association between a coding SNP (rs1015443) in TAS2R13 gene with increased susceptibility to alcohol consumption. Oral cancer patients were selected for the study since chronic alcohol dependence is considered a lifestyle risk factor for oral cancer (Dotson et al., 2012).

There have been several studies conducted to investigate the influence of T2R polymorphism on adiposity, eating behavior, a risk of cancers and coronary heart disease traits. In a cohort study of colorectal adenoma cases, the researchers explored association among colorectal adenoma risk, dietary intake, and genetic variation in three bitter taste receptor genes: TAS2R38 (rs713598, rs1726866, rs10246939), TAS2R16 (rs846672) TAS2R50 (rs1376251). No significant associations were observed between the TAS2R38 PAV/PAV diplotype or the TAS2R16 (rs846672) polymorphism with the selected diet variables (Schembre et al., 2013).

These findings do not support a link between these TAS2R genotypes/haplotypes and dietary intake that could impact colorectal adenoma risk. There has been no association found between TAS2R38 haplotype status and eating behavior, coronary heart disease risk factors in British women (Timpson et al., 2005). TAS2R38 polymorphism did not influence the waist circumference and BMI in a study conducted in females of a genetically isolated population from Italy. However, PROP non-taster showed a higher BMI compared to taster phenotypes (Tepper et al., 2008). In a sex-stratified analysis conducted in older Amish people, it was observed that TAS2R38 (rs1726866) allelic variation is correlated to ingestive behavior (restraint, disinhibition, and hunger) in women, but not in men (Dotson et al., 2010). In a recent study conducted with a sample size of 941 humans, it was observed that there is a statistically significant correlation between TAS2R16 polymorphism (rs978739) and the aging process (Campa et al., 2012). In addition, TAS2R38 polymorphism has been associated with the risk of dental caries. The TAS2R38, AVI haplotypes (non-tasters) are associated with increased risk of dental caries (Wendell et al., 2010). Recently a study showed an association between oral bacterial composition and taste preferences, with higher abundance of five bacterial genera in supertaster group compared to non-tasters(Cattaneo et al., 2019).

1.2.7 Role of T2Rs in cancer

Taste is referred to as the body's 'nutritional gatekeeper'. Variation in taste receptor genes can give rise to a differential perception of sweet, umami and bitter tastes. Many phytochemicals, including phenols, flavonoids, isoflavones, and glucosinolates, have been shown to have antioxidant, anticarcinogenic and a wide spectrum of tumor-blocking properties (Craig, 1997). Most of these phytochemicals taste bitter. Bitterness is the most commonly cited reason for

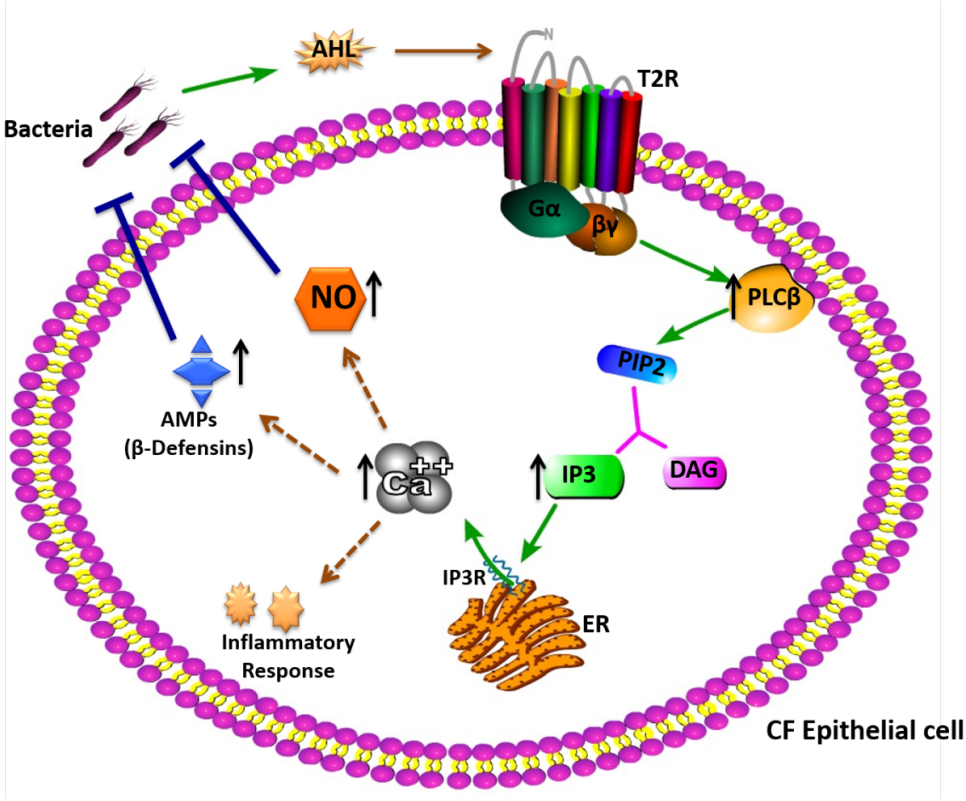

Figure 1.2.2 A schematic showing how quorum sensing molecules such as acyl-homoserine lactones (AHLs) acting through cell surface receptors might induce an increase in intracellular calcium leading to multiple responses in a bronchial epithelial cell (Lee et al., 2012;Jaggupilli et al., 2017;Freund et al., 2018). Colonized bacteria secrete AHLs as autoinducers or other QSMs that bind to an unknown receptor and activate phospholipase C-β (PLC-β) causing an increase in IP_3 and calcium mobilization. The increase in intracellular calcium subsequently can lead to diverse responses (represented by broken arrows) that lead to contrasting effects. These responses can lead to host cell inflammation or have bactericidal effects involving the production of nitric oxide (NO) and antimicrobial peptides (AMPs) such as β-defensins.

disliking a particular food and has been shown to lead to food rejection (Drewnowski et al., 1997a;b). Increasing fruit and vegetable consumption is the key dietary strategy for cancer prevention. Diets high in plant foods, notably cruciferous and green vegetables, allium vegetables, soy products, tomatoes, and citrus fruit, offers protection against cancer (Steinmetz and Potter, 1996). Experimental data shows that bitter vegetables inhibit the matrix metalloproteinase (MMP) activity in MDA-MB-231 cells (Rose et al., 2005).

Previous studies showed that many bitter compounds such as quinine, quinidine, chloroquine, and bitter melon extracts induced apoptosis and inhibit cell proliferation in breast cancer cells (Zhou et al., 2002;Ray et al., 2010). However, the potential role of cell membrane receptors in mediating the bitter compound induced anticancer effects is unclear. Novel findings by Singh et al., (2014) showed the differential expression of TAS2Rs in both non-cancerous and cancerous breast epithelial cells. Activation of T2Rs with bitter agonists dextromethorphan, quinine and PTC led to an increase in an intracellular calcium release (Singh et al., 2014). However, the signalling mechanism and physiological functions of these T2Rs in breast cancer need to be investigated. Recently, the role of T2R38 in pancreatic cancer was studied. It was reported that T2R38 was expressed and localized in lipid droplets of tumor cells from pancreatic cancer patients and tumor derived cell lines. Additionally, stimulation with AHL-12 and phenylthiourea (PTU) lead to T2R38 mediated activation of key transcription factors. These results indicate a potential involvement of T2R38 in pancreatic cancer progression (Gaida et al., 2016b). Furthermore, it was suggested that T2R10 played a role in improving the chemosensitivity of pancreatic cell lines (Stern et al., 2018) and in human neuroblastoma cells, T2R8 and T2R10 induced anti-invasive and anti-cancer stemness responses were reported (Seo et al., 2017). Recently, TAS2R14 expression pattern was shown to greatly vary in prostate and

ovarian cancer patient samples, while its involvement in inducing apoptosis was also demonstrated (Martin et al., 2018).

Additionally, reports by Campa et al., (2010) showed no evidence of statistically significant associations between TAS2R14 gene polymorphism and colorectal cancer risk. (Campa et al., 2010). A study by Tustumi et al., (2015) showed the effect of chemotherapy on the expression of taste receptors in head and neck cancer patients (Tsutsumi et al., 2015). Chemotherapy specifically changed the gene expression of TAS1R3 and TAS2R5 in head and neck cancer patients with mild/moderate stomatitis, resulting in both dysgeusia of umami and sweet tastes as well as phantogeusia. Further studies are needed to investigate the chemosensory role of T2Rs in cancer.

1.2.8 Role of T2Rs in pulmonary vasculature

Proteomic screens confirmed the expression of T2R46 in human bone marrow derived mesenchymal (hMSC) and vascular smooth muscle cells (VSMCs) (Lund et al., 2013). Treatment of human VSMCs with denatonium benzoate (DB) induced a T2R46 mediated Ca^{2+} release. In addition, systemic administration of DB in rats induced a transient drop in blood pressure. It was hypothesized that the observed changes in vascular tone in response to a prototypical T2R agonist was a T2R mediated effect (Lund et al., 2013). A recent study investigated the effect of T2R agonists in human and rodent VSMCs (Manson et al., 2014). It was found that bitter agonists induced relaxation in pre-contracted rodent and human VSMCs. However, the underlying involvement of T2R in mediating vasorelaxation was not established (Manson et al., 2014).

In contrast to this, studies by two different groups suggest bitter ligand induced smooth muscle contractility in pulmonary VSMCs and gastric smooth muscle cells or hGSMCs (Upadhyaya et al., 2014) (Avau et al., 2015). An elaborate study by Upadhyaya et al., (2014) reported TAS2R1 mediated Ca^{2+} responses and vasoconstriction in pulmonary artery, whereas relaxation in the airways in response to the bitter agonist dextromethorphan (Upadhyaya et al., 2014). In addition, a recent publication has reported the mechanism underlying bitter tastant induced effects on hGSMCs (Avau et al., 2015). It was shown that T2R agonist, DB induces hGSMC contractions in a concentration-dependent manner. DB induced an increase in intracellular Ca^{2+} levels via canonical taste signal transduction pathway. Along with this, the involvement of ERK-phosphorylation in DB induced hGSMC contractility was also reported (Avau et al., 2015). Discrepancies between the studies in the vasculature might be explained by agonist specificity, dose-related changes and type of T2Rs expressed in these tissues. Alternatively, these observations might underlie a physiologically relevant differential response to bitter treatment between the systemic and pulmonary circulation, although further studies need to be carried out. The expression of T2Rs has been recently reported in human and mouse hearts along with other taste GPCRs (Foster et al., 2013). TAS2R14 was found to be highly expressed in the human heart. It was proposed that T2Rs might be involved in a potential nutrient sensing role in the cardiovascular system (Foster et al., 2013). Moreover, the developmental regulation of TAS2R expression throughout the lifespan of rats was studied. It was found that the expression patterns of TAS2Rs (108, 126, 135, 137, 143) in heart tissue, decreased with age. Additionally, in nutrient deprived state, the expression of T2Rs in rat cardiomyocytes was found to be upregulated (Foster et al., 2013). Taken together, these results indicate a potential physiological

role played by T2Rs in cardiovascular physiology. An illustration summarizing T2Rs role in various pathophysiological conditions is shown in **figure 1.2.3**.

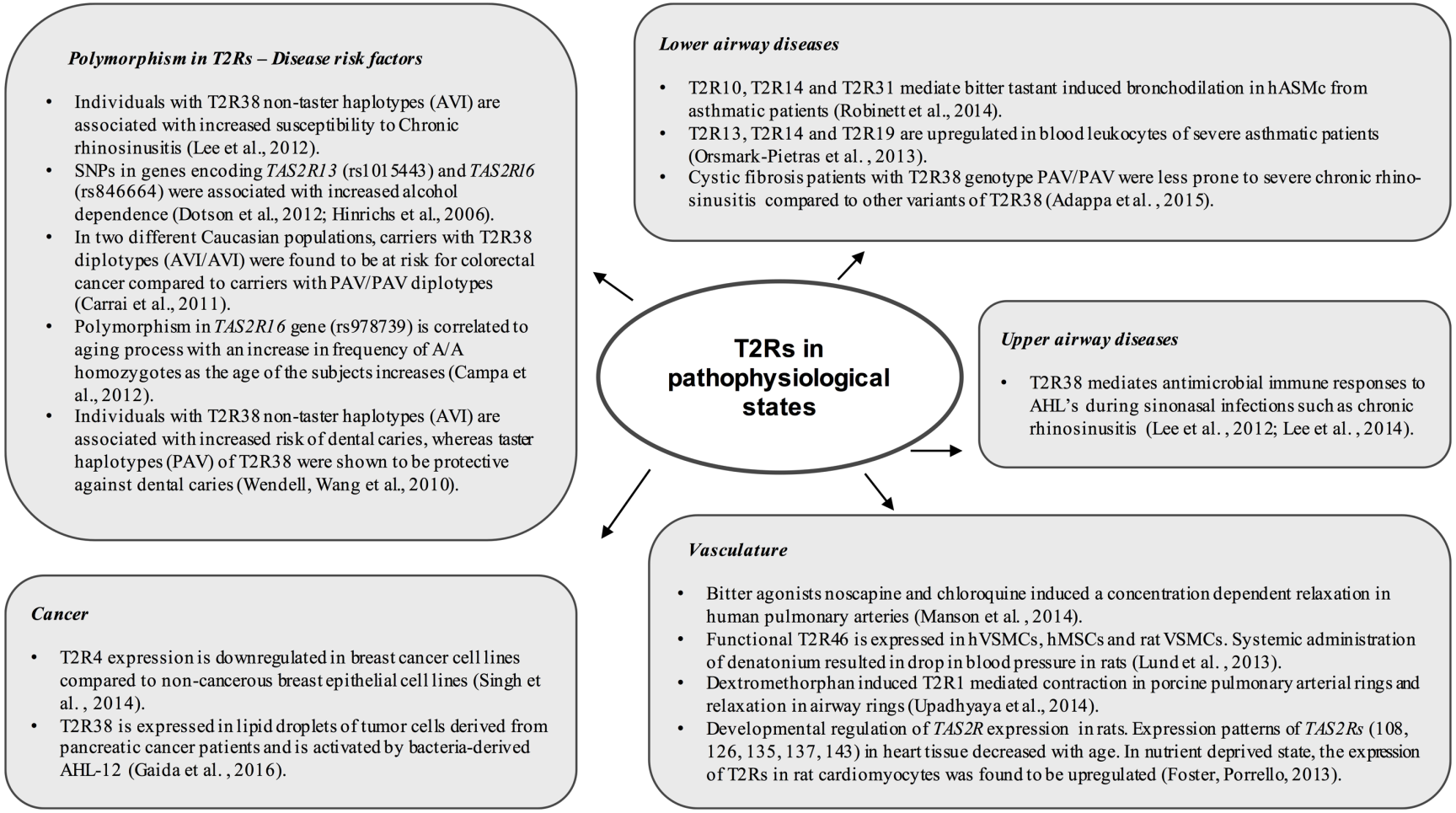

Figure 1.2.3 T2Rs in pathophysiological states. A summary diagram of T2R expression and physiological functions in various pathological states.

CHAPTER 2

2.0 HYPOTHESIS AND OBJECTIVES

2.1 Study Rationale

Rationale for T2R-Breast cancer study

In recent times, many studies have shown the expression of T2Rs in various extraoral regions of the human body (Shaik et al., 2016;Lu et al., 2017). The activation of T2Rs in these extraoral regions resulted in physiological responses like smooth muscle relaxation, airway immune responses and gut hormone secretion (Deshpande et al., 2010;Lee et al., 2012;Robinett et al., 2014;Sharma et al., 2017). Moreover, due to high expression and broad tuning breadth (i.e., receptor could be activated by structurally diverse ligands) T2Rs are considered potential pharmacological targets in various pathological conditions. While the role of T2Rs in different cancers is being explored, one of the first reports suggesting a potential pathophysiological role for T2Rs was in breast cancer (Singh et al., 2014).

Breast cancer is one of the major cause for cancer-related mortality in women. Global statistics from the World Health Organization for the year 2018 shows an estimated 626,679 women have died due to breast cancer (WHO). Improved diagnostic and therapeutic options are necessary for early detection and treatment of breast cancer. Aberrant GPCR expression and its concomitant dysregulated signaling has been implicated in breast cancer tumorigenesis, e.g. chemokine receptors regulate breast cancer metastasis as overexpression of GPR161 is correlated to breast cancer proliferation and migration (Muller et al., 2001;Yagi et al., 2011;Feigin et al., 2014). In addition, several GPCR mutations and dysregulated autocrine and paracrine GPCR

activation have been associated with breast tumor progression (Liu et al., 2016c;Nieto Gutierrez and McDonald, 2018).

T2Rs are aberrantly expressed in breast cancer cell lines, MDA-MB-231, compared to non-tumorigenic breast epithelial cells (MCF 10A). The TAS2R4 and TAS2R14 transcript expression analysis using nCounter platform (NanoString Technologies) reveals that TAS2R4 expression is less in MDA-MB-231 cells compared to MCF 10A cells whereas, T2R14 expression is increased in MDA-MB-231 in comparison to MCF 10A cells. Moreover, TAS2R gene profiling data from online clinical sample data repositories (TCGA and GTEx) shows that T2R4 and T2R14 expression in tumor samples is lower compared to normal samples (Data not shown). In the present work, I focussed on characterizing the effect of T2R4 and T2R14 activation on breast cancer pathophysiology.

Rationale for molecular determinants in T2R14 signaling studies

As mentioned earlier, T2R14 plays an important role in airway cellular pathophysiology. For example, in airway epithelial cells, activation of T2R14 resulted in anti-microbial responses whereas in human airway smooth muscle (HASM) cells, T2R14-mediated HASM cell relaxation as well as HASM cell growth inhibitory effects have been reported. Due to the important role played by T2R14 in airway physiology, additional factors regulating its function will be beneficial in understanding innate mechanisms governing T2R14 function. Membrane lipids like cholesterol and sphingolipids regulate the conformation and function of various GPCRs. In light of the key role played by T2R14 in airways, I studied the lipid sensitivity of T2R14 signaling in airway cells.

Emerging evidence suggests T2R14 as a potential pharmacological target, especially in alleviating respiratory tract related disease conditions. Thus, a better understanding of structural determinants governing its ligand inducing efficacy will be useful in providing insights into its molecular basis of function.

2.2 Hypothesis

T2R4 and T2R14 activation in breast cancer cells influences their proliferation and migration. Membrane lipids and conserved intracellular amino acid residues regulate T2R14 signaling.

2.3 Objectives

To test the hypothesis I pursued biochemical, pharmacological and physiological studies on select T2Rs. The specific objectives are as follows:

2.3.1 Characterize the role of T2R4 and T2R14 in the pathophysiology of breast cancer

The focus of this objective is to first, analyze the expression of T2R4 and T2R14 in breast cancer patient samples, normal breast samples, breast cancer cell lines and non-tumorigenic breast epithelial cell lines. Second, using a combination of approaches, which includes gene knockdown, pharmacological, biochemical and physiological assays, we examined the bitter agonist-induced effects of T2R4 and T2R14 on breast cancer cell apoptosis, proliferation, and migration.

2.3.2 Role of membrane cholesterol in T2R14 signaling

Here, the focus is to understand the role of membrane cholesterol in agonist induced T2R14 signaling in HASM cells and airway epithelial cells. Further, to elucidate the molecular

mechanisms involved in T2R14-cholesterol interaction, amino acids in the putative cholesterol binding motifs in T2R14 were analysed by mutational studies.

2.3.3 Elucidate role of membrane sphingolipids in T2R14 signaling

To investigate the role of membrane sphingomyelin in T2R14 signaling, a combination of bioinformatics analysis, live-cell functional assays, and second messenger induced protein phosphorylation studies were utilized.

2.3.4 Characterize the molecular determinants in agonist induced T2R14 efficacy

Here the objective is to obtain mechanistic insights into the role of intracellular conserved H208 residue in T2R14 efficacy.

CHAPTER 3

3.0 GENERAL METHODS

3.1 Materials

3.1.1 Chemicals and reagents

Diphenhydramine (DPH), quinine hydrochloride (QUI), flufenamic acid (FFA), dimethyl sulphoxide (DMSO), fetal bovine serum (FBS), horse serum, L-glutamine, hydrocortisone, insulin, human epidermal growth factor (hEGF), trypsin-EDTA, puromycin, cholesterol, methyl-β-cyclodextrin (MβCD), cholesterol oxidase (COase), collagen type 4 (Cat. #C7521), U73122, angiotensin II human (AngII), sphingomyelinase (SMase, Cat. #S8633), phosphatase inhibitor cocktail 3 (Cat. #P0044) were acquired from Sigma Aldrich (Oakville, ON, Canada). Apigenin (API) was purchased from Cayman Chemical (Ann Arbor, MI, USA). Fluo-4 NW calcium assay kit, Dulbecco's modified Eagle medium (DMEM)/Ham's F12 (F12), DMEM (High glucose), penicillin (10,000 U/ml)-streptomycin (10,000 µg/ml), hygromycin B (Cat. #10687010), lipofectamine 2000, opti-MEM, amplex red cholesterol assay kit (Cat. # A12216), amplex Red sphingomyelinase assay kit (Cat. #A12220), cyquant NF cell proliferation assay kit (Cat. # C35007,) western blot stripping buffer, superScript III reverse transcriptase (Cat. #18080093), and SYBR green PCR master mix (Cat. #4309155) were acquired from ThermoFisher Scientific (Burlington, ON, Canada). Gallein (Cat. #3090) was acquired from Tocris. Protease inhibitor cocktail (Cat. #539131) was obtained from Millipore Sigma and Bovine serum albumin (Cat. #0332) was acquired from VWR life sciences. Bronchial epithelial cell growth basal medium or BEBM (Cat. #CC-3171) and BEGM supplements and growth factors (Cat. #CC-4175) were purchased from Lonza Inc. (Walkersville, MD). QIAprep plasmid extraction kit, QIAquick gel

extraction kit, and RNeasy Mini Kit (Cat. #74104) were acquired from Qiagen (Toronto, ON, Canada). N-Dodecyl-β-D-maltopyranoside (DM) was acquired from Anatrace (Maumee, OH, USA). Propidium Iodide (Cat. #421301) and Alexa Fluor 647 Annexin V (Cat. #640912) were obtained from Biolegend (San Diego, CA, USA). ETSAHRL (T2R14 inhibitor peptide) was acquired from commercial sources (Genscript Inc. NJ, USA). CIM-plate 16 (Cat. #5665817001) was obtained from ACEA Biosciences (San Diego, CA, USA). Human MMP-9 quantikine ELISA kit (Cat. # DMP900) was from R&D Systems (Minneapolis, MN, USA). All the chemicals were of analytical grade.

3.1.2 Media for bacterial culture

Luria-Bertani (LB) media: 10 g/l Tryptone, 10 g/l NaCl, 5 g/l Yeast extract.

LB Agar-Ampicillin plates: 15 g of Agar was dissolved in 1l of LB media and sterilized. Upon cooling, 100 µg/ml Ampicillin was added to LB-Agar media. Next, the media was poured into 100 mm petri dishes and allowed to solidify in sterile conditions.

SOB media: 2% Bacto-Tryptone, 0.5% Yeast extract, 10 mM NaCl, 2.5 mM KCl (pH 7.0).

The SOB media was supplemented with 10 mM $MgCl_2$ before use.

3.1.3 Buffers

Phosphate buffered saline (PBS): 137 mM NaCl, 2.7 mM KCl, 10 mM Na_2HPO_4, 1.8 mM KH_2PO_4 (pH 7.6)

SDS-PAGE running buffer: 25 mM Tris base, 192 mM Glycine, 0.1% SDS (pH 8.3)

Tris acetate EDTA (TAE) buffer: 40 mM Tris base, 20 mM Acetic acid, 10 mM EDTA (pH 8.0)

Tris-buffered saline (TBS): 20 mM Tris base, 150 mM NaCl (pH 7.6)

TBST: TBS + 0.05% Tween20

Transfer (TB) buffer: 25 mM Tris base, 192 mM Glycine, 20% Methanol

Cell lysis buffer (Immunoblot analysis): 50 mM Tris base, 150 mM NaCl, 10% Glycerol, 1% DM with 1X protease inhibitor and 1X phosphatase inhibitor cocktails.

Cell lysis buffer (cell membrane preparation): 10 mM Tris base, 5 mM EDTA with 1X protease inhibitor cocktail

Storage buffer (cell membrane preparation): 50 mM Tris base with 1X protease inhibitor cocktail

Sample loading buffer (2X Laemmli buffer): 125 mM Tris base, 10% 2-Mercaptoethanol, 20% Glycerol, 4% SDS, 0.004% Bromophenol blue (pH 6.8).

Agarose loading buffer: 10 mM Tris-base (pH 7.6), 60 mM EDTA, 60% Glycerol, 0.03% Bromophenol blue.

Transformation buffer: 10 mM Hepes, 250 mM KCl, 15 mM $CaCl_2$, 55 mM $MnCl_2.4H_2O$ (pH 6.7).

FACS buffer: 1X PBS with 0.5% BSA

3.2 Molecular Biology and Cell Culture

3.2.1 Human TAS2R14 gene

The N-terminal FLAG epitope tagged human TAS2R14 gene was codon-optimized for expression in mammalian cells and cloned into Kpn1-Not1 multiple restriction sites of the pcDNA3.1-Hygro(+) expression vector. The synthetic FLAG-TAS2R genes were designed by

introducing a Kpn1 restriction site at 5' end followed by a Kozak consensus (GCCACCATGG) 5' to the ATG start codon. An octa-peptide FLAG tag (DYKDDDDK) was included after the start codon and followed by the TAS2R14 gene sequence. Not1 restriction site was introduced at the 3' end of the gene. The gene sequences encoding the recombinant human T2R14 **(Figure 3.2.1)** was optimized for mammalian cell codon usage, and genes were synthesized commercially (GenScript, NJ, USA). The DNA sequence for each gene was verified by automated DNA sequencing (MICB DNA Sequencing Facility, Winnipeg). The TAS2R14 gene cloned into pcDNA 3.1-Hygro (+) was used for transfection experiments and the empty vector, pcDNA3.1-Hygro (+) was used for mock transfection.

3.2.2 Preparation of competent *E. coli* cells

The competent *E.coli* cells were prepared following the Inoue method (Inoue et al., 1990). DH5α *E.coli* cells were added to 5 ml of LB media and allowed to grow overnight at 37°C. Then, 0.1 ml of saturated culture was inoculated in 100 ml of SOB media in a 1L flask and allowed to grow at 22°C under constant shaking (200-250 rpm) for 18 h, until an A_{260} value of 0.6 was reached. Then the flask was transferred onto the ice for 10 min, followed by centrifugation of cells at 2500 x g for 10 min at 4°C. The cell pellet was re-suspended in 32 ml of ice-cold transformation buffer and placed on ice for 10 min. The suspension was centrifuged again as described in the previous step. The cell pellet was re-suspended gently in 8 ml of transformation buffer and DMSO was added to a final concentration of 7% while swirling the cell suspension. The cells were placed on ice for another 10 min. Then, the cells were aliquoted in sterile microcentrifuge tubes and stored at -80°C until further use.

```
Kpn1   kozak            FLAG tag
GGTACCGCCACCATGGACTACAAGGACGACGATGACAAAGGTGGTGTCATAAAGAGCATATTTACATTCGTTTTAAT
TGTGGAATTTATAATTGGAAATTTAGGAAATAGTTTCATAGCACTGGTGAACTGTATTGACTGGGTCAAGGGAAGAA
AGATCTCTTCGGTTGATCGGATCCTCACTGCTTTGGCAATCTCTCGAATTAGCCTGGTTTGGTTAATATTCGGAAGC
TGGTGTGTGTCTGTGTTTTTCCCAGCTTTATTTGCCACTGAAAAAATGTTCAGAATGCTTACTAATATCTGGACAGT
GATCAATCATTTTAGTGTCTGGTTAGCTACAGGCCTCGGTACTTTTTATTTTCTCAAGATAGCCAATTTTTCTAACT
CTATTTTTCTCTACCTAAAGTGGAGGGTTAAAAAGGTGGTTTTGGTGCTGCTTCTTGTGACTTCGGTCTTCTTGTTT
TTAAATATTGCACTGATAAACATCCATATAAATGCCAGTATCAATGGATACAGAAGAAACAAGACTTGCAGTTCTGA
TTCAAGTAACTTTACACGATTTTCCAGTCTTATTGTATTAACCAGCACTGTGTTCATTTTCATACCCTTTACTTTGT
CCCTGGCAATGTTTCTTCTCCTCATCTTCTCCATGTGGAAACATCGCAAGAAGATGCAGCACACTGTCAAAATATCC
GGAGACGCCAGCACCAAAGCCCACAGAGGAGTTAAAAGTGTGATCACTTTCTTCCTACTCTATGCCATTTTCTCTCT
GTCTTTTTTCATATCAGTTTGGACCTCTGAAAGGTTGGAGGAAAATCTAATTATTCTTTCCCAGGTGATGGGAATGG
CTTATCCTTCATGTCACTCATGTGTTCTGATTCTTGGAAACAAGAAGCTGAGACAGGCCTCTCTGTCAGTGCTACTG
TGGCTGAGGTACATGTTCAAAGATGGGGAGCCCTCAGGTCACAAAGAATTTAGAGAATCATCTTGAGCGGCCGC
                                                                      Not1

GGTACCGCCACCATGGACTACAAGGACGACGATGACAAAGGTGGTGTCATAAAGAGCATA
 G  T  A  T  M  D  Y  K  D  D  D  D  K  G  G  V  I  K  S  I
TTTACATTCGTTTTAATTGTGGAATTTATAATTGGAAATTTAGGAAATAGTTTCATAGCA
 F  T  F  V  L  I  V  E  F  I  I  G  N  L  G  N  S  F  I  A
CTGGTGAACTGTATTGACTGGGTCAAGGGAAGAAAGATCTCTTCGGTTGATCGGATCCTC
 L  V  N  C  I  D  W  V  K  G  R  K  I  S  S  V  D  R  I  L
ACTGCTTTGGCAATCTCTCGAATTAGCCTGGTTTGGTTAATATTCGGAAGCTGGTGTGTG
 T  A  L  A  I  S  R  I  S  L  V  W  L  I  F  G  S  W  C  V
TCTGTGTTTTTCCCAGCTTTATTTGCCACTGAAAAAATGTTCAGAATGCTTACTAATATC
 S  V  F  F  P  A  L  F  A  T  E  K  M  F  R  M  L  T  N  I
TGGACAGTGATCAATCATTTTAGTGTCTGGTTAGCTACAGGCCTCGGTACTTTTTATTTT
 W  T  V  I  N  H  F  S  V  W  L  A  T  G  L  G  T  F  Y  F
CTCAAGATAGCCAATTTTTCTAACTCTATTTTTCTCTACCTAAAGTGGAGGGTTAAAAAG
 L  K  I  A  N  F  S  N  S  I  F  L  Y  L  K  W  R  V  K  K
GTGGTTTTGGTGCTGCTTCTTGTGACTTCGGTCTTCTTGTTTTTAAATATTGCACTGATA
 V  V  L  V  L  L  L  V  T  S  V  F  L  F  L  N  I  A  L  I
AACATCCATATAAATGCCAGTATCAATGGATACAGAAGAAACAAGACTTGCAGTTCTGAT
 N  I  H  I  N  A  S  I  N  G  Y  R  R  N  K  T  C  S  S  D
TCAAGTAACTTTACACGATTTTCCAGTCTTATTGTATTAACCAGCACTGTGTTCATTTTC
 S  S  N  F  T  R  F  S  S  L  I  V  L  T  S  T  V  F  I  F
ATACCCTTTACTTTGTCCCTGGCAATGTTTCTTCTCCTCATCTTCTCCATGTGGAAACAT
 I  P  F  T  L  S  L  A  M  F  L  L  L  I  F  S  M  W  K  H
CGCAAGAAGATGCAGCACACTGTCAAAATATCCGGAGACGCCAGCACCAAAGCCCACAGA
 R  K  K  M  Q  H  T  V  K  I  S  G  D  A  S  T  K  A  H  R
GGAGTTAAAAGTGTGATCACTTTCTTCCTACTCTATGCCATTTTCTCTCTGTCTTTTTTC
 G  V  K  S  V  I  T  F  F  L  L  Y  A  I  F  S  L  S  F  F
ATATCAGTTTGGACCTCTGAAAGGTTGGAGGAAAATCTAATTATTCTTTCCCAGGTGATG
 I  S  V  W  T  S  E  R  L  E  E  N  L  I  I  L  S  Q  V  M
GGAATGGCTTATCCTTCATGTCACTCATGTGTTCTGATTCTTGGAAACAAGAAGCTGAGA
 G  M  A  Y  P  S  C  H  S  C  V  L  I  L  G  N  K  K  L  R
CAGGCCTCTCTGTCAGTGCTACTGTGGCTGAGGTACATGTTCAAAGATGGGGAGCCCTCA
 Q  A  S  L  S  V  L  L  W  L  R  Y  M  F  K  D  G  E  P  S
GGTCACAAAGAATTTAGAGAATCATCTTGAGCGGCCGC
 G  H  K  E  F  R  E  S  S  -  A  A
```

Figure 3.2.1 Nucleotide and amino acid sequence of codon-optimized TAS2R14. Kpn1 and Not1 restriction sites were included at the 5' and 3' ends of the gene (green). Kozak sequence (blue) was introduced before the start codon (blue) followed by the FLAG sequence (red).

3.2.3 Plasmid DNA transformation of competent *E. coli* cells

Wild-type (WT) TAS2R or mutant TAS2R genes cloned into a mammalian expression vector pcDNA3.1 were transformed into competent DH5α cells using the heat shock method. 2 µl of plasmid DNAs was added to 50 µl of DH5α cells in an microcentrifuge tube and allowed to incubate on ice for 30 min on ice. Then, the microcentrifuge tube with plasmid DNA and DH5α cells was placed at 42°C for 45 sec followed by immediate transfer onto ice for 2 min. Next, 0.5 ml of LB media was added to DH5α cells and incubated at 37°C with gentle shaking. Then, 0.1 ml of bacterial suspension was transferred onto LB-Amp plates and spread evenly followed by overnight incubation of plates at 37°C.

3.2.4 Plasmid DNA purification and restriction digestion

The ampicillin-resistant bacterial colonies were picked up using a sterile tip and added to 5 ml of LB media supplemented with 100 µg/ml ampicillin and grown overnight at 37°C for 16 hr under constant shaking. The bacterial cultures were subjected to either plasmid DNA purification or frozen as glycerol stocks for further use. The plasmid DNA was isolated from the DH5α cells using the QIAprep plasmid extraction kit as per the manufacturer's instructions. The $A_{260/280}$ ratio value in the range of 1.7-2.0 as measured by Nanodrop spectrophotometer confirmed the purity of the isolated plasmid DNA. The gene of interest cloned into the multiple cloning sites (Kpn1 and Not1 restriction sites) of pcDNA3.1 was confirmed by cleaving the plasmid DNA using restriction digestion enzymes Kpn1 and Not1 followed by separating cleaved plasmid fragments using agarose electrophoresis on a 1% agarose gel. Additionally, the quality of the isolated plasmid DNAs was confirmed by automated DNA sequencing (MICB, DNA Sequencing Facility, Winnipeg).

3.2.5 Mammalian cell culture

For all experiments, HASM cells of passages 2-4 were used and maintained in DMEM media. NuLi-1 cells were cultured in BEGM media with supplements in collagen coated cell culture dishes. HEK293T and MDA-MB-231 cells were maintained in DMEM/F12 growth media. MCF 10A cells were cultured in MCF 10A media. All cells were maintained at 37°C in a humidified atmosphere with 5% CO_2.

CHAPTER 4

4.0 Chemosensory Bitter Taste Receptors T2R4 and T2R14 Activation Attenuates Proliferation and Migration of Breast Cancer Cells

Nisha Singh, **Feroz Ahmed Shaik**, Yvonne Myal, Prashen Chelikani

4.1 ABSTRACT

The emerging significance of the bitter taste receptors (T2Rs) role in the extraoral tissues alludes to their potential role in many pathophysiological conditions. The dysregulation of T2R expression and function in disease has now been demonstrated in airways diseases, neurological disorders and in some cancers. However, the role of T2Rs in the pathophysiology of breast cancer is unexplored thus far. Previously we demonstrated differential expression of the 25 T2Rs in breast cancer (BC) cells. Based on our previous findings we selected two T2Rs, T2R4 and T2R14 for this work. The objective of the current study is to investigate the expression of T2R4 and T2R14 in BC clinical samples and to examine their physiological role using highly metastatic BC and non-cancerous cell lines. Using approaches, which involve receptor knockdown, pharmacological activation and biochemical assays we report that; i) T2R4 and T2R14 expression patterns are dissimilar, with decreased levels of T2R4 and increased levels of T2R14 in BC clinical samples compared to non-cancerous controls. ii) Activation of T2Rs with their respective agonist elicited physiological responses in metastatic breast cancer cells, and no responses were seen in non-tumorigenic breast epithelial cells. iii) Agonist activation of T2Rs (irrespective of T2R subtype) induced anti-proliferative, pro-apoptotic and anti-migratory responses in highly metastatic breast cancer cells. Taken together, our findings demonstrate that the chemosensory T2R signaling network is involved in evoking physiological responses in the metastatic breast cancer cell line.

4.2 INTRODUCTION

Breast cancer is a leading cause for cancer-related mortality in women and better diagnostic and treatment options are needed to improve the survival rate and prognosis with a good outcome. Experimental and clinical data reveal that G protein-coupled receptors (GPCRs) have a crucial role in cancer progression and cancer metastasis (Dorsam and Gutkind, 2007). Thus, GPCRs and their ligands are important therapeutic targets in the treatment of cancer (Liu et al., 2016c;Nieto Gutierrez and McDonald, 2018). GPCRs control many aspects of tumorigenesis, proliferation, migration and cancer cell invasion as well as several cancer related signaling pathways (Dorsam and Gutkind, 2007).

A myriad of environmental and chemical stimuli activate the widely expressed repertoire of GPCRs, including bitter and sweet taste modalities recognized by a sub-class of GPCRs referred to as bitter taste receptors (T2R) and sweet taste receptors (T1R) respectively (Adler et al., 2000;Chandrashekar et al., 2000;Munk et al., 2016). The function of the 25 T2Rs was initially purported to only detect the taste of the ingested food and thereby perform a defensive role against ingesting toxic bitter tasting xenobiotics. However, in recent years, T2R expression has been uncovered in several extraoral regions of the human body (Shaik et al., 2016;Lu et al., 2017). Furthermore, their activation was shown to result in physiological responses, which were comparable to the ones elicited by well-characterized GPCRs. In light of their propensity to induce divergent physiological responses, T2Rs are considered potential therapeutic targets in several pathological conditions; especially T2Rs role in airway pathophysiology has been an area of active investigation (Deshpande et al., 2010;Lee et al., 2012;Robinett et al., 2014;Sharma et al., 2017). Moreover, some characteristic features of T2Rs including their abundant expression and broadly-tuned nature (i.e., receptor could be activated by various structurally diverse

ligands) further provides a strong rationale to consider them as targets for therapeutic intervention in pathological states.

In addition to their newly emerging role in airway physiology, T2Rs are also implicated in the pathophysiology of various cancers and in metabolic and developmental disorders (Jeon et al., 2008;Ansoleaga et al., 2015;Clark et al., 2015;Shaik et al., 2016;Kim et al., 2018b). In pancreatic cancer cells, functional expression and activation of T2R38 by bacterial metabolites (AHL-12) were shown and thereby proposed T2R38 as a potential link between microbiota and cancer (Gaida et al., 2016a). Furthermore, it was suggested that T2R10 played a role in improving the chemosensitivity in pancreatic cell lines (Stern et al., 2018). In human neuroblastoma cells, T2R8 and T2R10 induced anti-invasive and anti-cancer stemness (Seo et al., 2017). Recently, TAS2R14 expression pattern was shown to greatly vary in prostate and ovarian cancer patient samples, while their involvement in inducing apoptosis was demonstrated (Martin et al., 2018). We have previously reported the differential expression of T2Rs in breast cancer and non-tumorigenic mammary epithelial cell lines (Singh et al., 2014). Comparative genomic expression analysis of all 25 human TAS2Rs in highly metastatic triple negative breast cancer (TNBC) epithelial cell line (MDA-MB-231), a luminal-like breast estrogen positive epithelial cell line (MCF7), and a non-tumorigenic breast epithelial cell line (MCF 10A) has shown expression pattern disparity not only amongst the three cell lines but also between the TAS2Rs themselves (Jaggupilli et al., 2017). For example, while TAS2R4 gene expression was lower in cancerous cell lines compared to normal cell line, TAS2R14 was higher (Singh et al., 2014;Jaggupilli et al., 2017). Thus, in the present work, we focused on the above two well characterized T2Rs (T2R4 and T2R14) and studied their potential role in breast cancer cell pathophysiology.

We hypothesize that in breast cancer cells, activation of the chemosensory receptors T2R4 and T2R14, regulates the cell biological properties including proliferation and chemotaxis. We first confirmed the expression of T2R4 and T2R14 in human breast tissues. Next, we used two established breast cell line models, TNBC cell line MDA-MB-231 and immortalized breast epithelial cell line MCF 10A, in our studies. Using a combination of approaches, which includes gene knockdown, pharmacological, biochemical and physiological assays, we examined the bitter agonist-induced effects of T2R4 and T2R14 on breast cancer cell apoptosis, proliferation, and migration.

4.3 MATERIALS AND METHODS

4.3.1 Materials

Chemicals were obtained from the following sources: Quinine, Nα,Nα-bis(carboxymethyl)-L-lysine (BCML), Dimethyl sulphoxide, Fetal bovine serum, Horse serum, L-glutamine, Hydrocortisone, Insulin, Human epidermal growth factor, Thiazolyl Blue Tetrazolium Bromide, Puromycin were acquired from Sigma-Aldrich Canada. Apigenin (API) was purchased from Cayman Chemical. Cell culture media, supplements, Fluo-4 NW calcium assay kit, were purchased from Invitrogen and Cedarlane. Cyquant NF cell proliferation assay kit (Cat. # C35007,) western blot Stripping buffer, SuperScript III Reverse transcriptase (Cat. #18080093), SYBR® Green PCR master mix (Cat. #4309155) were obtained from ThermoFisher Scientific. The synthetic oligonucleotide primer sequences for human TAS2R4, TAS2R14 and GAPDH were purchased from Invitrogen. The HUGO gene nomenclature of TAS2R is used wherever the gene is mentioned. RNeasy Mini Kit (Cat. #74104) was acquired from Qiagen. N-Dodecyl-β-D-maltopyranoside was acquired from Anatrace. Propidium Iodide (Cat. #421301) and Alexa Fluor® 647 Annexin V (Cat. #640912) were obtained from Biolegend.

Antibodies were obtained from the following sources: T2R14 antibody (#C120957, LSBio), T2R4 antibody (Cat #OSR00153W, ThermoFisher Scientific), ß-actin antibody (# A5441, Sigma-Aldrich), Anti-rabbit secondary antibody (Cat. #170-6515, Bio-Rad), Anti-mouse secondary antibody Cat. #31430, Thermofisher Scientific). CIM-plate 16 (# 5665817001) was obtained from ACEA Biosciences. Human MMP-9 Quantikine ELISA kit (Cat. # DMP900) was from R&D Systems.

4.3.2 Cell culture and shRNA mediated knockdown

MCF 10A, MDA-MB-231 cell lines were cultured as per our earlier published work (Singh et al., 2014). Short hairpin (sh) RNA constructs for TAS2R4 (50832), TAS2R14 (50840) and non-targeting shRNA control (RHS6848) were purchased from Dharmacon. The details of the lentiviral shRNA constructs (cloned into pLKO.1 vector) are as follows: TAS2R4 shRNA (ID: TRCN0000014068; 5'-GCTATGAAGCTGATGGTCTAT-3'), TAS2R14 shRNA (ID: TRCN0000014039; 5'-CCAGCTTTATTTGCCACTGAA-3'), Scrambled shRNA (ID: RHS6848). The packaging of lentiviral vectors and subsequent production of the lentivirus particles was performed at the Lentiviral core facility (University of Manitoba). The lentiviral transduction of MDA-MB-231 and MCF 10A cells was done to silence the gene expression of TAS2R4 and TAS2R14. Corresponding scrambled shRNA infected cells were used as controls throughout the study. Post transduction, the cell lines were cultured in their respective media for a few days followed by replacement of growth media with the selection media i.e., media supplemented with puromycin (3 µg/ml). To ensure monoclonality, the clones were picked using trypsin disc methodology and further expansion of the clones was carried out in the selection media. Screening of clones was done using qPCR to select the ideal stable knockdown cell lines. All treatments were carried out at 37°C and in a humidified atmosphere with 5% $C0_2$.

Throughout the study, the scrambled shRNA cells (either MDA-MB-231 or MCF 10A) will be denoted as "control", and the corresponding T2R4 shRNA cells (either MDA-MB-231 or MCF 10A) will be denoted as "shT2R4" and T2R14 shRNA cells will be denoted as "shT2R14".

4.3.3 Normal (non-cancerous) and breast tumor samples

The anonymized normal (non-cancerous) and breast cancer patient tissue samples were acquired from Manitoba Breast Tumor Bank (MBTB, University of Manitoba) which operates with the approval from the Research Ethics Board at the Bannatyne campus, Faculty of Health Sciences, University of Manitoba. The protocols pertaining to the collection, handling and histopathological assessment of tumor tissue has been previously described (Skliris et al., 2008;Blanchard et al., 2009). The clinical samples used to characterize the TAS2R4 and TAS2R14 gene expression levels were derived from tumor tissue of patients diagnosed with invasive ductal carcinoma (n=7) or from mammary tissue from non-cancerous individuals (n=7). The tumor tissue specimens used ranged from well differentiated to poorly differentiated tumor grades. The tissue samples used for the T2R4 and T2R14 protein expression analyses were from non-cancerous (n=2) or patients in stage four (highly metastatic) of breast cancer (n =4).

4.3.4 RNA Preparation and qPCR

Total RNA isolation from the cell lines and tissues samples was performed using RNeasy mini kit according to the manufacturer's instructions. The purity and quantity of the RNA was determined using Nanodrop 2000 spectrophotometer. cDNA synthesis from the purified RNA was performed using 1 µg of RNA, SuperScript III Reverse transcriptase, oligo dT's and first strand buffer. Synthesized cDNA was used as a template to amplify the gene of interest using sequence specific primers. The details of the primers used are as follows, TAS2R4: For- 5'

TCCTGCTGAAGCGGAATATC 3' Rev- 5' GAAAAGGTGATGCCTGGCTA 3'; TAS2R14: For- 5' AAATATCCGGAGACGCCAGC 3' Rev- 5' CCTCCAACCTTTCAGAGGTCC 3'; GAPDH: For- 5' CAATGACCCCTTCATTGACC 3' Rev-5' ACCCAGAAGACTGTGGATGG 3'. The final reaction volume was 30 µl which constituted of cDNA, primers and SYBR Green PCR master mix. The PCR cycling parameters used were as follows, a pre-amplification cycle (Initial denaturation at 95°C for 60 s) followed by 50 cycles of amplification (denaturation at 94°C for 30 s, annealing 60°C for 30 s, extension at 72°C for 30 s and final extension at 72°C for 120 s). GAPDH was used as a reference gene. A control group devoid of cDNA was used to ensure that there was no genomic contamination. The target gene expressed was normalized to that of the reference gene and the fold change in gene expression of the experimental group relative to control group was calculated using $2^{-\Delta\Delta Ct}$ method (Livak and Schmittgen, 2001). Analysis was performed using Eco Real-Time PCR detection system (Montreal Biotech) and the EcoStudy software was used for data analysis.

4.3.5 Western blot analysis

Sample preparation from breast tumor tissue and normal breast tissue for western blot analysis was performed as previously described (Skliris et al., 2008;Blanchard et al., 2009). Cell lysates were prepared from control and shT2R specific cells. Next, protein estimation was done in the samples using Bio-rad DC protein estimation kit. All samples (20 µg each) were run on a 12% SDS-polyacrylamide gel electrophoresis and the separated polypeptides were transferred on to a nitrocellulose membrane. Next, the membrane was blocked with 5% skimmed milk for 1 hour at room temperature and incubated with the respective primary antibodies overnight at 4°C. Chemiluminescence based detection of antigen-antibody complex was done using HRP conjugated secondary antibodies and ECL substrate and imaged using Vilber Lourmat Fusion

FX7 imager. The blot exposure time for chemiluminescence detection was 30 sec for T2R4 and T2R14, and 5 sec for loading control (ß-actin). Pixel density analysis of the bands was performed using ImageJ software (NIH). The target protein specificity for the Anti-T2R4 and Anti-T2R14 antibodies used in this study was confirmed by performing western blot analysis of cell lysates from cells expressing the respective target proteins at different densities. Stable cell lines of HEK293T cells overexpressing either T2R4 or T2R14 were used as overexpression system and HEK293T cells (base cells used to generate stable cell lines) was used as controls. The generation and characterization of HEK293T-T2R4 and HEK293T-T2R14 stable cells was as previously described (Chakraborty et al., 2015).

4.3.6 Intracellular calcium mobilization assay

Measurement of intracellular Ca^{2+} mobilized post stimulation with agonist was used to characterize the functionality of the receptors of interest and the experiments were performed as previously described (Jaggupilli et al., 2018a). In brief, for the experimental groups which involved characterization of T2R4 receptor (i.e. shT2R4 and control cell lines) we used quinine (QUI), and apigenin (API) for pharmacological characterization of T2R14 (Roland et al., 2013;Pydi et al., 2014c;Hariri et al., 2017). MDA-MB-231 and MCF10A cell lines (both control and shRNA variants) were seeded at a density of $1x10^5$ cells per well of a black-walled 96 well plates and cultured 12-16 h in growth media. Then, the cells were loaded with calcium sensitive Fluo-4 NW dye and incubated for 30 min at 37°C followed by an additional 30 min incubation at RT. Agonist induced changes in intracellular levels are detected by measuring the changes in fluorescence intensity (Excitation at 494nm, Emission at 525nm) using a Flex station-3 microplate reader (Molecular Devices).

4.3.7 Cell proliferation assay

Bitter agonist induced effect on proliferation of MDA-MB-231 and MCF 10A cells were determined using CyQUANT NF cell proliferation assay kit as per manufacturer's instructions (Jones et al., 2001). Briefly, cells were seeded in black walled 96 well plates at a density of $5x10^3$ cells per well and then serum starved overnight, followed by agonist treatment for 48 h. The agonist (QUI and API) were dissolved in cell line specific growth media and added to the respective cells. To delineate the receptor specificity of the agonist induced effects, cell proliferative changes of control cell lines was compared with that of the corresponding T2R4 or T2R14 knockdown cell lines.

4.3.8 Real-time cell migration assay

Cell migration rate was monitored in real-time using the xCELLigence RTCA-DP instrument (ACEA Biosciences) as described (Ungefroren et al., 2011;Limame et al., 2012). The CIM-16 assay plate consisted of detachable upper and lower panels. The chemoattractant solutions (with or without T2R agonist) were added to the lower wells and the cells to the upper wells. Serum (5%) containing basal growth media was included as a chemoattractant. API or QUI containing chemoattractant solution driven chemotaxis relative to their buffer (i.e. buffer containing chemoattractant solution) was calculated. Cells were serum starved approximately 18-24 h prior to conducting the experiments. Cells (MDA-MB-231 and MCF 10A control, shT2R4 and shT2R14) were seeded in the upper chamber at a concentration of $4x10^4$ cells/well in serum-free media. Fresh DMEM media with or without QUI (125 µM) and API (50µM), was added to each well of the lower chamber, and 5% serum was used as chemoattractant. The CIM-plates were left undisturbed in an incubator for 1 h to allow the cells to attach. The impedance value of each well was monitored automatically by the xCELLigence system for the duration of 48 h and expressed as a cell index (CI) value for measuring the cell migration (Limame et al., 2012).

4.3.9 Matrix metalloproteinase 9 (MMP-9) activity assay

Cell supernatant concentration of MMP-9 was determined using a Human MMP-9 Elisa kit as per the manufacturer's instructions (Straat et al., 2009). Briefly, MDA-MB-231 and MCF 10A (shT2R14 and control; shT2R4 and control) were seeded in 12-well plates at a density of $1x10^5$ cells/well and allowed to grow overnight. Cells were then subjected to overnight serum starvation followed by treatment with their respective agonists QUI (T2R4 group) and API (T2R14 group) for 24 h. The supernatants were collected and the MMP-9 levels in the agonist treated vs. untreated groups were compared. Similarly, cell supernatants from API treated and untreated MDA-MB-231 cells (control and shT2R14) were collected and the MMP-activity was quantified using the human MMP-9 Elisa kit as per the manufacturer's instructions. API treatments were done for 24 h at 37°C and 5% CO_2.

4.3.10 Apoptosis Assay

Apoptosis was induced in the cell lines using bitter taste receptor agonists QUI and API. The Annexin V and PI labelling procedure was followed as described in (Lakshmanan and Batra, 2013). MCF 10A and MDA-MB-231 (scrambled control, shT2R4, shT2R14) cell lines were cultured in their respective growth media and serum starved overnight prior to 24 h bitter agonist treatment. The scrambled control and shT2R4 cell lines of both MDA-MB-231 and MCF 10A were treated with QUI and buffer and API was used for shT2R14 and scrambled control cell lines. The rate of apoptosis induced was assessed using Alexa Fluor® 647 Annexin V apoptosis detection kit as per the manufacturer's instructions. Cell sorting into apoptotic, necrotic and live cells was performed using Flow cytometry (BD FACS Canto-II analyzer).

4.3.11 Statistical analysis

Data shown is the mean ± SEM and unless specified results are from at least three independent experiments. Student's t-test and one-way ANOVA analysis coupled with Tukey's post hoc multiple comparison test were performed to determine statistical significance in experiments which involved two and more than two groups respectively. A p value of less than 0.05 was considered statistically significant. Statistical analysis was performed using Graph Pad Prism 6.0 (San Diego, CA).

4.4 RESULTS

4.4.1 T2Rs are differentially expressed in MDA-MB-231 and MCF 10A cells

We have previously reported the differential expression of T2Rs in breast cancer and non-tumorigenic mammary epithelial cell lines **(Figure 4.4.1)** (Singh et al., 2014). Comparative genomic expression analysis of all 25 human TAS2Rs in highly metastatic triple negative breast cancer (TNBC) epithelial cell line (MDA-MB-231), a luminal-like breast estrogen positive epithelial cell line (MCF7), and a non-tumorigenic breast epithelial cell line (MCF 10A) has shown expression pattern disparity not only amongst the three cell lines but also between the TAS2Rs themselves **(Figure 4.4.2)** (Jaggupilli et al., 2017). For example, while TAS2R4 gene expression was lower in cancerous cell lines compared to normal cell line whereas TAS2R14 was higher **(Figures 4.4.1 and 4.4.2)** (Singh et al., 2014;Jaggupilli et al., 2017). Thus, in the present work, the focus was on the above two well characterized T2Rs (T2R4 and T2R14) and to analyze their potential role in breast cancer cell pathophysiology.

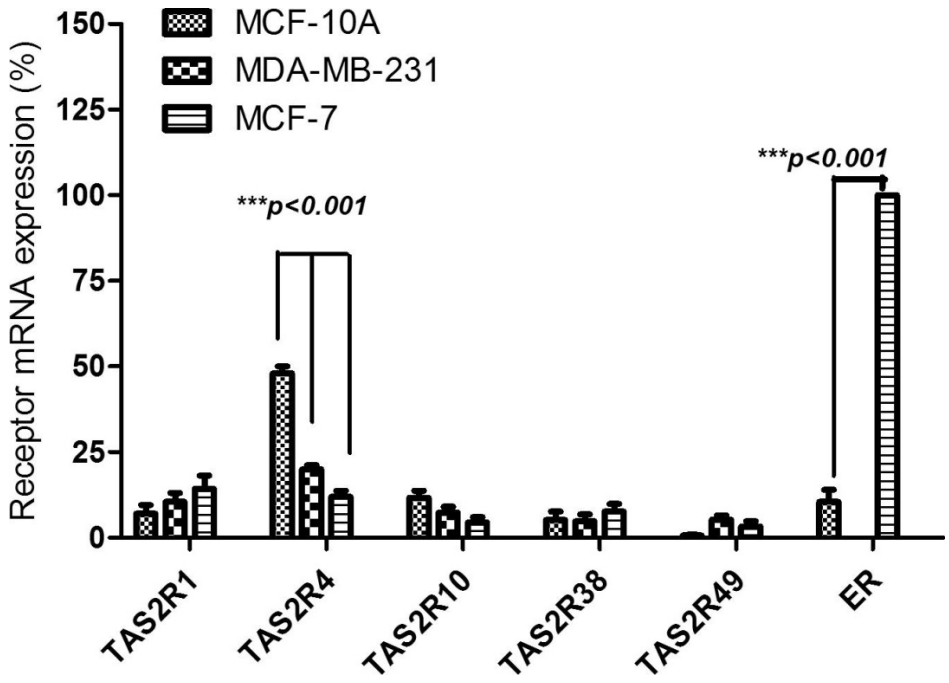

Figure 4.4.1 Quantitative (q) PCR expression analysis of TAS2R1, TAS2R4, TAS2R10, TAS2R38 and TAS2R49 transcripts in non-cancerous breast epithelial cell line MCF 10A, and breast cancer cell lines MDA-MB-231 and MCF7. Relative expression is normalized to that of estrogen receptor (ER) in MCF 7, which is considered as 100%. The MDA-MB-231 cell line is ER negative. Data presented are from 2 to 4 independent experiments done in triplicate. GAPDH was used as an internal control. Values are plotted as mean ± SEM. Relative expressions were computed using 2 DCT methods. Melt-curve analysis confirmed the presence of a single PCR product in each reaction. Statistically significant values are shown by asterisk. **(Image used with permission from Biochem Biophys Res Commun, 2014. 446(2): p. 499-503, License number-4566030987453 © by Elsevier).**

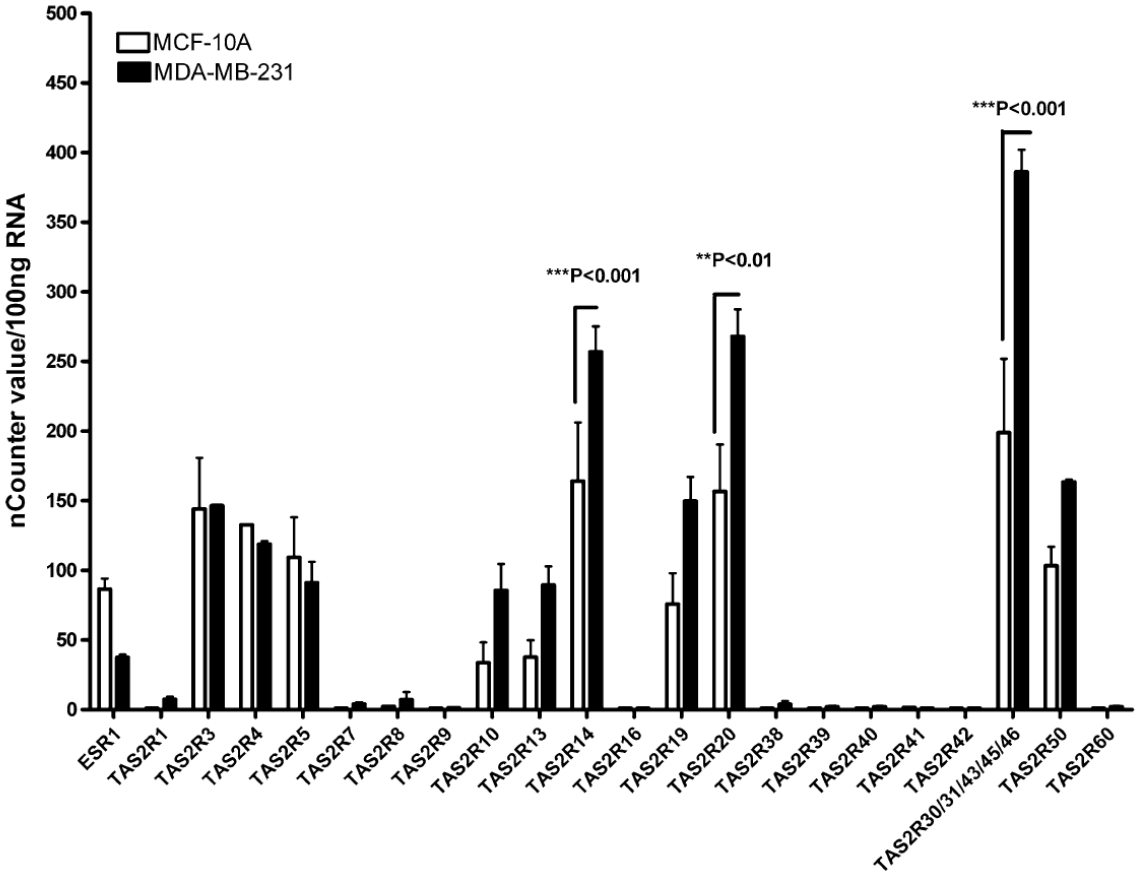

Figure 4.4.2 The mRNA expression levels of TAS2R genes in normal breast epithelial cells MCF10A and in highly invasive breast cancer cells MDA-MB-231. The MDA-MB-231 cell line is estrogen receptor (ESR1) negative, and ESR1 was used as a control gene. nCounter values were represented on the Y axis and the genes analyzed were on the X axis. The expression of TAS2R14 and 20 showed a significant difference between MCF 10A and MDA-MB-231. Data presented are from two independent experiments and the values are plotted as mean ± SEM. The results were analyzed using two-way ANOVA. Statistically significant values are shown by asterisk. **(Image used with permission from Mol Cell Biochem, 2017. 426(1-2): p. 137-14, License number-4561460516967 © by Springer Nature).**

The hypothesis was that in breast cancer cells, activation of the chemosensory receptors T2R4 and T2R14, regulates the cell biological properties including proliferation and chemotaxis. We first confirmed the expression of T2R4 and T2R14 in human breast tissues. Next, we used two established breast cell line models, TNBC cell line MDA-MB-231 and immortalized breast epithelial cell line MCF 10A, in our studies. Using a combination of approaches, which includes gene knockdown, pharmacological, biochemical and physiological assays, we examined the bitter agonist-induced effects of T2R4 and T2R14 on breast cancer cell apoptosis, proliferation, and migration.

4.4.2 Characterization of T2R4 and T2R14 expression in normal human breast tissue and breast tumor samples

Gene expression analysis was carried out using breast tissue samples obtained from 7 patients with highly differentiated breast tumor and 7 normal individuals following mammoplasty to characterize the relative mRNA expression of TAS2R4 and TAS2R14. The TAS2R4 gene expression in breast cancer (ER and PR negative) patients was found to be significantly lower compared to normal controls **(Figure 4.4.3A)**. Whereas the expression of TAS2R14 was found to be higher in tumor conditions compared to normal controls **(Figure 4.4.3B).** Additionally, the protein levels of T2R4 and T2R14 in clinical samples were characterized using western blot analysis. As shown in **figure 4.4.3C-D**, two individual tissue samples from mammoplasty (control) and four breast cancer tissue samples were used for western blot analysis. Based on the pixel density of the bands obtained, the pooled T2R4 in the control samples tested was lower compared to tumor samples **(Figure 4.4.3C)**. In contrast, the T2R14 expression was higher ($p<0.05$) in tumor samples compared to normal samples **(Figure 4.4.3D)**. Of note, the clinical samples used for mRNA expression analysis shown in **figures**

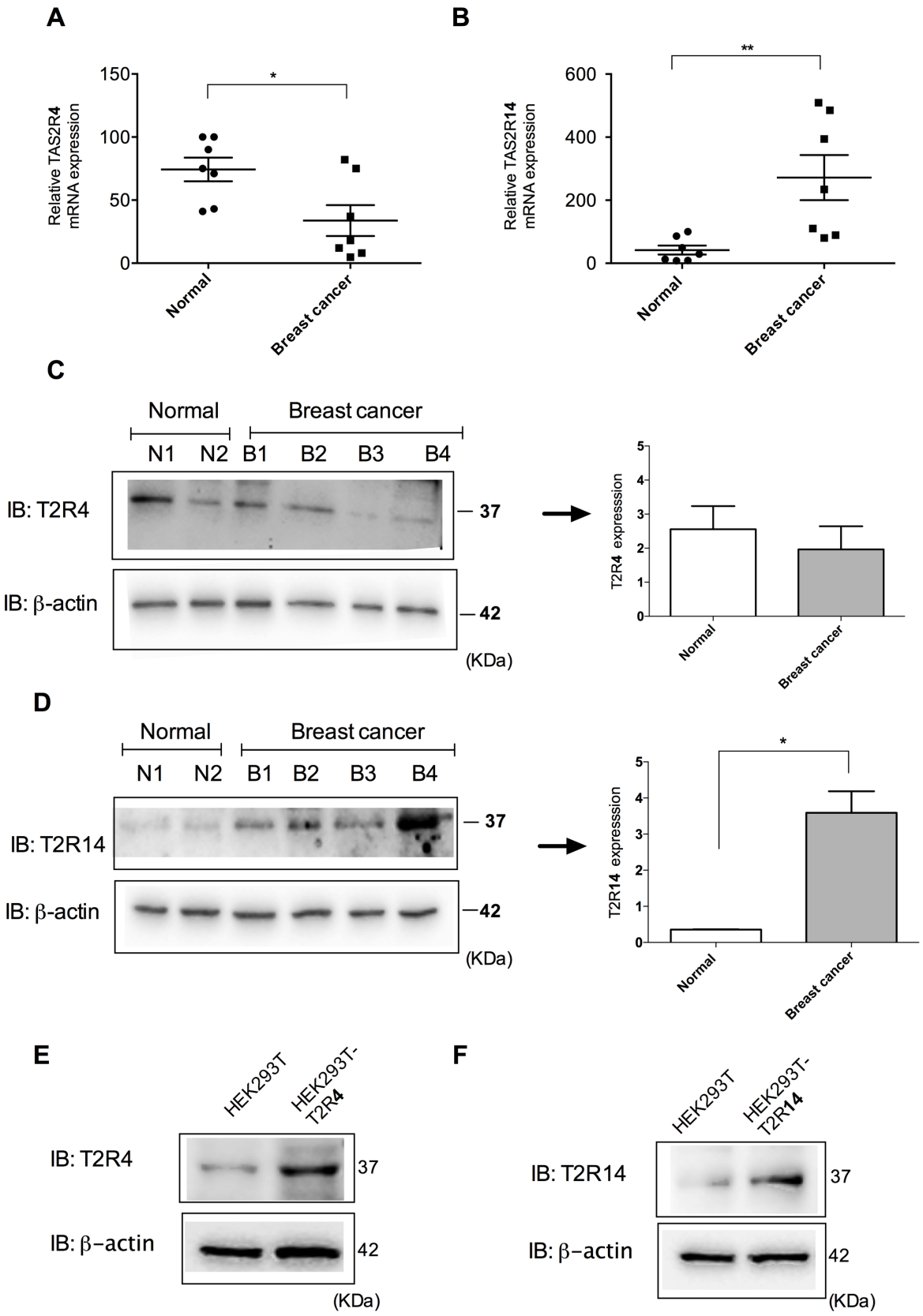
A
Relative TAS2R4 mRNA expression
150
100
50
0
*
Normal
Breast cancer
B
Relative TAS2R14 mRNA expression
600
400
200
0
**
Normal
Breast cancer
C
Normal
Breast cancer
N1 N2 B1 B2 B3 B4
IB: T2R4
37
IB: β-actin
42
(KDa)
T2R4 expresssion
Normal
Breast cancer
D
Normal
Breast cancer
N1 N2 B1 B2 B3 B4
IB: T2R14
37
IB: β-actin
42
(KDa)
T2R14 expresssion
*
Normal
Breast cancer
E
HEK293T
HEK293T-T2R4
IB: T2R4
37
IB: β-actin
42
(KDa)
F
HEK293T
HEK293T-T2R14
IB: T2R14
37
IB: β-actin
42
(KDa)

Figure 4.4.3 T2R4 and T2R14 are differentially expressed in breast tissue samples from breast cancer patients and normal (non-cancerous) individuals. **A, B)**. TAS2R4 and TAS2R14 gene expression in breast tumor specimens from patients diagnosed with invasive ductal carcinoma (n=7) relative to normal individuals (n=7). Data shown is mean ± S.E, and each data point represents an individual. **C, D)** The breast tissue samples used for T2R4 and T2R14 protein expression analysis were from patients in stage IV of breast cancer (n=4) and normal breast tissue (n=2). The pixel density analysis shown is the pooled band density of the clinical samples (B1, B2, B3, and B4) versus the same done for normal samples (N1 and N2). Shown is a representative blot of two independent experiments. The antibody dilutions used are as follows, T2R4 (1:300); T2R14 (1:1000); ß-actin 1:5000; Rabbit IgG secondary (1:5000), Mouse IgG secondary (1: 25,000). **E, F)** Characterization of T2R4 and T2R14 antibody specificity. Total cell lysates isolated from HEK293T, HEK293T-T2R4, HEK293T-T2R14 stable cells were loaded and western blots were run as discussed in methods. * $p<0.05$; ** $p<0.01$.

4.4.3A-B are different from the samples used for western blot analysis shown in **figures 4.4.3C-D**. Due to paucity of clinical samples for protein expression analysis, only two biological replicates could be included for samples from normal individuals. The band density from the western blot analysis of cell lysates isolated T2R4 or T2R14 overexpressing cell systems and control cells confirms the target specificities of the T2R4 and T2R14 antibodies used (**figures 4.4.3E-F)**.

4.4.3 Characterization of T2R4 and T2R14 knockdown in MDA-MB-231 and MCF 10A cell lines

TAS2R4 expression in control (scrambled shRNA) and shT2R4 (TAS2R4 shRNA) of both MDA-MB-231 and MCF 10A was examined using qPCR. Results show a 62 ± 3 % reduction of TAS2R4 expression in MDA-MB-231 cells and 86 ± 3 % reduction in MCF 10A cells **(Figure 4.4.4A, B)** in shT2R4 groups compared to control. To characterize protein levels of T2R4 in control and shT2R4 cell lines, western blot analysis of cell lysates was performed by probing with T2R4 antibody. We detected T2R4 protein bands around 37 KDa and shT2R4 mediated knockdown induced a 47.3 ± 5.1 % reduction in T2R4 expression in MDA-MB-231 and 40.1 ± 4.6 % reduction in MCF 10A cells **(Figure 4.4.4C)**. Furthermore, using Ca^{2+} mobilization assay, we examined the agonist induced activation of T2R4 dependent Ca^{2+} signals in MDA-MB-231 and MCF 10A cells. T2R4 specificity of the agonist induced Ca^{2+} mobilization was demonstrated by using corresponding T2R4 knockdown cell lines. The concentration-response curves were generated for QUI (0-1000 μM) in control and shT2R4 cells and results show that the magnitude of agonist induced intracellular Ca^{2+} release in control cells was higher compared to shT2R4 cells **(Figure 4.4.4D-F)**. The results pertaining to shRNA-mediated T2R14

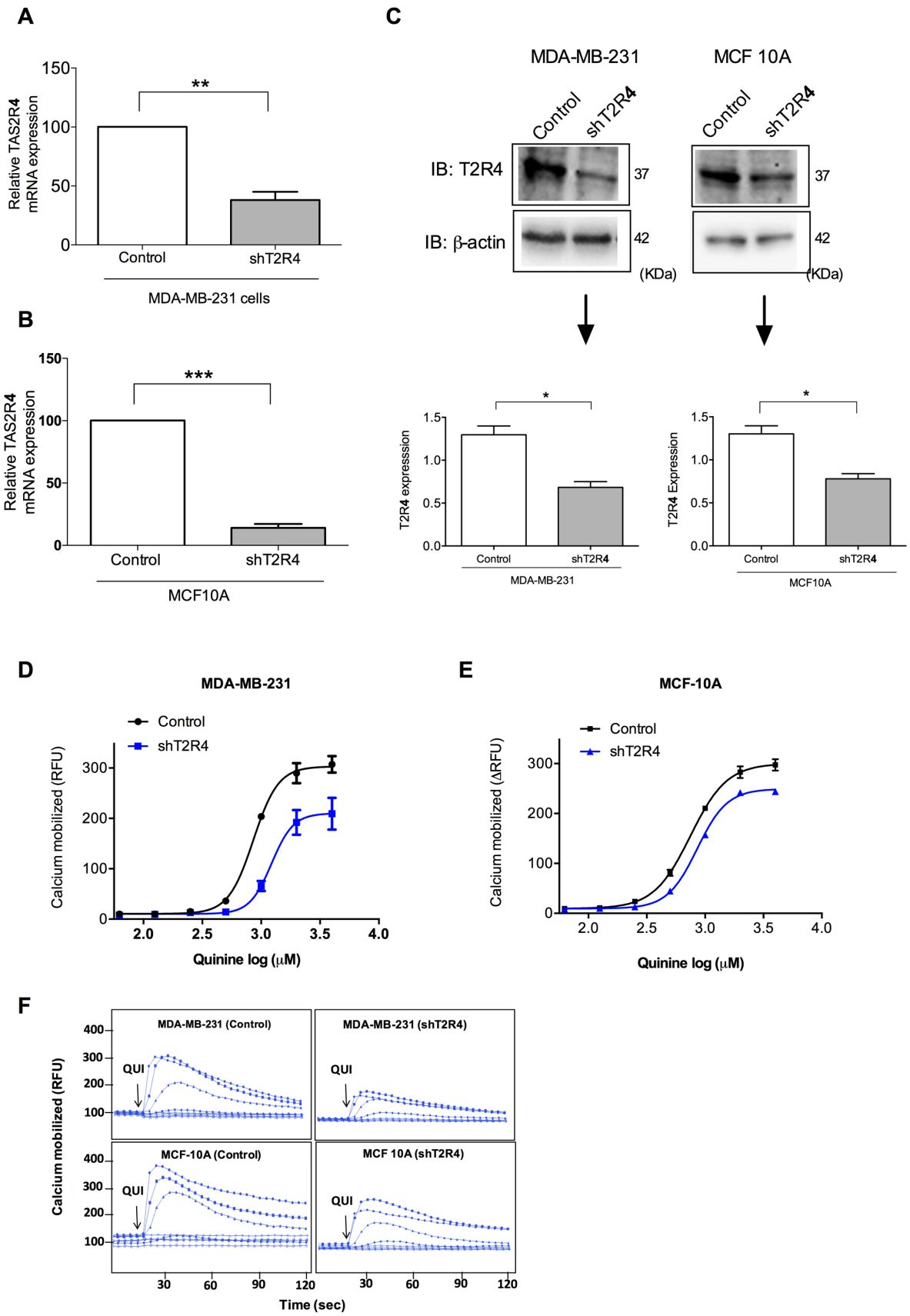
A
Relative TAS2R4 mRNA expression
150
100
50
0
**
Control
shT2R4
MDA-MB-231 cells
B
Relative TAS2R4 mRNA expression
150
100
50
0
***
Control
shT2R4
MCF10A
C
MDA-MB-231
MCF 10A
Control
shT2R4
Control
shT2R4
IB: T2R4
IB: β-actin
37
42
(KDa)
37
42
(KDa)
T2R4 expresssion
1.5
1.0
0.5
0.0
*
Control
shT2R4
MDA-MB-231
T2R4 Expression
1.5
1.0
0.5
0.0
*
Control
shT2R4
MCF10A
D
MDA-MB-231
Control
shT2R4
Calcium mobilized (RFU)
300
200
100
0
2.0
2.5
3.0
3.5
4.0
Quinine log (μM)
E
MCF-10A
Control
shT2R4
Calcium mobilized (ΔRFU)
300
200
100
0
2.0
2.5
3.0
3.5
4.0
Quinine log (μM)
F
MDA-MB-231 (Control)
MDA-MB-231 (shT2R4)
MCF-10A (Control)
MCF 10A (shT2R4)
QUI
Calcium mobilized (RFU)
400
300
200
100
30
60
90
120
Time (sec)

Figure 4.4.4 Characterization of T2R4 knockdown in MDA-MB-231 and MCF 10A cells. **A, B)** The TAS2R4 gene knockdown in MDA-MB-231 and MCF 10A cells (control vs. shT2R4) was confirmed using qPCR. Data are shown in mean ± S.E (n=3-4). **C)** The protein level knockdown of T2R4 was confirmed using western blot analysis. Shown are representative blots from at least three independent experiments (* $p<0.05$). **D, E)** Concentration-dependent intracellular Ca^{2+} mobilization responses for QUI (0-4000 μM; half-log dilutions) in control and T2R4 knockdown cell lines (shT2R4). "Control" denotes the MDA-MB-231 or MCF 10A cells transduced with scrambled shRNA. Data shown is mean ± S.E (n=3). **F**) Representative calcium traces corresponding to concentrations used in panels D and E. QUI was added at the 20 sec time point, which is indicated with an arrow. *$p<0.05$, **$p<0.01$, *** $p<0.001$.

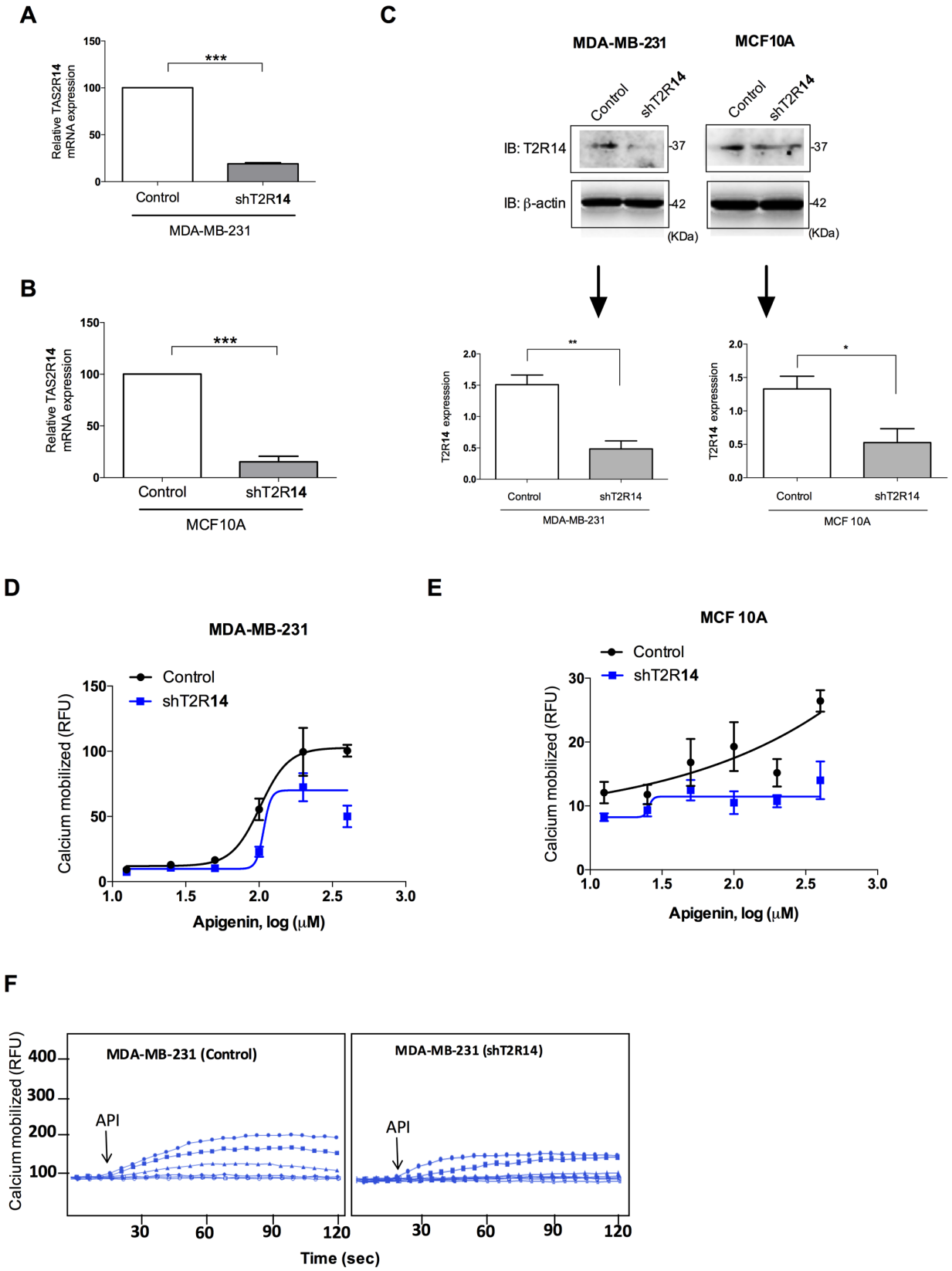
A
Relative TAS2R14 mRNA expression
150
100
50
0
***
Control
shT2R14
MDA-MB-231
B
Relative TAS2R14 mRNA expression
150
100
50
0
***
Control
shT2R14
MCF10A
C
MDA-MB-231
MCF10A
Control
shT2R14
Control
shT2R14
IB: T2R14
IB: β-actin
37
42
(KDa)
37
42
(KDa)
T2R14 expresssion
2.0
1.5
1.0
0.5
0.0
**
Control
shT2R14
MDA-MB-231
T2R14 expresssion
2.0
1.5
1.0
0.5
0.0
*
Control
shT2R14
MCF 10A
D
MDA-MB-231
Control
shT2R14
Calcium mobilized (RFU)
150
100
50
0
1.0
1.5
2.0
2.5
3.0
Apigenin, log (μM)
E
MCF 10A
Control
shT2R14
Calcium mobilized (RFU)
30
20
10
0
1.0
1.5
2.0
2.5
3.0
Apigenin, log (μM)
F
Calcium mobilized (RFU)
400
300
200
100
MDA-MB-231 (Control)
API
MDA-MB-231 (shT2R14)
API
30
60
90
120
30
60
90
120
Time (sec)

Figure 4.4.5 Characterization of T2R14 knockdown in MDA-MB-231 and MCF10A cells. **A, B)** The TAS2R14 gene knockdown in the MDA-MB-231 and MCF10A cells (control vs. shT2R14) was confirmed using qPCR. Data are shown in mean ± S.E (n=3-4). **C)** The protein level knockdown of T2R14 was confirmed using western blot analysis. Shown are representative blots from at least three independent experiments (* $p<0.05$). **D, E)** Concentration-dependent intracellular Ca^{2+} mobilization responses for API (0-400 µM; half-log dilutions) in control and T2R14 knockdown cell lines (shT2R14). "Control" denotes the MDA-MB-231 or MCF 10A cells transduced with scrambled shRNA. Data shown is mean ± S.E (n=3). **F**) Representative calcium traces corresponding to concentrations used in panel D. API was added at the 20 sec time point, which is indicated with an arrow. *$p<0.05$, **$p<0.01$, *** $p<0.001$.

silencing in MDA-MB-231 cells are as follows, mRNA expression analysis showed a 80.9 ± 0.6 % decrease in shT2R14 relative to control. The protein expression analysis showed a 53.8 ± 9.6 % decrease in T2R14 expression compared to control. A concentration-dependent decrease in functional responses to API (0-400 μM) in shT2R14 vs. control was observed. In MCF10A cells, an mRNA decrease of 84.6± 3 %; decrease in T2R14 protein levels of 61 ± 9.2 % and a sigmodal concentration-dependent responses for API were not observed in MCF 10A cells and this may be due to the lower levels of API induced Ca^{2+}mobilized in MCF 10A cells **(Figure 4.4.5 D-F)**.

4.4.4 T2R4 and T2R14 activation attenuates MDA-MB-231 cell proliferation

To evaluate the potential functional role of T2R4 and T2R14 on cell proliferation, we used the cyquant NF cell proliferation assay kit (ThermoFisher Scientific), a fluorescence-based assay, which quantitates the cell number based on the cellular nucleic acid content. MDA-MB-231 and MCF 10A cells were treated with QUI or API to activate T2R4 and T2R14 respectively and their effect on cell proliferation after 48 h was examined. As shown in **figure 4A**, in MDA-MB-231 cells (control group) QUI treatment (0-1000 μM) significantly attenuated the cell proliferation in a concentration dependent manner compared to buffer treated group. In MDA-MB-231 (shT2R4 group) statistically significant differences were observed at only at higher concentrations relative to buffer **(Figure 4.4.6A)**. In MCF 10A cells, QUI treatment did not have any effect on its proliferation, however at higher concentrations a decrease in cell proliferation was observed **(Figure 4.4.6B)**. T2R14 activation with API (0-800 μM) attenuated cell proliferation in control MDA-MB-231 cells in a concentration dependent manner, however in shT2R14 cells, no statistical significant decrease in cell proliferation was observed at low concentrations **(Figure 4.4.6C)**. In contrast, in MCF 10A (both control and shT2R14 cells), T2R14 activation did not have any effect on cell proliferation **(Figure 4.4.6D)**. Agonist activation of T2R4 and T2R14

attenuated the proliferation of metastatic breast cancer cells (MDA-MB-231), whereas non-tumorigenic breast epithelial cells (MCF 10A) did not exhibit these responses.

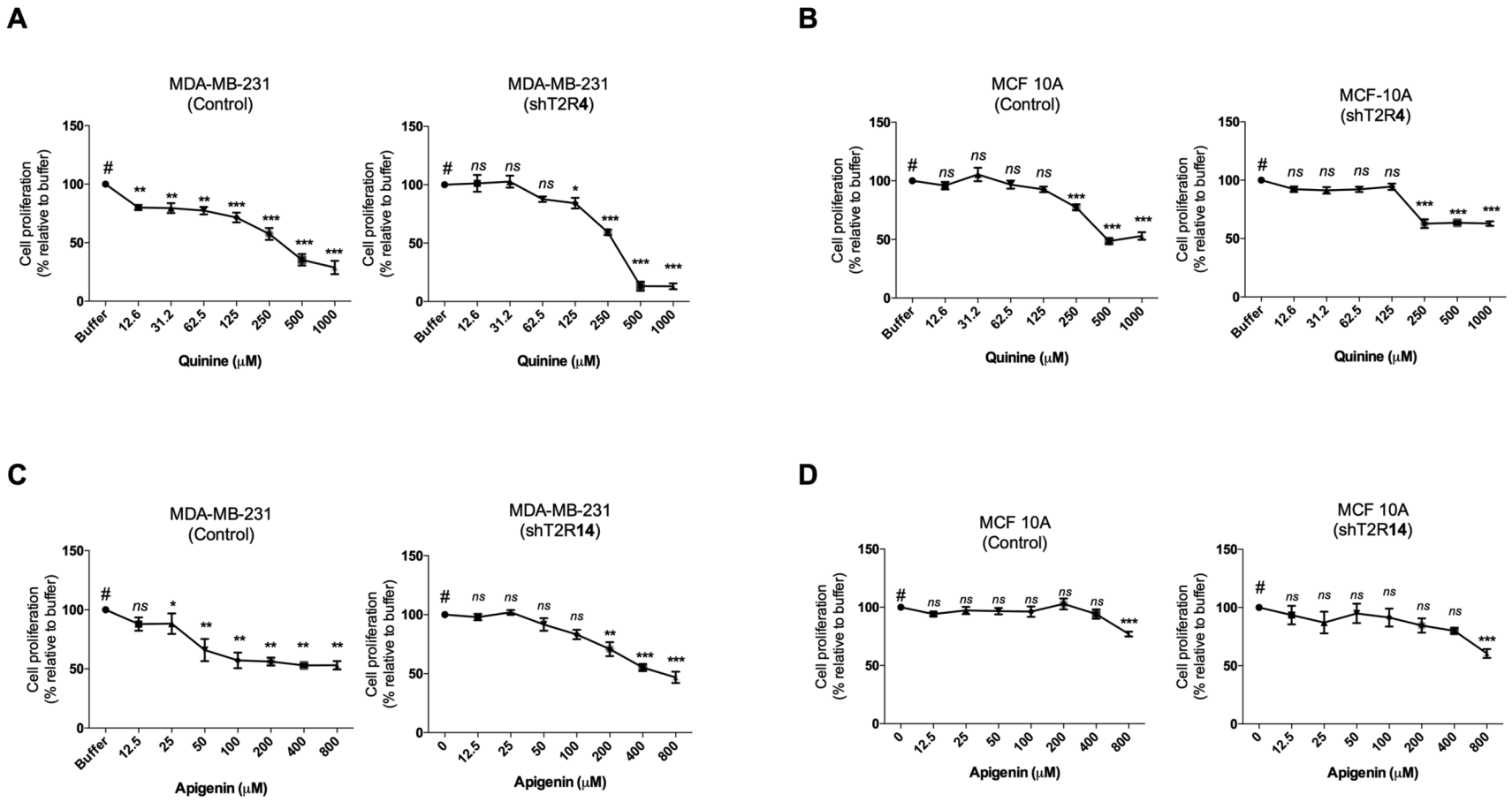

Figure 4.4.6 Cell proliferation following activation of T2R4 and T2R14. **A, B)** QUI (0-1000 μM) induced effect on cell proliferation in MDA-MB-231 and MCF 10A cells (control and T2R4 shRNA) relative to buffer. **C, D)** API (0-800 μM) induced effect on cell proliferation in MDA-MB-231 and MCF 10A cells (control and T2R14 shRNA) relative to buffer. "Control" denotes the cells transduced with scrambled shRNA. Data shown is mean ± S.E.M (n=4-6). # indicates buffer treatment. *p<0.05, **p<0.01, ***p <0.001, ns- non-significant p value vs. buffer.

4.4.5 T2R4 and T2R14 promotes pro-apoptotic responses in MDA-MB-231 cells

To examine the role of T2R4 and T2R14 activation in inducing apoptosis in breast cancer cells, we used the flow cytometry based Annexin V (AV)/ Propidium iodide (PI) double staining approach as described in the methods section. The population of cells undergoing early apoptosis is stained positive for AV and negative for PI (AV+/PI-) and the ones in late apoptotic state are AV+/PI+ and necrotic cells are AV-/PI+. As shown in **figure 4.4.7A and figure 4.4.7B**, QUI treatment in MDA-MB-231 cells resulted in an increase in cells in early apoptotic state compared to buffer treated group. In T2R4 shRNA cells, statistically significant differences in the rate of apoptosis were not detected in intrinsic versus basal groups. **Figure 4.4.7C and 4.4.7D** shows that intrinsic activation of T2R14 with API (50 μM) resulted in an increase of cells in early apoptotic state. The T2R14-specificity of the API induced effects are confirmed by results obtained in shT2R14 cells, in which there was no significant agonist-promoted increase in the rate of apoptosis **(Figure 4.4.7C)**. As a positive control for activating apoptotic pathways, we treated the MDA-MB-231 cells with 100 μM H_20_2 which resulted in an increase in the rate of apoptosis **(Figure 4.4.7E and 4.4.7F)**. Congruent with the cell proliferation data, T2R-mediated apoptotic effects observed seems to have implications in metastatic breast cancer cells. The rationale for using a single concentration of agonist to study T2R-mediated effects on apoptosis (in this section), migration and MMP-9 assays (in the subsequent sections) is on the basis of the results obtained from cell proliferation studies involving different dose of agonists and its effect on viability of cells at 48 h in MDA-MB-231 cells. The regression analysis of the cell viability data resulted in an IC_{50} in the range of 125 μM for QUI and 100 μM for API (data not shown). Moreover, from the literature we found that API at a concentration of 50 μM has been used for proliferation studies in various cancer cell line models.

4.4.6 T2R4 and T2R14 activation inhibits chemotactic migration of MDA-MB-231 cells

We examined whether activation of T2R4 and T2R14 has a role in chemotactic migration of breast cancer cells. For this, we used real-time cell migration analysis of MDA-MB-231 cells in the presence of a chemotactic gradient (5% serum containing media). To delineate the receptor specificity of effects observed, we used stable shT2R4 or shT2R14 (MDA-MB-231) and scrambled (MDA-MB-231) cells as controls. Human epidermal growth factor (hEGF) was used as a positive control chemoattractant for inducing in vitro cell migration. As shown in **figures 4.4.8A and 4.4.8B**, T2R4 activation with QUI attenuated the migration of MDA-MB-231 cells up to 46 ± 9% relative to buffer treatment. No differences were observed in the migration index of QUI and buffer treated MDA-MB-231 (shT2R4) cell line, confirming a role for the native T2R4 in abating migration in a metastatic breast cancer cell line **(Figure 4.4.8A)**. T2R14 activation with API decreased the migration of MDA-MB-231 cells **(Figure 4.4.8C)**, and receptor specificity of the effects observed was confirmed with shT2R14 results **(Figures 4.4.8C and 4.4.8D)**. As expected, hEGF induced pro-migratory responses compared to the respective buffer treated groups **(Figures 4.4.8E and 4.4.8F)**.

4.4.7 T2R4 and T2R14 activation abrogates MMP-9 secretion in MDA-MB-231 cells

To further investigate the components involved in T2R mediated inhibitory effects of cell migration observed, we examined if the expression of tumor migration triggering proteins such as matrix metalloproteinases (MMP) was down-regulated. Upregulation of MMP-9 expression and secretion is associated with breast cancer metastasis and as a cancer prognostic biomarker (Radisky et al., 2017). In our study, T2R4 and T2R14 activation with their agonists, QUI and API respectively, resulted in a decrease in MMP-9 secretion compared to the buffer treated

groups. The inhibitory effects observed, were not detected with corresponding knockdown cell lines **(Figure 4.4.9A-B)**.

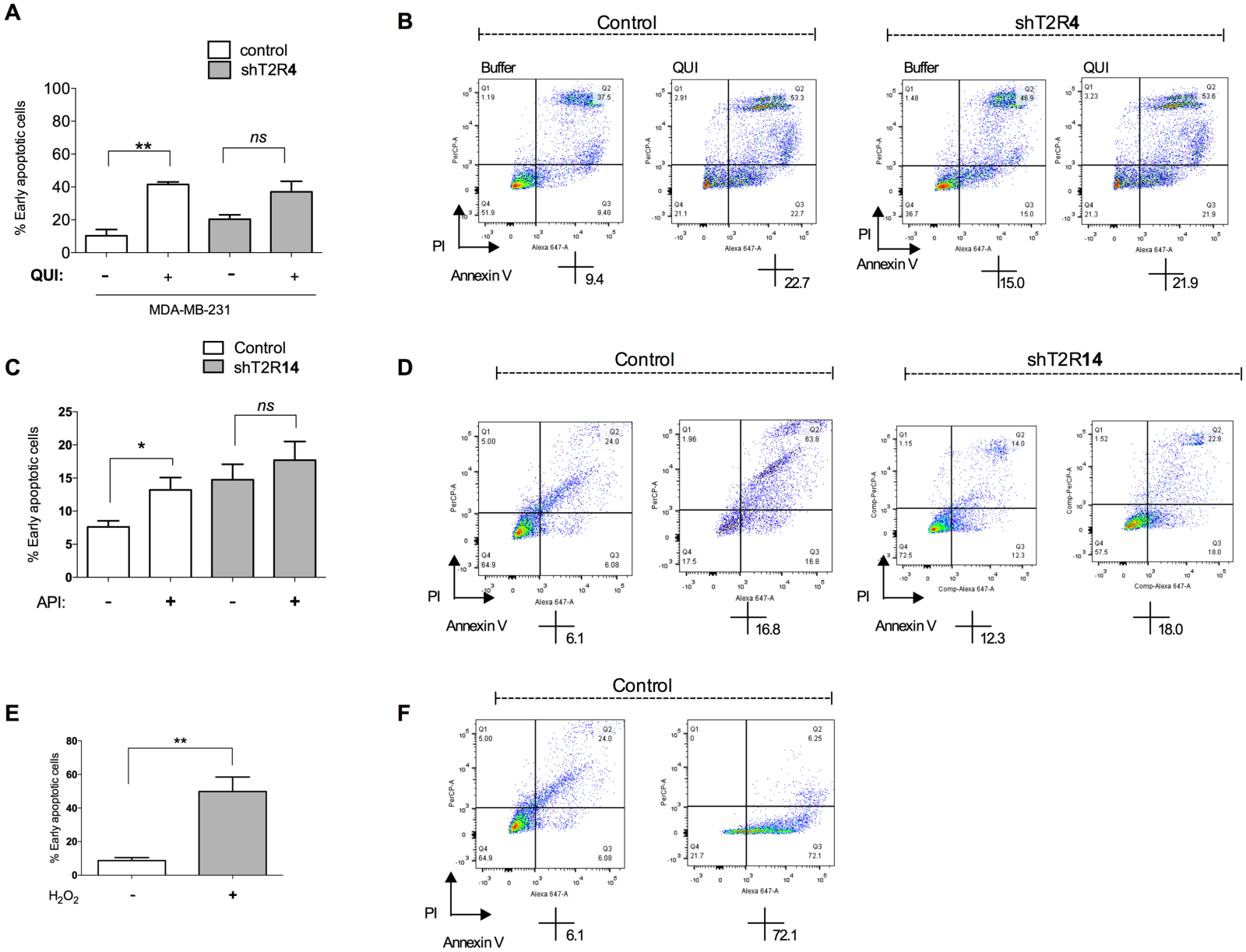
A
control
shT2R4
% Early apoptotic cells
100
80
60
40
20
0
**
ns
QUI:
-
+
-
+
MDA-MB-231
B
Control
shT2R4
Buffer
QUI
Buffer
QUI
PI
Annexin V
9.4
22.7
15.0
21.9
C
Control
shT2R14
% Early apoptotic cells
25
20
15
10
5
0
*
ns
API:
-
+
-
+
D
Control
shT2R14
PI
Annexin V
6.1
16.8
12.3
18.0
E
% Early apoptotic cells
80
60
40
20
0
**
H2O2
-
+
F
Control
PI
Annexin V
6.1
72.1

Figure 4.4.7 T2R4 and T2R14 activation induce apoptosis in MDA-MB-231 cells. Apoptosis induced by QUI (125 μM), API (50 μM) and H_2O_2 (100 μM) treatment was examined using Annexin V and PI labeling procedure. Cell sorting was done using Flow cytometry (BD FACS Canto-II analyzer). Y-axis corresponds to the percentage of cells in early apoptotic phase (AV+ and PI-) out of total intact cells. **A)** Bar plot representation of MDA-MB-231 cells (control and shT2R4) in the early apoptotic phase, post treatment with QUI (+) or buffer (-). **B)** Representative scatter plots of data shown in panel A. The percentage of cells in the early apoptotic phase are shown in the third quadrant below each scatter plot. **C)** Bar plot representation of MDA-MB-231 cells (control and shT2R14) in early apoptotic phase, post treatment with API (+) or buffer (-). **D)** Representative scatter plots of data shown in panel C. The percentage of cells in the early apoptotic phase are shown in the third quadrant below each scatter plot. **E)** Bar plot representation of MDA-MB-231 cells in early apoptotic phase, post treatment with H_2O_2 (+) or buffer (-). **F)** Representative scatter plots of data shown in panel E. The percentage of cells in the early apoptotic phase are shown in the third quadrant below each scatter plot. "Control" denotes the cells transfected with scrambled shRNA. Data shown is from at least n=3 independent experiments performed in duplicate. *p< 0.05, **p<0.01, ns, non-significant vs. buffer.

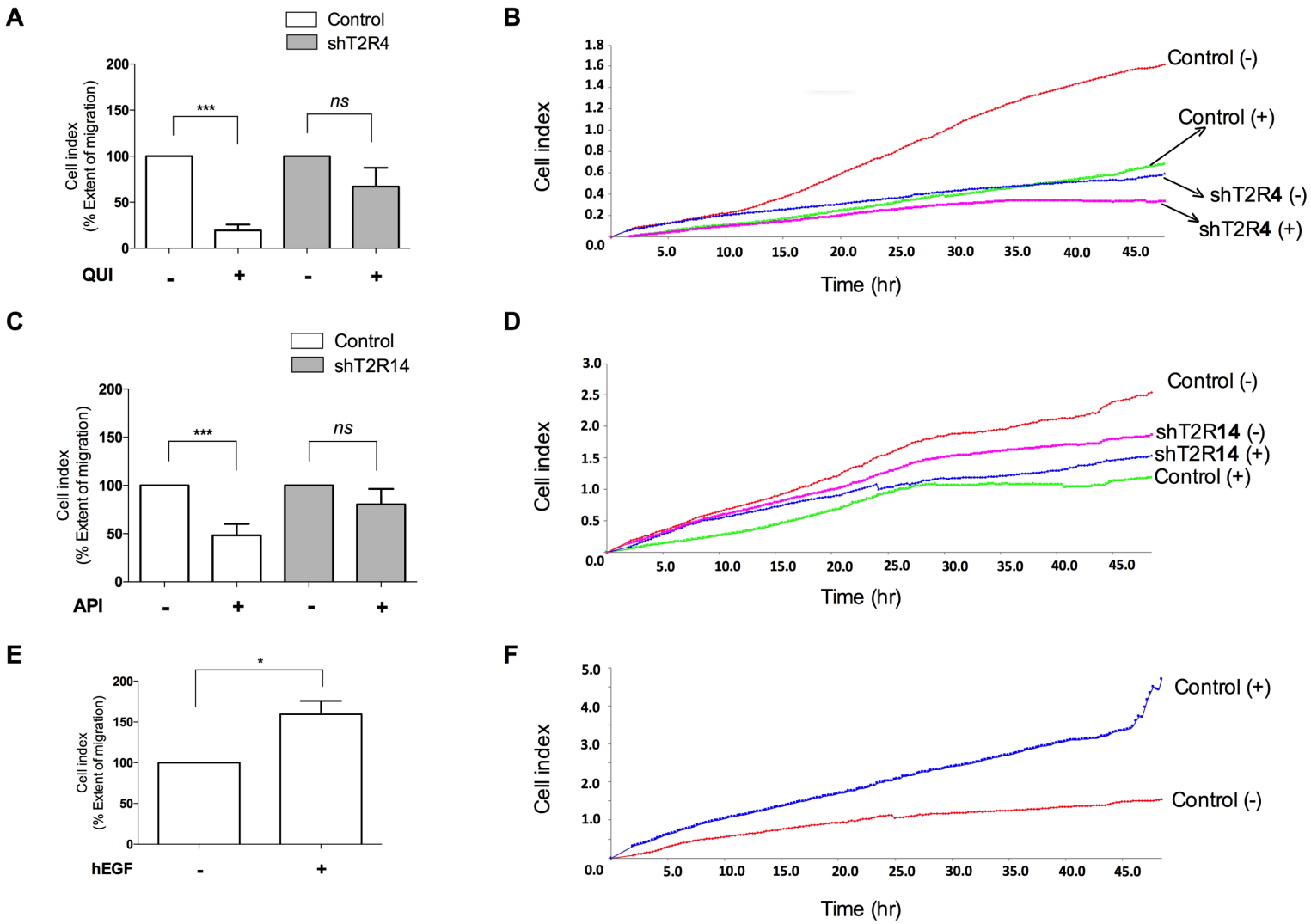
A
Control
shT2R4
Cell index
(% Extent of migration)
200
150
100
50
0
***
ns
QUI
-
+
-
+
B
Cell index
1.8
1.6
1.4
1.2
1.0
0.8
0.6
0.4
0.2
0.0
5.0
10.0
15.0
20.0
25.0
30.0
35.0
40.0
45.0
Time (hr)
Control (-)
Control (+)
shT2R4 (-)
shT2R4 (+)
C
Control
shT2R14
Cell index
(% Extent of migration)
200
150
100
50
0
***
ns
API
-
+
-
+
D
Cell index
3.0
2.5
2.0
1.5
1.0
0.5
0.0
5.0
10.0
15.0
20.0
25.0
30.0
35.0
40.0
45.0
Time (hr)
Control (-)
shT2R14 (-)
shT2R14 (+)
Control (+)
E
Cell index
(% Extent of migration)
200
150
100
50
0
*
hEGF
-
+
F
Cell index
5.0
4.0
3.0
2.0
1.0
0.0
5.0
10.0
15.0
20.0
25.0
30.0
35.0
40.0
45.0
Time (hr)
Control (+)
Control (-)

Figure 4.4.8 T2R4 and T2R14 activation impair the chemotactic migration in MDA-MB-231 cells. Real time cell migration (cell index) induced by QUI (125 μM), API (50 μM) and hEGF (20 ng/ml) treatment in MDA-MB-231 cells examined using xCELLigence DP system. **A**) Effect of QUI (+) induced T2R4 activation on the chemotactic migration of MDA-MB-231 cells (control and shT2R4 cells) relative to buffer (-). **B)** Representative real time traces of cell index vs. time course corresponding to the data shown in panel A. **C**) Effect of API (+) induced T2R4 activation on the chemotactic migration of MDA-MB-231 cells (control and shT2R14 cells) relative to buffer (-). **D)** Representative real time traces of cell index vs. time course corresponding to the data shown in panel C. **E**) Effect of hEGF (+) treatment on the chemotactic migration of MDA-MB-231 cells relative to buffer (-). **F)** Representative real time traces of cell index vs. time course corresponding to the data shown in panel E. "Control" denotes the cells transfected with scrambled shRNA. Data analysis was performed using RTCA 2.0 software. Data shown is from at least n=3 independent experiments performed in duplicate. *$p < 0.05$, ***$p < 0.001$, ns, non-significant vs. buffer.

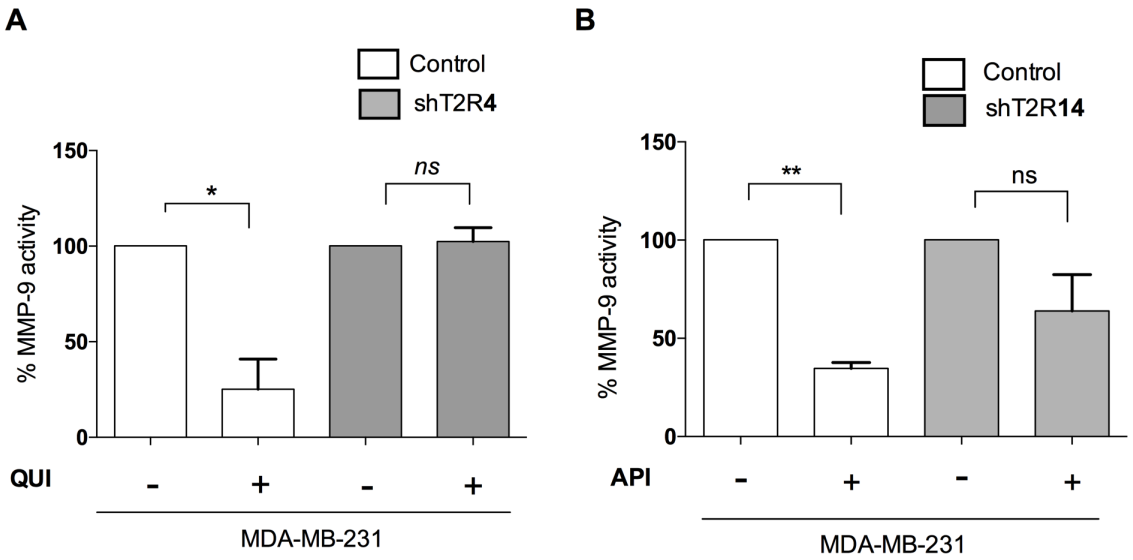

Figure 4.4.9 Effect of T2R activation on MMP-9 activity. **A)** QUI (125 μM) induced effect on MMP-9 activity relative to buffer in MDA-MB-231 (control and shT2R4) cells. **B)** API (50 μM) induced effect on MMP-9 activity relative to buffer in MDA-MB-231 (control and shT2R14) cells. "Control" denotes the cells transfected with scrambled shRNA. Data shown is from at least n=3 independent experiments performed in duplicate. *p< 0.05, **p<0.01, ns, non-significant vs. buffer.

4.5 Discussion

Despite increasing advances in the diagnosis and adjuvant targeted therapies, breast cancer remains the second most common cause of cancer death among women in North America. Triple negative breast cancer is characterized by lack of ER, PR and HER-2 receptors has poor treatment options and shows early recurrence (Foulkes et al., 2010). Therefore, developing novel strategies for early diagnosis, prevention and/or treatment of breast cancer with TNBC phenotype is very much needed. Hence, unconventional or unattended targets come into focus of research; among these are bitter-tasting compounds and foods such as bitter melon extract, epigallocatechin-3-gallate, caffeine or quinine which have some anticancer activities (Kwatra et al., 2013;Liu et al., 2016b;Stern et al., 2018). However, the molecular mechanisms by which these compounds exert anticancer properties are not well understood.

T2R polymorphic variants including those of TAS2R4 and TAS2R14 have been reported to have an influence on increased cancer risk (Carrai et al., 2011;Yamaki et al., 2017;Choi et al., 2018;Lambert et al., 2018). Moreover, T2Rs are activated by a gamut of naturally occurring compounds of plant origin, many of whom have anti-cancer properties. Plant crude extracts or isolated active constituents from vegetables such as broccoli, bitter melon, and brussel sprouts have shown anti-breast cancer properties (Levitsky and Dembitsky, 2014;Muhammad et al., 2017). Moreover, flavonoids such as apigenin, quercetin, genistein, tangeritin and epigallocatechin-3-gallate were shown to have inhibitory effects on breast cancer (Jeong et al., 2009;Lin et al., 2015;Seo et al., 2015;Rivera Rivera et al., 2016;Bauer et al., 2017;Lin et al., 2017). Strikingly, many of these compounds are characterized as T2R14 agonists (Roland et al., 2013;Hariri et al., 2017). However, it is unclear if T2Rs are cell surface targets in mediating anticancer effects evoked by these bioactive phytochemicals. Thus, in this study, we show how

quinolone alkaloids (QUI) and flavonoids (API) display their anticancer activities through activation of T2R4 and T2R14.

Our results show that T2R4 and T2R14 are differentially expressed in breast cancer. In the breast cancer patient samples T2R14 expression was higher compared to normal individuals, and vice versa, in the case of T2R4. These results are consistent with our previous publications, in which we used the nCounter platform (NanoString Technologies) and qPCR to demonstrate TAS2R4 and TAS2R14 expression patterns in MCF 10A and MDA-MB-231 cells (Singh et al., 2014;Jaggupilli et al., 2017). Moreover, aberrant expression of GPCRs is also a hallmark of cancer progression (Allen et al., 1991;O'Hayre et al., 2013;Nieto Gutierrez and McDonald, 2018). For example, GPR161, GPR30, CXCR4, LPAR2, PAR1 expression is dysregulated in breast cancer cells compared to normal cells (Liu et al., 2016c;Nieto Gutierrez and McDonald, 2018). More specifically, a decrease in the expression of the T2Rs, TAS2R8 and TAS2R10 was found in less differentiated neuroblastoma cells (more malignant) compared to the same in a more differentiated state (Seo et al., 2017). In ovarian and prostate cancer, the TAS2R14 expression is down-regulated in cancer cells compared to non-cancerous cells (Martin et al., 2018). However, currently, it is difficult to assess if there is a correlation between the expression pattern of T2Rs and tumorigenic transformation of normal cells. Additional genomic analyses with a larger sample size of breast tumor samples in different stages would provide a better understanding of the potential underlying association of T2R expression variances and breast cancer development.

To confirm the functionality of the T2R4 and T2R14 in breast cancer cells and normal breast epithelial cells we measured the agonist induced Ca^{2+} mobilization. T2R14 is known to be activated by several structurally diverse agonists and evoke varying degrees of efficacy. A

specific T2R14 agonist with high affinity and efficacy still remains elusive; therefore, in this study, we selected API a T2R14 agonist with reported anticancer properties. QUI is promiscuous in its specificity for activation of T2Rs. However, previous reports from our lab have demonstrated specificity for T2R4 compared to other T2Rs. The specificity for activating endogenous T2R4 and T2R14 by the respective agonists in MDA-MB-231 and MCF10A is demonstrated by their decreased responses in the corresponding receptor knock down cells (shT2R4 and shT2R14). These findings suggest that T2Rs expressed in cancer conditions are functional and could be activated by exogenous ligands. Endogenous ligands for T2Rs are poorly characterized, barring a single study which highlighted a steroid hormone, progesterone activating mouse T2R110 and T2R114 (Lossow et al., 2016). Interestingly, autocrine and paracrine activation of GPCRs by neuropeptides and steroid hormones promotes breast cancer tumorigenesis. Therefore, it is plausible that T2Rs activated by endogenous ligands may play a role in breast cancer tumorigenicity. T2R-mediated inhibition of cell proliferation has recently been demonstrated in healthy human airway smooth muscle cells and in ovarian and prostate cancer cell lines (Sharma et al., 2016;Martin et al., 2018). This is similar to our finding in which we showed that in metastatic breast cancer cell lines, activation of T2R4 and T2R14 attenuated the proliferation of breast cancer cells and in non-tumorigenic breast epithelial cells the agonist-promoted anti-proliferative effects were not observed. A number of possibilities exist for why activation of T2R4 and T2R14 did not attenuate the MCF 10A cell proliferation, which includes the different culture media in which the two cells (BC and non-BC) were grown. Non-BC cells (MCF 10A) are grown in media consisting of different growth factors including 20 ng/ml human epidermal growth factor (hEGF) whereas hEGF is absent in MDA-MB-231 culture media. hEGF is a common mitogenic factor that stimulates the proliferation of different types of cells,

especially epithelial cells. Therefore, though T2R4 expression is higher in MCF 10A, the activation of T2R4 signaling may not be enough to overcome the mitogenic effect of hEGF. Furthermore, the pharmacology and effect of these growth factors (including hEGF) on T2R signaling, whether they are T2R agonists or antagonists are not elucidated, yet. While this observation is new to the T2Rs, it is not surprising and previously shown in the BC field. It was shown in multiple studies that anti-carcinogenic phytochemicals inhibited the proliferation of BC cells, in contrast they showed no effect on the proliferation on non-tumorigenic breast epithelial cell lines (Katdare et al., 1998;Gache et al., 1999;Lewinska et al., 2017).

A variety of pathways like PPARα1 and FOXM1 pathways are upregulated in the cancer phenotype which affects cell proliferation, differentiation and apoptosis compared to normal cells (Narrandes et al., 2018). This may explain the discernible anti-proliferative effects evoked by T2Rs in MDA-MB-231 cells as opposed to the ones evoked in MCF 10A cells. Moreover, another characteristic feature of tumor cell signaling is a loss of equilibrium between the stimuli-induced cell proliferation and stimuli-induced apoptosis (Liu et al., 2001). To test the possibility that T2R activation influences apoptotic mechanisms in the cells, we determined the rate of apoptosis using Annexin V/PI staining procedure. T2R4 and T2R14 agonist activation caused an increase in the percentage of apoptotic cells in MDA-MB-231 cells. These results suggest that both T2R4 and T2R14 activation induce anti-tumor biological responses i.e. anti-proliferative and pro-apoptotic responses. The key unanswered question, however, will be to identify the complex cellular signal transduction pathways interlinking the anti-tumorigenic effects observed. Our findings are in agreement with a recent report suggesting, T2R14 activation induced pro-apoptotic and anti-proliferative effects in ovarian and prostate cancer cells (Martin et al., 2018).

The effects of pharmacological activation of T2R4 and T2R14 on the migration of MDA-MB-231 cells were also examined. T2R4 or T2R14 activation by QUI or API respectively mitigated the migration of cells in the presence of a chemotactic gradient and the receptor specificity of the agonist induced effects are demonstrated in the corresponding receptor knockdown cell lines. These results confirm the potential role of T2R4 and T2R14 pathway in the motility of highly invasive breast cancer cells. These results are in agreement with the previously reported role of T2R8 and T2R10 in abrogating migration of neuroblastoma cells (Seo et al., 2017). Notably, GPCRs engage in multiple downstream pathways to modulate the migration and metastasis of breast cancer cell. Most notable of them includes MAPK/ERK1/2, $G\alpha_{12/13}$-RhoGTPase pathways and GPCR transactivation of other key cell membrane non-GPCR proteins thereby indirectly regulating other downstream signaling modules. The T2R driven downstream effectors involved in evoking physiological responses are varied and tissue specific, however the one commonality in all T2R signaling is $G\alpha_q$-PLCβ-IP_3 mediated release of intracellular calcium. Interestingly, elevated intracellular Ca^{2+} levels are implicated in regulating breast cancer cell migration (Cross et al., 2014). Therefore, we hypothesize that downstream Ca^{2+} could play a central role in the anti-migratory responses elicited through T2R4 and T2R14 activation. However additional studies are required, considering some recent reports highlighting the direct T2R (T2R10 and T2R14) mediated activation of downstream effectors involving ERK1/2 and AMPK phosphorylation in extraoral T2R physiology (Camoretti-Mercado et al., 2015;Kim et al., 2018a;Kim et al., 2018b).

MMP-9 are endopeptidases secreted by highly invasive tumor cells which degrade extracellular matrix, thereby facilitating breast cancer migration. MMP-9 are considered a prognostic biomarker and druggable target in the alleviation of breast cancer metastasis (Radisky et

al., 2017). We examined a potential role of MMP-9 secretion in T2R4 and T2R14 induced migration inhibitory responses observed in MDA-MB-231 cells. Results show that T2R4 and T2R14 activation by QUI and API treatment resulted in suppression of MMP-9 secretion, which could be one of the mechanisms underlying the migration inhibitory responses observed. Taken together, our findings demonstrate a role for chemosensory T2R signaling network in evoking beneficial physiological responses in breast cancer. Nevertheless, more studies directed at identifying the downstream signaling cascades activated via basal or agonist T2R activation in several breast cancer cell line models are needed, as they will provide deeper insights into role of T2Rs in pathology of breast cancer.

BRIDGE TO CHAPTER 5

In chapter 4, as part of the overall theme of the thesis i.e., elucidating the role of chemosensory T2Rs in extraoral tissues, the role of T2R4 and T2R14 in breast cancer cells and normal breast epithelial cells was characterized. Previously, the role of membrane cholesterol in influencing T2R4 activity was studied using heterologous expression systems. Given that T2R14 is expressed at higher levels in a number of extraoral tissues compared to T2R4, therefore it is important to study how membrane lipids influence T2R14 signaling in native systems and the molecular basis for these interactions. In the following chapter (5), I studied membrane cholesterol's role in regulating T2R14 signaling in human airway smooth muscle cells and human airway epithelial cells. Furthermore, the molecular basis of cholesterol-T2R14 interaction was also studied.

CHAPTER 5

5.0 Cholesterol modulates the signaling of chemosensory bitter taste receptor T2R14 in human airway cells

Feroz Ahmed Shaik, Manoj Reddy Medapati, Prashen Chelikani

Am J Physiol Lung Cell Mol Physiol. 2019 Jan 1;316(1):L45-L57.

5.1 ABSTRACT

Bitter taste receptors (T2Rs) are a group of 25 chemosensory receptors expressed at significant levels in the human airways. In human airways bitter taste receptor 14 (T2R14) mediated physiological response in ameliorating obstructive airway disorders is an active area of investigation. Therefore, understanding various factors regulating the structure and function of T2R14 will be beneficial. We hypothesize that membrane lipids like cholesterol play a regulatory role in T2R14 signaling in airway cells. We confirmed the expression and signaling of T2R14 in primary human airway smooth muscle (HASM) cells, and human airway epithelial cell line (NuLi-1) using immunoblot analysis and $[Ca^{2+}]_i$ mobilization experiments respectively. Next, T2R14 signaling was examined in membrane cholesterol altered environments by methyl-β-cyclodextrin (MβCD) or cholesterol oxidase treatments. In the cells analysed, cholesterol depletion affected the agonist induced T2R14 signaling, and cholesterol replenishment rescued its efficacy. An alternative approach for cholesterol depletion (with cholesterol oxidase pretreatment) also negatively affected the agonist potency for T2R14 in HASM cells. To understand the molecular mechanism of interaction between cholesterol and T2R14, we used site-directed mutagenesis coupled with functional assays and examined the role of putative cholesterol binding motif's (CRAC and CARC) in T2R14. Functional characterization of wild-type and mutant T2R14 receptors suggest that amino acid residues K110, F236 and L239 are crucial in T2R14-cholesterol functional interaction. In conclusion, our results show that cholesterol influences the T2R14 signaling efficacy by forming direct interactions with the receptor and consequently plays a regulatory role in T2R14 mediated signaling in human airway cells.

5.2 INTRODUCTION

The bitter taste sensation in humans is mediated by a specialized class of chemosensory receptors known as the bitter taste receptors (T2Rs). T2Rs are integral membrane proteins that belong to G protein-coupled receptor (GPCR) superfamily and consist of a characteristic seven-transmembrane architecture (Hoon et al., 1999;Chandrashekar et al., 2000). In humans, 25 T2Rs are expressed in oral and extraoral tissues. The principal function of T2Rs was believed to be in detection of bitter-tasting food substances, however, in the past decade, a plethora of extra-gustatory roles for T2Rs have been uncovered (Shaik et al., 2016). In airways, the expression and physiological effects elicited via T2R has been demonstrated in various cell types, viz. airway smooth muscle cells, airway epithelial cells and pulmonary sensory neurons (Deshpande et al., 2011;Lee et al., 2012;Gu et al., 2017). T2R38 and T2R14 expressed in the sino-nasal epithelial cells mediate anti-microbial immune responses and thereby proposed as potential therapeutic targets in the management of upper respiratory tract infections (Lee et al., 2014;Hariri et al., 2017). In human airway smooth muscle (HASM) cells, activation of T2Rs by cognate bitter agonists induced a calcium pathway dependent relaxation of HASM (Deshpande et al., 2011;Zhang et al., 2013;Camoretti-Mercado et al., 2015;Kim et al., 2017a). In addition, T2R agonists induced antimitogenic responses in healthy and asthmatic HASM cellular models further provides evidence for T2R signaling pathway as a potential target in mitigating some aspects of airway remodeling (Sharma et al., 2016;Pan et al., 2017). In contrast to differences observed in the expression and/or dysregulation of β_2-adrenergic receptors (β_2AR) in HASM cells from asthmatic and non-asthmatic patients, T2Rs expression or efficacy was not altered (Robinett et al., 2014). Taken together, these studies suggest T2Rs as novel therapeutic targets in the treatment of obstructive airway diseases.

The paradoxical HASM relaxation induced by T2R signaling pathway (T2R-PLCβ-Ca^{2+}) involving increase in intracellular Ca^{2+} level is novel, however the mechanisms involved remains to be clearly understood (Deshpande et al., 2010;Zhang et al., 2013). Therefore, it would be beneficial to examine additional determinants regulating T2R function in the HASM. One of the major factors influencing GPCR function in HASM is membrane cholesterol (Schlenz et al., 2010). Membrane cholesterol regulates the function of several GPCRs either directly, by forming specific interactions with the receptors or indirectly, by altering the physical state of the membrane or a combination of both (Gimpl et al., 1997;Pucadyil and Chattopadhyay, 2006). In addition, cholesterol-rich membrane microdomains like lipid-rafts and caveolae, also play a key role in the recruitment of GPCRs and in facilitating GPCR mediated signaling events (Brown and London, 2000;Barnett-Norris et al., 2005;Insel et al., 2005). Moreover, in HASM, membrane proteins involved in contractile signaling events have been shown to be cholesterol sensitive (Gosens et al., 2006;Hunter and Nixon, 2006;Schlenz et al., 2010).

Previously, we have shown the cholesterol sensitivity of T2R4 signaling in Chinese Hamster Ovary (CHO) cells (Pydi et al., 2016). In this study, we investigated the role of membrane cholesterol in the T2R14 signaling in two types of airway cells, HASM and NuLi-1 cells. The rationale for examining T2R14 subtype in the current study is based on its predominant expression in many extra-oral tissues compared to other T2R subtypes. Moreover, the expression levels of T2R14 in epithelial cells of upper airways, gastrointestinal tract and in HASM cells is comparable to the physiologically important Class A GPCRs (Jaggupilli et al., 2017;Liszt et al., 2017). We hypothesize that membrane cholesterol might regulate T2R14 signaling in airways. To test this hypothesis, first, we examined the role of membrane cholesterol in agonist induced T2R14 signaling. Second, to elucidate the molecular mechanisms involved in

T2R14-cholesterol interaction, we mutated the amino acids in the putative cholesterol binding motifs in T2R14 and characterized their function. Together, these studies provide novel insights into innate mechanisms governing T2R14 signaling in airways.

5.3 MATERIALS AND METHODS

5.3.1 Materials

Diphenhydramine (DPH), flufenamic acid (FFA), cholesterol, methyl-β-cyclodextrin (MβCD), cholesterol oxidase, fetal bovine serum, collagen type 4 (C7521), Dimethyl sulphoxide, U73122 and other chemicals were purchased from Sigma Chemical Co. (Oakville, ON). Fluo-4 NW calcium assay kit, Dulbecco's modified Eagle medium (DMEM), Amplex Red cholesterol assay kit were purchased from Invitrogen Life Technologies (Carlsbad, CA). Detergent n-Dodecyl-β-D-maltopyranoside (DM) was purchased from Anatrace (Maumee, OH) and gallein from Tocris (Oakville, ON). Bronchial epithelial cell growth basal medium or BEGM (CC-3171) and BEGM supplements and growth factors (CC-4175) were purchased from Lonza Inc. (Walkersville, MD). Polyclonal Anti-T2R14 antibody (C120957, LSBio Inc.), Monoclonal Anti-β-Actin antibody (A5441, Sigma), Goat Anti-Rabbit IgG-HRP conjugate secondary antibody (170-6515, Bio-Rad), Goat Anti-Mouse IgG-HRP secondary antibody (31430, Thermofisher scientific), APC conjugated Monoclonal Anti-Flag antibody, (637308, Biolegend). ETSAHRL (T2R14 inhibitor peptide) was synthesized commercially (GenScript Inc. NJ, USA).

5.3.2 Cell culture

Primary human airway smooth muscle (HASM) cells was a kind gift from Dr. Andrew Halayko, Department of Physiology, University of Manitoba. For all experiments, HASM cells of passages 2-4 were used and cells were grown to full confluency. HASM cells were maintained

in DMEM media supplemented with 10% Fetal bovine serum (FBS), 100 units/ml Penicillin and 0.1 mg/ml Streptomycin and at 5% CO_2 and 37°C. Growth media and conditions used for HEK293T cells were similar to the one used for HASM cells with one exception, DMEM/F12 (1:1) was used in place of DMEM. Human bronchial epithelial cell line from normal lung (NuLi-1) was purchased from ATCC. NuLi-1 cells were cultured in BEGM media with supplements in collagen coated cell culture dishes.

5.3.3 Recombinant plasmid DNA and transfections

The TAS2R14 wild-type (encoding T2R14) and twelve TAS2R14 mutant genes (encoding $T2R14^{L103A}$, $T2R14^{L103I}$, $T2R14^{Y107A}$, $T2R14^{Y107F}$, $T2R14^{K110A}$, $T2R14^{K110R}$, $T2R14^{K231A}$, $T2R14^{K231R}$, $T2R14^{F236A}$, $T2R14^{F236Y}$, $T2R14^{L239A}$, $T2R14^{L239I}$) codon-optimized for expression in the mammalian cells were synthesized commercially (GenScript Inc., MA, USA). All the gene sequences consisted of a FLAG epitope coding sequence at the 5' end and genes were cloned into mammalian expression vector, pcDNA3.1-Hygro (+). Transient transfections of plasmid DNA's in HEK293T was performed using Lipofectamine 2000 (Invitrogen) as per the manufacturers protocol.

5.3.4 Membrane cholesterol modulation

Membrane cholesterol was depleted by treating the cells with MβCD. For cholesterol estimation in HASM or NuLi-1 cell membranes, cells were grown to full confluency in 100 mm cell culture dishes. Cells were serum starved for 3hrs by incubating the cells in DMEM basal media. This short period of serum-starvation of cells prior to MβCD treatment is an established protocol and is done to stabilize the cells in serum-free basal media, prior to MβCD (which is dissolved in basal media) treatment (Pucadyil and Chattopadhyay, 2007;Jafurulla et al., 2017b).

After a wash with PBS, cells were incubated in different concentrations (5 mM or 10 mM) of MβCD solution (prepared in DMEM basal media) for 30 min. Post MβCD treatment, cell membrane preparation and membrane cholesterol quantification were performed as per our previously published procedures (Pydi et al., 2016). For depletion of membrane cholesterol, live cells were seeded in a black walled, clear bottom 96 well plates at a density of 40,000 cells per well and were allowed to grow overnight. Cells were serum starved for 3hrs followed by treatment with MβCD (10 mM) for 30 min. Post MβCD treatment, cholesterol depleted and control cells were used for functional assays. Membrane cholesterol replenishment was performed as described elsewhere (Jafurulla and Chattopadhyay, 2017). Briefly, cholesterol replenishment in cell membranes was carried out by first depleting the membrane cholesterol with MβCD (10mM) treatment for 30 min followed by incubation of cells with cholesterol: MβCD complex (1 mM:10 mM) for 30 min. Cholesterol depletion and replenishment treatments were performed at 37°C in a humidified atmosphere with 5% CO_2.

5.3.5 Cholesterol oxidase treatment

Cholesterol oxidase (COase) treatment was done to enzymatically alter the cholesterol and thereby decreasing the unoxidized form of membrane cholesterol. Cells were serum starved for 3hrs followed by incubation with COase (1 unit/ml) for 30 min at 37°C (Pucadyil and Chattopadhyay, 2006;Jafurulla et al., 2017b). Functional assays for COase treated cells were performed immediately after COase treatment.

5.3.6 Estimation of plasma membrane cholesterol content

Enzymatic determination of membrane cholesterol content in control and cholesterol altered HASM, NuLi-1 and HEK293T cell membrane preparations were done using the Amplex Red Cholesterol assay kit (Amundson and Zhou, 1999).

5.3.7 Immunoblot analysis

HASM and NuLi-1 cell membrane enriched lysates of control and cholesterol modulated cells were prepared by lysing the cells in a lysis buffer consisting of 20 mM n-Dodecyl-β-D-Maltopyranoside (DM), 20 mM Tris-HCl, 500 mM NaCl, 10% Glycerol and protease inhibitor cocktail (pH 7.4). Following lysis, cell debris was removed by centrifugation at 12,000 RPM for 15 min at 4°C. The samples were resolved on a 12% SDS-PAGE, followed by transfer onto a nitrocellulose membrane. Immunoblotting was performed with the corresponding primary antibodies at 4°C overnight followed by secondary antibody incubation at room temperature for 1 hour. Bands were visualized using chemiluminescence based detection and for imaging, Vilber Lourmat Fusion FX7 imager was used.

5.3.8 Flow cytometry

HEK293T cell surface expression of FLAG tagged T2R14 WT receptor and T2R14 mutants was quantified using BD FACS canto flow cytometer. Briefly 50,000 cells were washed in ice-cold FACS buffer (0.5% BSA in 1xPBS) and incubated with APC conjugated mouse monoclonal anti-FLAG M2 antibody (1:500 dilution) for 1 hour on ice. The cells were then washed 3 times with FACS buffer and resuspended in 300µl of FACS buffer. The fluorescent intensity was measured using a FACS canto analyzer and mean fluorescent intensity (MFI) values were obtained. The results were expressed in terms of percent cell surface expression compared to the mock transfected (pcDNA 3.1) cells.

5.3.9 Intracellular calcium $[Ca^{2+}]_i$ measurement

Agonist induced $[Ca^{2+}]_i$ mobilization assays were performed as in procedures previously described (Pydi et al., 2014c). Briefly, in HASM cells, T2R14 specific agonists DPH and FFA were used to characterize the endogenously expressed T2R14. HASM cells were seeded at a density of 40,000 cells per well in a clear bottom, black walled 96 well plates and grown overnight to full confluency. In experiments which required cholesterol modulation, cells were serum starved for 3hrs by maintaining cells in serum free DMEM media. Post various aforementioned cholesterol-altering pretreatments, the cells were washed with Hank's balanced salt solution (HBSS), followed by loading of cells with Ca^{2+} sensitive Fluo-4 NW dye and incubation at 37°C for 30 min in dark. An additional incubation of 30 min is done at RT, prior to agonist stimulation. In assays which involved U73122 and Gallein pretreatments, during the second incubation step, the Fluo-4NW dye is replaced with buffer containing U73122 or Gallein and further incubated for 30 min at RT. Flexstation-3 fluorescence plate reader (Molecular Devices) was used to measure the fluorescence changes as a result of $[Ca^{2+}]_i$ mobilization elicited by respective agonists or vehicles. Fluorescence was measured for 120 secs at 525nm with excitation at 494nm. Data are expressed as relative fluorescence units (ΔRFU) after subtracting fluorescence values from the vehicle treated cells. Signals were normalized to background fluorescence. Dose-response curves were generated by Non-linear regression analysis of the data using GraphPad Prism 6.0.

5.3.10 Statistical analysis

One-way ANOVA and Tukey's multiple comparisons tests were used to determine the statistically significant differences in experiments which involved more than two sample groups. Student's T-Test was used to determine the statistical differences in experiments with two

sample groups. Half-maximal effective concentrations values (EC_{50}) for the compounds used, was calculated using the Nonlinear regression analysis of the dose-response data. Unless specified, the experimental data shown is mean ± S.E, from at least three independent experiments done in triplicate. A p value of less than 0.05 was considered statistically significant. All the above mentioned statistical analysis was performed using Graph pad prism 6.0 software (San Diego, CA).

5.4 RESULTS

Previously, using nCounter sequencing analysis, we reported the mRNA expression of TAS2R14 in primary HASM cells and bronchial epithelial immortalized cell line NuLi-1. The TAS2R14 expression was higher compared to the other T2R subtypes in the assayed cell types (Jaggupilli et al., 2017). As T2R14 was found to signal in both the airway cell types, therefore we pursued studies in both these airway cells to investigate whether the role of membrane cholesterol in T2R14 signaling is cell-type dependent or independent. We examined the role of membrane cholesterol in endogenous T2R14 signaling in these airway cells by physical depletion of membrane cholesterol methyl-β-cyclodextrin (MβCD) treatment. Cyclodextrins are sterol-specific carriers, used to extract lipids from the cell membranes. Due to its high cholesterol specificity, MβCD is widely used for acute modulation of membrane cholesterol content (Pucadyil and Chattopadhyay, 2006). Moreover, cholesterol and MβCD complex at a stoichiometric ratio of 1:10 is normally used for plasma membrane cholesterol enrichment.

5.4.1 Membrane cholesterol alters T2R14 signaling in primary HASM cells

Treatment of HASM cells with MβCD (10 mM) depleted the cholesterol content in the membranes by 36%, which was statistically significant compared to the control cells **(Figure**

5.4.1E). For cholesterol replenishment in cholesterol depleted group, cholesterol (1 mM): MβCD (10 mM) ratio was found to be optimal to restore the membrane cholesterol levels to the wild-type levels **(Figure 5.4.1E)**. Membrane cholesterol differentially affects the conformation, signaling and trafficking of many GPCRs. To elucidate these effects on T2R14, we pursued pharmacological characterization of the T2R14 in control versus cholesterol altered membrane environments. T2R14 specific agonists DPH and FFA induced $[Ca^{2+}]_i$ mobilization was studied. We observed that in cholesterol depleted conditions, there was a rightward shift in the EC_{50} of the agonists (DPH and FFA) which indicates a decrease in potency **(Figure 5.4.1A)**. For agonist DPH, an EC_{50} of 606 ± 1.04 μM for control, 791 ± 1.03 μM for cholesterol depleted, and 553 ± 1.06 μM for cholesterol replenished HASM cells were obtained **(Figure 5.4.1A)**. For agonist FFA, an EC_{50} of 5 ± 1.09 μM for control, 11 ± 1.06 μM for cholesterol depleted, and 7 ± 1.1 μM for cholesterol replenished HASM cells were obtained **(Figure 5.4.1A).** However, at saturating concentrations, an increase in the E_{max} values of the agonist was observed in cholesterol depleted conditions compared to control conditions. In cholesterol replenished conditions, the responses were restored to control levels, both in terms of EC_{50} and E_{max} measures **(Figure 5.4.1A)**. Additionally, T2R14 specificity of the Ca^{2+} responses elicited by DPH and FFA was confirmed by blocking the downstream effectors (PLC and Gβγ) of the canonical bitter taste signal transduction pathway. Pretreatment of cells with U73122 and Gallein (small molecule inhibitors of PLC and Gβγ respectively), resulted in attenuation of DPH and FFA evoked $[Ca^{2+}]_i$ signals **(Figure 5.4.1B)**. This shows that major proportion of the intracellular Ca^{2+} mobilization is mediated through T2R14 in these cells. In addition, we used a peptide (EHSARHL), which we recently reported to be a T2R14 inhibitor (Jaggupilli et al., 2018a). Here, we characterized the half-maximal inhibitory concentration (IC_{50}) for ETSARHL against DPH treatment in HASM

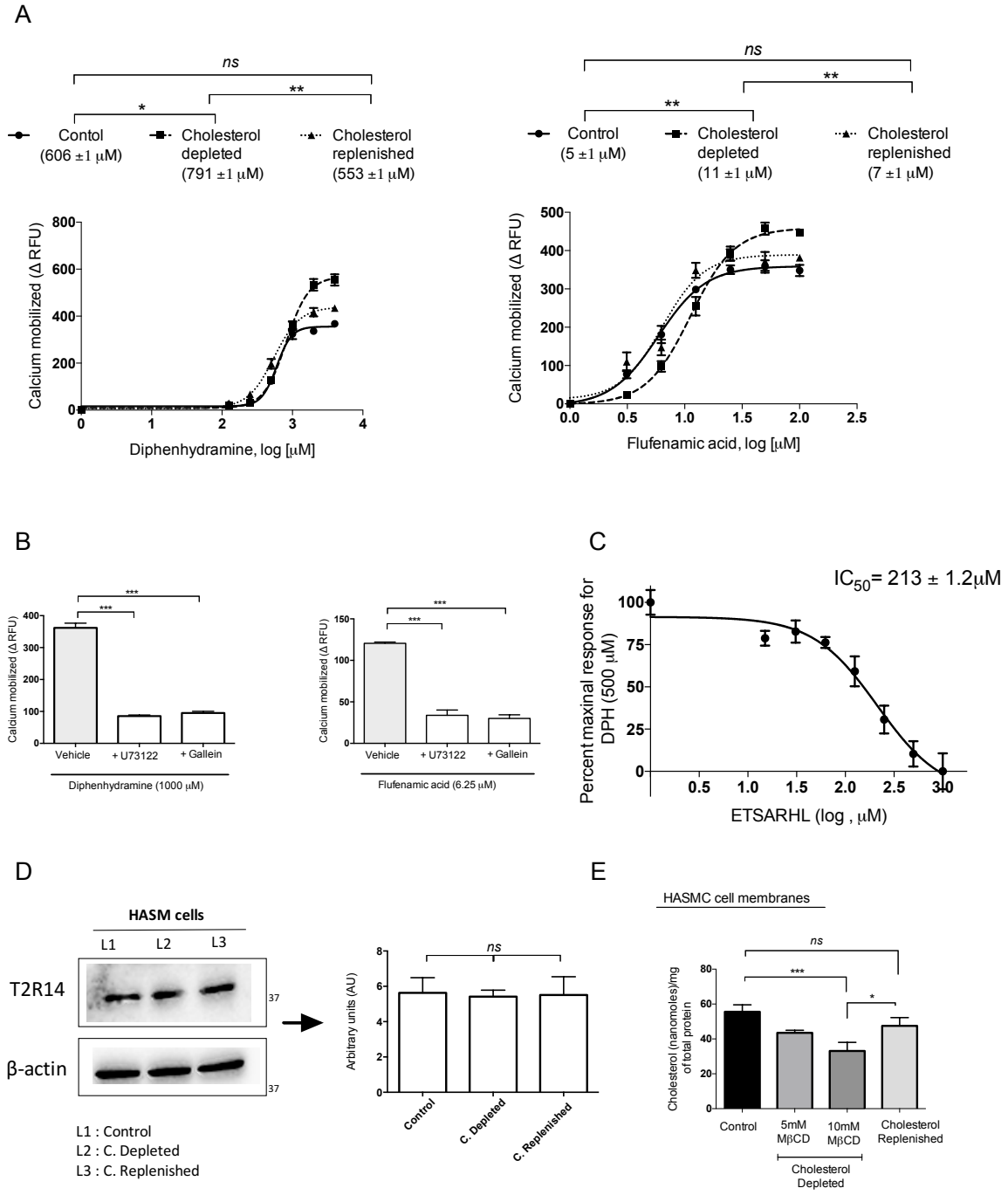

Figure 5.4.1 Agonist-induced T2R14 signaling in HASM cells is cholesterol dependent. **A)** Diphenhydramine (DPH) and Flufenamic acid (FFA) induced $[Ca^{2+}]_i$ in HASM cells in cholesterol altered conditions. The dose response curves were generated using a concentration

range of 62.5 μM – 4000 μM for DPH and 0.78 μM – 100 μM for FFA in control conditions (untreated; solid curve with circles), cholesterol depleted cells (10mM MβCD treated; dashed curve with squares) cholesterol replenished cells (1mM cholesterol :10mM MβCD treated; dotted curve with triangles). The EC_{50} values were calculated by non-linear regression analysis using Graph pad prism version 6.0 (San Diego, CA). Data shown in mean ± S.E from at least three independent experiments. A p value of < 0.05 was considered statistically significant. The agonist(s) were added at 20 seconds and fluorescence changes measured for the next 100 seconds. **B)** Single concentration (~ EC_{50} value) of DPH (1000 μM) and FFA (6.25 μM) induced $[Ca^{2+}]_i$ in HASM cells in presence of small molecule inhibitors of PLC-β (5 μM) and Gallein (5 μM). **C)** Characterization of peptide ETSARHL as an inhibitor of DPH induced T2R14 signaling in HASM cells. Competition Ca^{2+} mobilization assay was performed with a single concentration of DPH in the presence of increasing concentration of ETSARHL (15.6 μM -1000 μM; half log dilutions). The IC_{50} value was calculated by non-linear regression analysis of the dose-response data. Date shown is from at least three independent experiments performed in triplicate. **D)** Immunoblot analysis of T2R14 expression in control and cholesterol-altered conditions. 20ug membrane enriched cell lysates of HASM cells analyzed on 12% SDS-PAGE gel. The antibody dilutions of 1:1000 for anti-T2R14 antibody, 1:5000 for anti-β actin, 1:5000 for HRP-conjugated anti-rabbit IgG antibody and 1:25,000 of anti-mouse IgG were used. The bands obtained were of the expected sizes (~37 kDa). The blot shown is a representative of at least three independent experiments. The band density analysis of three independent experiments was performed using AlphaView software (FluorChem systems). **E)** Quantification of membrane cholesterol. The membrane cholesterol of HASM cell membrane preparations of control and cholesterol-modulated groups was quantified by comparing to the fluorescence values obtained for the cholesterol standards (3 nanomoles – 0.04 nanomoles) from the Amplex Red Cholesterol assay. A 25 μg total protein equivalent of membrane sample was used. The fluorescence values obtained were normalized to nanomoles of cholesterol/mg of total protein. Data shown is mean ± S.E from at least three independent experiments. A p value of < 0.05 was considered statistically significant; $^{*}p<0.05$, $^{**}p<0.01$, $^{***}p<0.001$.

cells with endogenous T2R14 expression **(Figure 5.4.1C)**. As shown in **Figure 5.4.1C**, in HASM cells, DPH (500 μM; ~EC_{50} value) induced Ca^{2+} responses were attenuated in a dose-dependent manner, when challenged with increasing concentrations of ETSARHL with an IC_{50} value of 213 ± 1.2 μM.

To elucidate the effect of cholesterol-modulation on the cell surface expression of T2R14, immunoblot analysis of membrane-enriched cell lysates from control, cholesterol-depleted and cholesterol-replenished HASM cells. Immunoblot analysis using anti-T2R14 antibody shows that membrane cholesterol modulation did not affect the membrane expression levels of T2R14 **(Figure 5.4.1D)**.

5.4.2 Membrane cholesterol alters T2R14 signaling in NuLi-1 cells

NuLi-1 is an immortalized human bronchial epithelial cell line and is a model cell line for studies relating to airway innate immunity. Previously, it has been shown that membrane cholesterol and its derivatives regulate the function of airway epithelial transmembrane proteins like CFTR, TLR-3 and P2X7 receptor (Koarai et al., 2012;Robinson et al., 2014;Abu-Arish et al., 2015). Pharmacological characterization of T2R14 in control and cholesterol-altered conditions, suggest an, increase in EC_{50} values of DPH in cholesterol depleted group (649 ± 1.7 μM) compared to the control group (319 ± 1.1 μM). The EC_{50} values were restored to control levels in cholesterol replenished group (391 ± 1.1 μM) **(Figure 5.4.2A)**. U73122 and Gallein pre-treatment inhibited the T2R14 induced $[Ca^{2+}]_i$ release **(Figure 5.4.2B)**. Additionally, T2R14 specificity of DPH induced $[Ca^{2+}]_i$ release was confirmed in these airway epithelial cell line in a competition assay with ETSARHL (T2R14 inhibitor). As shown in **Figure 5.4.2C**, ETSARHL blocked the T2R14 induced signaling with an IC_{50} of 172 ± 1.5 μM. Similar to HASM cells cholesterol modulation did not have any effect on plasma membrane T2R14 expression in NuLi-

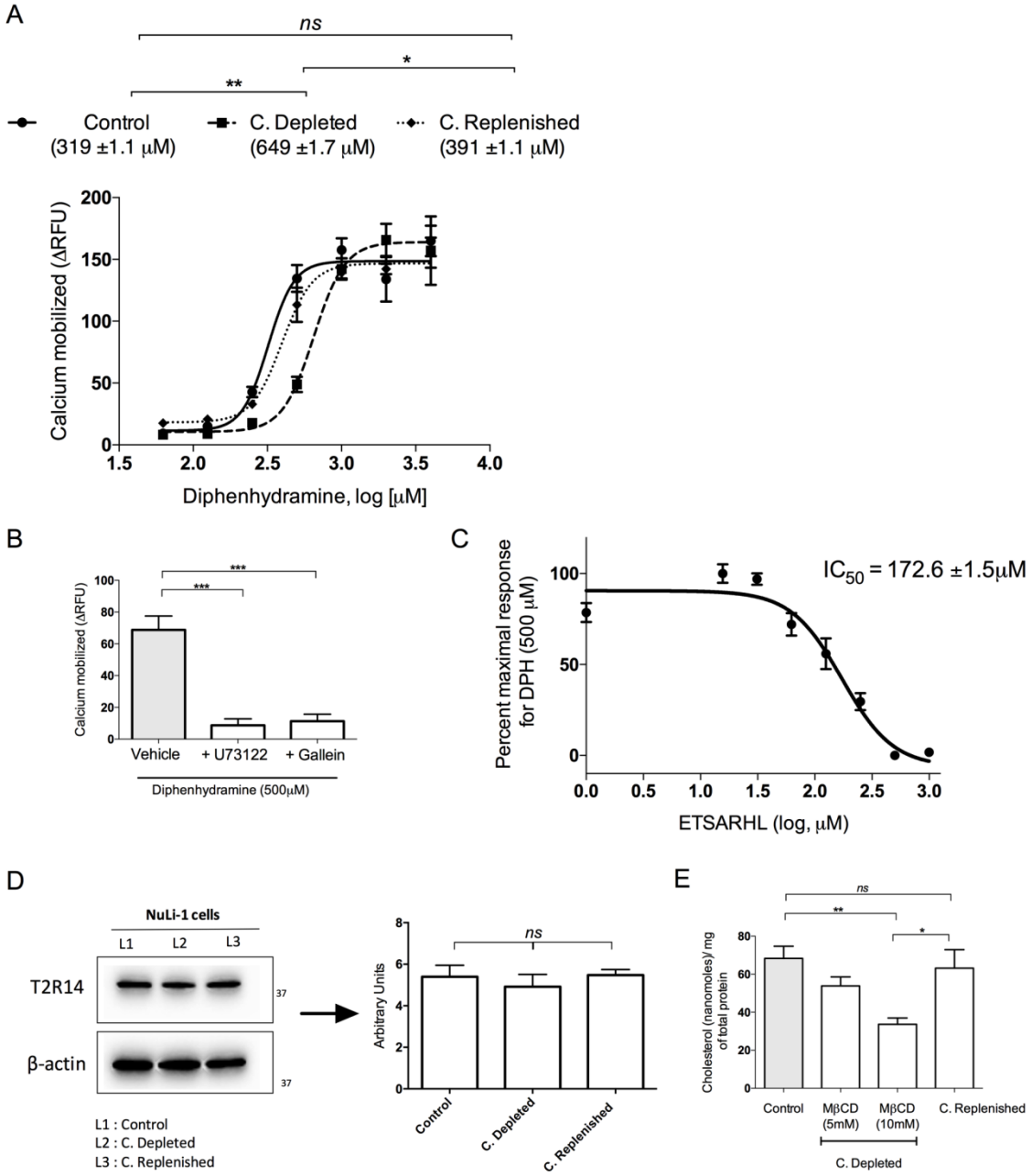

Figure 5.4.2 Membrane cholesterol regulates T2R14 signaling in NuLi-1 airway epithelial cells. **A)** Pharmacological characterization of T2R14 signaling is performed in control (solid curve), cholesterol-depleted (dash curve) and cholesterol replenished (dotted curve) conditions using Ca^{2+} mobilization assay. DPH (62.5 μM -4000μM) was used to generate dose-response curves. The EC_{50} values are shown in brackets along with the labels. Data ± SEM is from 3 independent experiments done in triplicate. One-way ANOVA was used to determine the statistical

differences between EC_{50} shifts. **B)** DPH (500 μM) induced T2R14 signaling in presence of U73122 and Gallein. **C)** DPH induced T2R14 signaling in NuLi-1 cells is attenuated in presence of increasing concentration of peptide ETSARHL (15.6 μM -1000 μM). IC_{50} value was calculated by non-linear regression analysis of dose-response data and y-axis in the graph corresponds to normalized ΔRFU values. **D)** Immunoblot analysis of T2R14 in NuLi-1 cells in cholesterol altered conditions. Representative immunoblot is shown. The treatments, antibody dilutions and blot analysis are similar to figure legend 5.4.1D. **E)** Membrane cholesterol estimation in NuLi-1 cell membranes were similar to the conditions mentioned earlier in figure legend 5.4.1E.

1 cells **(Figure 5.4.2D)**. MβCD at a concentration of 10mM, resulted in a decrease in membrane cholesterol content by ~51% compared to the untreated cells, which was found to be statistically significant **(Figure 5.4.2E)**.

5.4.3 Effect of cholesterol oxidase treatment on T2R14 signaling in HASM cells

The methodological approach of using MβCD treatment to alter membrane cholesterol involves physical depletion of cholesterol molecules. Cholesterol molecules provide rigidity to the plasma membrane and thereby physical depletion of it may potentially affect membrane fluidity (Gimpl et al., 1997). Fluorescence anisotropy studies using membrane probes have demonstrated that membrane cholesterol can indirectly modulate the function of cell membrane receptors including GPCRs by influencing membrane physical properties (Illinger et al., 1995;Paila and Chattopadhyay, 2009). To examine whether the reduced agonist efficacy at T2R14 in cholesterol depleted conditions is due to the direct or indirect effect of cholesterol on T2R14, we used an alternate approach to modulate membrane cholesterol. Cholesterol oxidase (COase) is an enzyme of bacterial origin, which catalyses the oxidation of accessible pool of membrane cholesterol to 4-Cholesten-3-one and consequently depletes the cholesterol levels without affecting membrane fluidity (Vrielink and Ghisla, 2009;Jafurulla et al., 2017b). The pre-treatment of HASM cells with cholesterol oxidase (1 unit/ml) for 30 min resulted in reduced efficacy for both bitter agonists (DPH and FFA) at T2R14 in HASM cells **(Figure 5.4.3A)**. This is corroborated by the increase in the EC_{50} for agonists in COase treated versus control group (DPH: EC_{50} of 554 ± 1.03 μM in control and 703 ± 1.05 μM in COase treated group; FFA: EC_{50} of 8 ± 1.2 μM in control and 15 ± 1.14 μM in COase treated group, **(Figure 5.4.3A)**. This data demonstrates that cholesterol regulates the signaling of T2R14 in HASM cells by direct

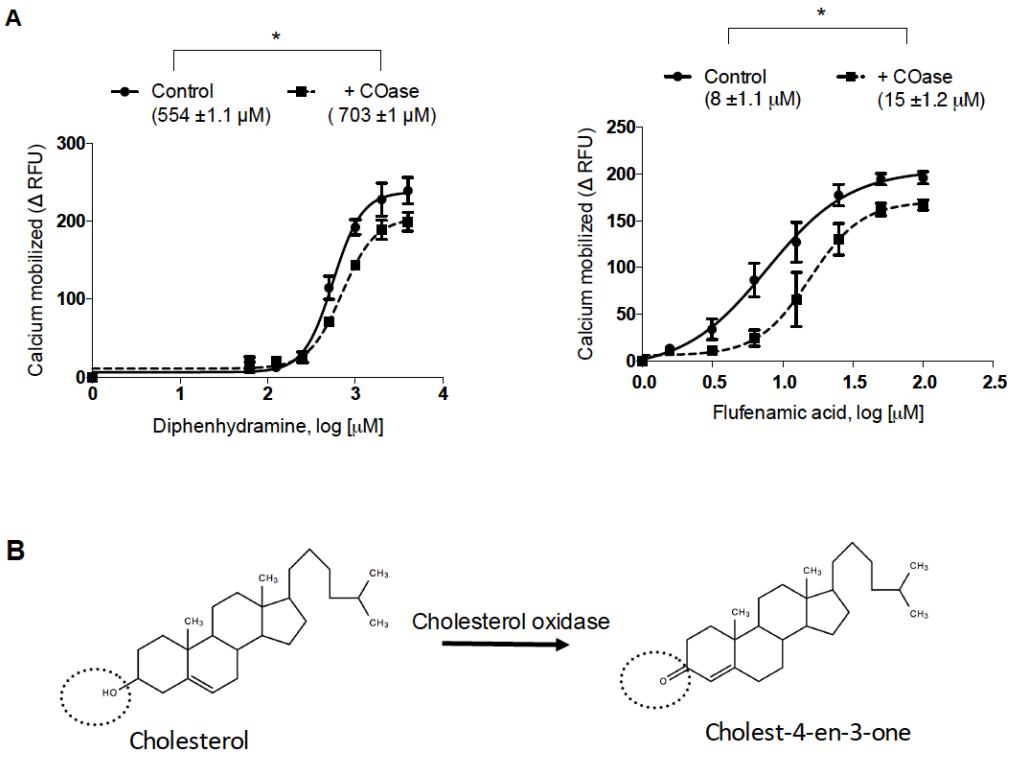

Figure 5.4.3 Cholesterol oxidase treatment affects agonist induced activation of T2R14. **A)** HASM cells were treated with cholesterol oxidase (COase; 1 unit/ml) for 30 min at 37°C followed by Ca^{2+} mobilization assay. DPH and FFA induced dose dependent responses were examined in control and cholesterol oxidase treated HASM cells. The concentrations used were DPH (62.5 μM – 4000 μM, solid curve with circles) and FFA (0.78 μM – 100 μM, dashed line with squares). The EC_{50} values are calculated by non-linear regression analysis and student's t-test was used to determine the statistical differences between the EC_{50} values of two groups. Data shown is mean ± S.E from at least three independent experiments done in triplicate. A p value of < 0.05 was considered statistically significant; *p<0.05. **B)** Molecular schematic showing the reaction catalyzed by COase, highlighting the structural differences between cholesterol and cholest-4-en-3-one.

interactions. To investigate the mechanisms by which this direct cholesterol-T2R14 interaction occurs, we targeted specific cholesterol binding motifs of T2R14 for structure-function analysis.

5.4.4 Molecular basis of membrane cholesterol sensitivity of T2R14: Role of putative CRAC and CARC motifs in cholesterol-T2R14 interaction

5.4.4.1 Identifying cholesterol binding motifs in T2R14

To identify putative cholesterol-binding motifs we pursued protein sequence alignment analysis using clustal omega program for all the 25 human T2Rs **(Figure 5.4.4)**. These cholesterol-binding motifs are termed as Cholesterol Recognition/interaction Amino acid Consensus or CRAC and CARC. CRAC motif is characterized by a conserved amino acid sequence $–NH_2$-L/V-$(X)_{1-5}$-Y-$(X)_{1-5}$-R/K-COOH (Li and Papadopoulos, 1998), in which $(X)_{1-5}$ represents between one and five of any amino acid. The CARC motif is the inverse amino acid sequence of CRAC motif and is characterized by $–NH_2$-R/K-$(X)_{1-5}$-F/Y-$(X)_{1-5}$-L/V-COOH (Di Scala et al., 2017). Our results show that 23 of the 25 T2Rs contain CRAC motif at the interface of transmembrane helix 3 (TM3) and intracellular loop 2 (ICL2), and 12 of the 25 T2Rs contain CARC motif at the interface of TM6 and ICL3 **(Figures 5.4.4 and 5.4.5)** We have also identified CRAC and CARC motifs in T2R14 to be conserved across higher order vertebrates **(Figure 5.4.5)**

5.4.4.2 Role of amino acids in CRAC and CARC motifs in membrane cholesterol sensitivity of T2R14

To study the effect of membrane cholesterol on T2R14, HEK293T cells transfected with T2R14 were pretreated with MβCD and the receptor activation was characterized by measuring intracellular calcium upon treating with increasing concentrations of the agonist DPH. In wild

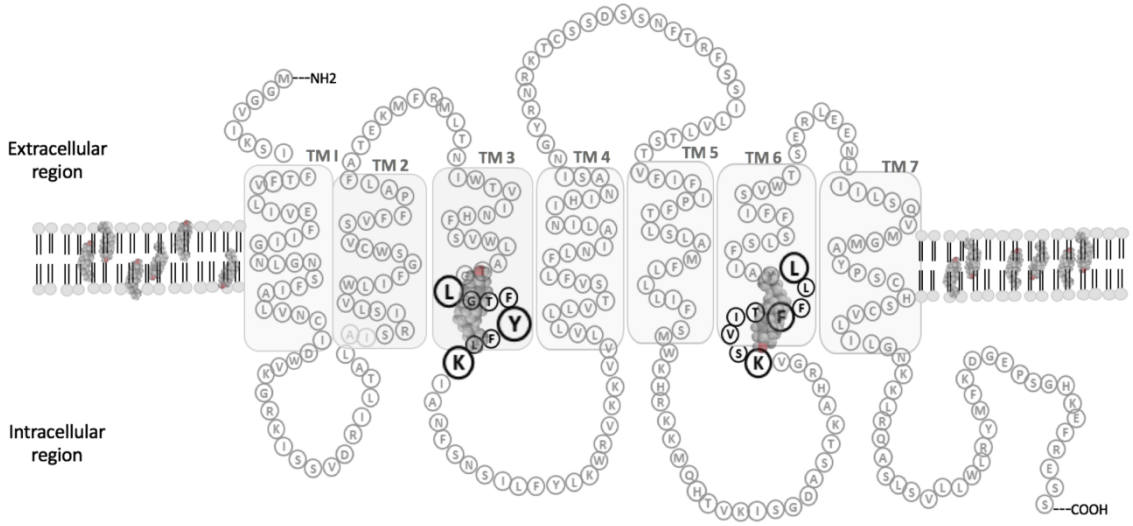

Figure 5.4.4 Two-dimensional representation of the T2R14 amino acid sequence. Shown is a secondary structure model of membrane embedded T2R14. The transmembrane segments of the protein were predicted using TMpred, TMHMM and HMMTOP servers. The putative cholesterol recognition motifs, CRAC and CARC are present in TM3 and TM6 respectively. The motifs are highlighted in bold circles and the residues within the motifs, which are conserved across human T2R family are shown in bold enlarged circles. Membrane cholesterol molecules are shown in a space-filled molecular representation close to the putative sites of interaction with T2R14.

```
A                    CRAC motif
T2R1       INELELWLATWLGVFYCAKVASVRHPLFIWLKMRISKLVPWMILGSLLYVSMICVF-
T2R3       TNHLSIWLATCLGVLYCLKIASFSHPTFLWLKWRVSRVMVWMLLGALLLSCGSTAS-
T2R4       LDSSSVWFVTLLNILYCVKITNFQHSVFLLLKRNISPKIPRLLLACVLISAFTTCL
T2R5       VSQASLWFATFLSVFYCKKITTFDRPAYLWLKQRAYNLSLWCLLGYFIINLLLTVQ-
T2R7       TNHLSIWFATCLSIYYFFKIGNFFHPLFLWMKWRIDRVISWILLGCVVLSVFISLP-
T2R8       ANYLNMWITTCLNVFYFLKIASSSHPLFLWLKWKIDMVVHWILLGCFAISLLVSLI-
T2R9       ANNSSLWFTSCLSIFYLLKIANISHPFFFWLKLKINKVMLAILLGSFLISLIISVP-
T2R10      GNQSSMWFATSLSIFYFLKIANFSNYIFLWLKSRTNMVLPFMIVFLLISSLLN
T2R13      SNHFNLWLATIFSIFYLLKIASFSSPAFLYLKWRVNKVILMILLGTLVFLFLNLIQ-
T2R14      INHFSVWLATGLGTFYFLKIANFSNSIFLYLKWRVKKVVLVLLLVTSVFLFLNIAL-
T2R16      FNILTFWLNSLLTVFYCIKVSSFTHHIFLWLRWRILRLFPWILLGSLMITCVTIIP-
T2R38      ANQANLWLAACLSLLYCSKLIRFSHTFLICLASWVSRKISQMLLGIILCSCICTVL-
T2R39      LNFCSLWFAAWLSFFYFVKIANFSYPLFLKLRWRITGLIPWLLWLSVFISFSHSM--
T2R41      LNSATFWFCSWLSVLFCVKIANITHSTFLWLKWRFPGWVPWLLLGSVLISFIITLL-
T2R42      TNHLTTWLATCLSIFYFFKIAHFPHSLFLWLRWRMNGMIVMLLILSLFLLIFDSLV-
T2R43      INHFSNWLATTLSIFYLLKIANFSNFIFLHLKRRVKSVILVMLLGPLLFLACHLFV-
T2R44      TGHFSNWLATSLSIFYLLKIANFSNLIFLHLKRRVKSVILVMLLGPLLFLACQLFV-
T2R45      TGHFSNWPATSLSIFYLLKIANFSNLIFLRLKRRVKSVILVVLLGPLLFLACHLFV-
T2R46      INHFSNWLATSLSIFYLLKIANFSNLIFLHLKRRVKSVVLVILLGPLLFLVCHLFV-
T2R47      TNHFSSWLATSLSMFYLLRIANFSNLIFLRIKRRVKSVVLVILLGPLLFLVCHLFV-
T2R48      TNHFSMWLAASLSIFCLLKIANFSNLISLHLKKRIKSVVLVILLGPLVFLICNLAV-
T2R49      TNHFSIWLATSLSIFYLLKIVNFSRLIFHHLKRKAKSVVLVIVLGSLFFLVCHLVM-
T2R50      TNHFSMWLAANLSIFYLLKIANFSNLLFLHLKRRVRSVILVILLGTLIFLVCHLLV-
T2R60      LNAATLWSSTWLSVFYCVKIATFTHPVFFWLKHKLSGWLPWMLFSSVGLSSFTTIL-
            .    *  : :      ::           :           :
                                                CARC motif
T2R1       AVLLLIFSLGRHTRQMRNTVAGSRVPGRGAPISALLSILSFLILYFSHCMIKVF-
T2R3       LLIFSLGRHTRQMLQNGTSSRDPTTEAHKRAIRIILSFFFLFLLYFLAFLIASF
T2R4       LLIHSLRRHIQKMQKNATGFWNPQTEAHVGAMKLMVYFLILYIPYSVATLVQYLPFY
T2R5       MLIVSLYTHHKKMKVHSAGRRDVRAKAHITALKSLGCFLLLHLVYIMASPFSITSKT
T2R7       LLILSLRRHIRRMQLSATGCRDPSTEAHVRALKAVISFLLLFIAYYLSFLIATSSYF
T2R8       LLVRSLWRHTKQIKLYATGSRDPSTEVHVRAIKTMTSFIFFFFLYYISSILMTFSYL
T2R9       LLLFSLVRHTKQIRLHATGFRDPSTEAHMRAIKAVIIFLLLLIVYYPVFLVMTSSAL
T2R10      FLIISLWRHNRQMQSNVTGLRDSNTEAHVKAMKVLISFIILFILYFIGMAIEISCFT
T2R13      SFLLLIFSLQKHLQKMQLNYKGHRDPRTKVHTNALKIVISFLLFYASFFLCVLI-
T2R14      LLLIFSMWKHRKKMQHTVKISGDASTKAHRGVKSVITFFLLYAIFSLSFFISVWTSE
T2R16      STIFLMASLTKQIQHHSTGHCNPSMKARFTALRSLAVLFIVFTSYFLTILITIIGTL
T2R38      MLTVSLGRHMRTMKVYTRNSRDPSLEAHIKALKSLVSFFCFFVISSCVAFISVPLLI
T2R39      LLILSLKRHTLHMGSNATGSNDPSMEAHMGAIKAISYFLILYIFNAVALFIYLSNM-
T2R40      LLILSLKRHTLHMGSNATGSRDPSMKAHIGAIKATSYFLILYIFNAIALFLSTSNI-
T2R41      LLINSLRRHTQRMQHNGHSLQDPSTQAHTRALKSLISFLILYALSFLSLIIDAAKFI
T2R42      FLFLSLVRHTRNLKLSSLGSRDSSTEAHRRAMKMVMSFLFLFIVHFFSLQVANWIFF
T2R43      LLICSLCKHLKKMQLHGKGSQDPSTKVHIKALQTVISFLLLCAIYFLSIMISVWSFG
T2R44      LLICSLCKHLKKMQLHGKGSQDPSTKVHIKALQTVIFFLLLCAVYFLSIMISVWSFG
T2R45      LLVCSLCKHLKKMQLHGKGSQDPSTKVHIKVLQTVISFFLLRAIYFVSVIISVWSFK
T2R46      LLICSLCKHLKKMQLHGKGSQDPSMKVHIKALQTVTSFLLLCAIYFLSIIMSVWSFE
T2R47      LLICSLCKHLKKMQLHGKGSQDPSTKVHIKALQTVTSFLLLCAIYFLSMIISVCNFG
T2R48      LLICSLCKHLKKMRLHSKGSQDPSTKVHIKALQTVTSFLMLFAIYFLCIITSTWNLR
T2R49      LLIYSLCKHLKKMQLHGKGSQDPSTKIHIKALQTVTSFLILLAIYFLCLIISFWNFK
T2R50      MLICSLCKHLKKMQLHGEGSQDLSTKVHIKALQTLISFLLLCAIFFLFLIVSVWSPR
T2R60      LLITSLGRHRKKALLTTSGFREPSVQAHIKALLALLSFAMLFISYFLSLVFSAAGIF
B                                                   CRAC motif
Homo    ISLVWLIFGSWCVSVFFPALFATEKMFRMLTNIWTVINHFSVWLATGLGTFYFLKIANFS
Gorilla ISLVWLIFGSWCVSVFLPALFATEKMFRMLTNIWTVINHFSVWLATGLGTFYFLKIANFS
Pan     ISLVWLIFGSWCVSVFFPALFATEKMFRMLTNIWTVINHFSVWLATGLGTFYFLKIANFS
Macaca  ISLVWSIFGSWCVSVFFPALFATEKLLRMLTNIWTVTNHFSVWLATILGTFYFLKIANFS
Mus     ICLVLILITEAYIKIFYPQLLSPVNIIELISYLWIIICQLNVWFATSLSIFYFLKIANFS
Rattus  ITLLWSLYILKSTFSMVPNFEVAIPSTRLTNLVWIISNHFNIWLATILSIFYFLKIGNFS
Xenopus FFWQWVLSL----MILYNYITFSLDFLQLLTYISNFLELSSLWLTFTLCFTYCVKITDHP
        :    :        :   :       .: . :  .    .:*::  *   * :** :.
         CARC motif
Homo    VK-SVITFFLLYAIFSLSFFISVWTSER--LEEN-LIILSQVMGMAYPSCHSCVLILGNK
Gorilla VK-SVITFFLLYAIFCLSFFISVWTSER--LEEN-LIILSQVMGMAYPSCHSCVLILGNK
Pan     VK-SVXTFFLLYAIFCLSFFISVWTSER--LEEN-LIILSQVMGMAYPSCHSCVLILGNK
Macaca  VMQTVITFLLLYAVFLLTFFISIWASVR--LKENQIIILSEMMGLAYPSGHSCVLILGNK
Mus     TIKVLLSFIILFILHFMGITINVICLLI--PESNLLFMFGLTTAFIYPGCHSLILILANS
Rattus  ALKTVVAFLLLYIIFILSLFAHVWSYDF--EEKKYFIFFCLVGMFALPSLHSYILILGNS
Xenopus VLKKIFFALFLYVMYFISSGLFLFKRQQMAHWERWLFII----YQFYPTAYLGWLILLNC
        .   :   ::*: :. :     :         .. ::::        *  :   *** *
```

Figure 5.4.5 A) Multiple sequence alignment of putative CARC and CARC motifs in 25 T2Rs. Alignment of sequences was carried out using clustal omega and the cholesterol-binding motif were manually identified. The conserved CRAC sequence with tyrosine (Y) in centre with leucine (L)/ valine (V) at the amino terminus and arginine (R)/lysine (K) at the carboxy terminus are highlighted in italicized bold alphabets. The CARC motif is reverse to CRAC motif with lysine (K)/arginine(R) at the amino terminus and leucine (L)/ valine (V) at the carboxy terminus. **B)** Multiple sequence alignment of putative CARC/CARC motifs of T2R14 orthologs. Alignment of sequences was carried out using clustal omega and the cholesterol-binding motifs

were manually identified. The conserved CARC sequence with tyrosine (Y) in centre with leucine (L)/ valine (V) at the amino terminus and arginine (R)/lysine (K) at the carboxy terminus are highlighted in italicized bold alphabets. The CARC motif is reverse to CRAC motif with lysine (K)/arginine(R) at the amino terminus and leucine (L)/ valine (V) at the carboxy terminus.

type (WT) T2R14 expressing cells, upon membrane cholesterol depletion, a decreased potency (EC_{50}) for the agonist and an increased efficacy (E_{max}) was observed **(Figure 5.4.6A)**. The EC_{50} for agonist DPH are as follows: 696 ± 2.1 μM in control, 758 ± 2.8 μM in cholesterol depleted cells, and 702 ± 2.8 μM in cholesterol replenished WT-T2R14cells. Both EC_{50} and E_{max} values were restored to control levels upon membrane cholesterol replenishment **(Table 5.4.1)**. To analyse the role of conserved amino acids in the putative cholesterol binding motifs we first characterized the alanine mutations of these residues and then pursued functional characterization of the complementary amino acid substitutions (for example, replacement of Lysine with Arginine), where appropriate **(Figure 5.4.6 and Table 5.4.1)**. The L103A, Y107A, and K231A tested response similar to WT-T2R14, hence complementary amino acid substitutions and cholesterol replenishment studies were not carried out at these amino acid positions **(Figures 5.4.6 B, C and F)**. Flow cytometry showed no significant difference in cell surface receptor protein expression between the WT-T2R14 and all the T2R14 mutants **(Figure 5.4.7)**. Our calcium mobilization assays identified K110 in CRAC motif and F236, L239 in CARC motif of T2R14 to be sensitive to membrane cholesterol alterations. K110A, F236A, and L239A expressing control cells showed increased calcium responses similar to cholesterol depleted cells, however the saturation response to DPH was not achieved **(Figure 5.4.6 D, G, I)**. K110A, F236A, L239A expressing control cells exhibited increased EC_{50} compared to T2R14 WT cells. Interestingly cholesterol replenished L239A mutant exhibited increased calcium response compared to control and depleted cells **(Figure 5.4.6I)**. K110A mutant cholesterol depleted cells showed similar dose response patterns compared to the control and cholesterol replenished cells **(Figure 5.4.6D)**. In the cells expressing complementary mutation K110R, an increase in EC_{50} upon cholesterol depletion similar to that of the WT receptor was observed

(Table 5.4.1). With F236A mutation, cholesterol depleted cells showed decreased EC_{50} values indicating potent agonist activity compared to the control and replenished cells. With complementary substitution F236Y, hyperactivation of the receptor was observed in control and the dose-response did not reach saturation **(Figure 5.4.6H)**. Hence, we were unable to determine the EC_{50} for this group. For the F236 mutants, there is no change in EC_{50} for cholesterol depleted and replenished treatments **(Table 5.4.1)**. In cells expressing complementary L239I mutation, control cells exhibited lower EC_{50} values indicating higher agonist potency, and EC_{50} for depleted and replenished were similar **(Table 5.4.1)**. This mutational data demonstrates that CRAC and CARC motifs are important structural requirements for membrane cholesterol binding in T2R14.

Immunoblot analysis of control and cholesterol modulation HEK293T-T2R14 cell lysates shows that there were no differences observed in the T2R14 expression levels **(Figure 5.4.8A).** Membrane cholesterol estimation in cell membrane extracts from HEK-T2R14 cell lines shows that 10 mM MßCD treatment resulted in a statistically significant reduction ($p<0.001$ vs. untreated) in membrane cholesterol **(Figure 5.4.8B)**.

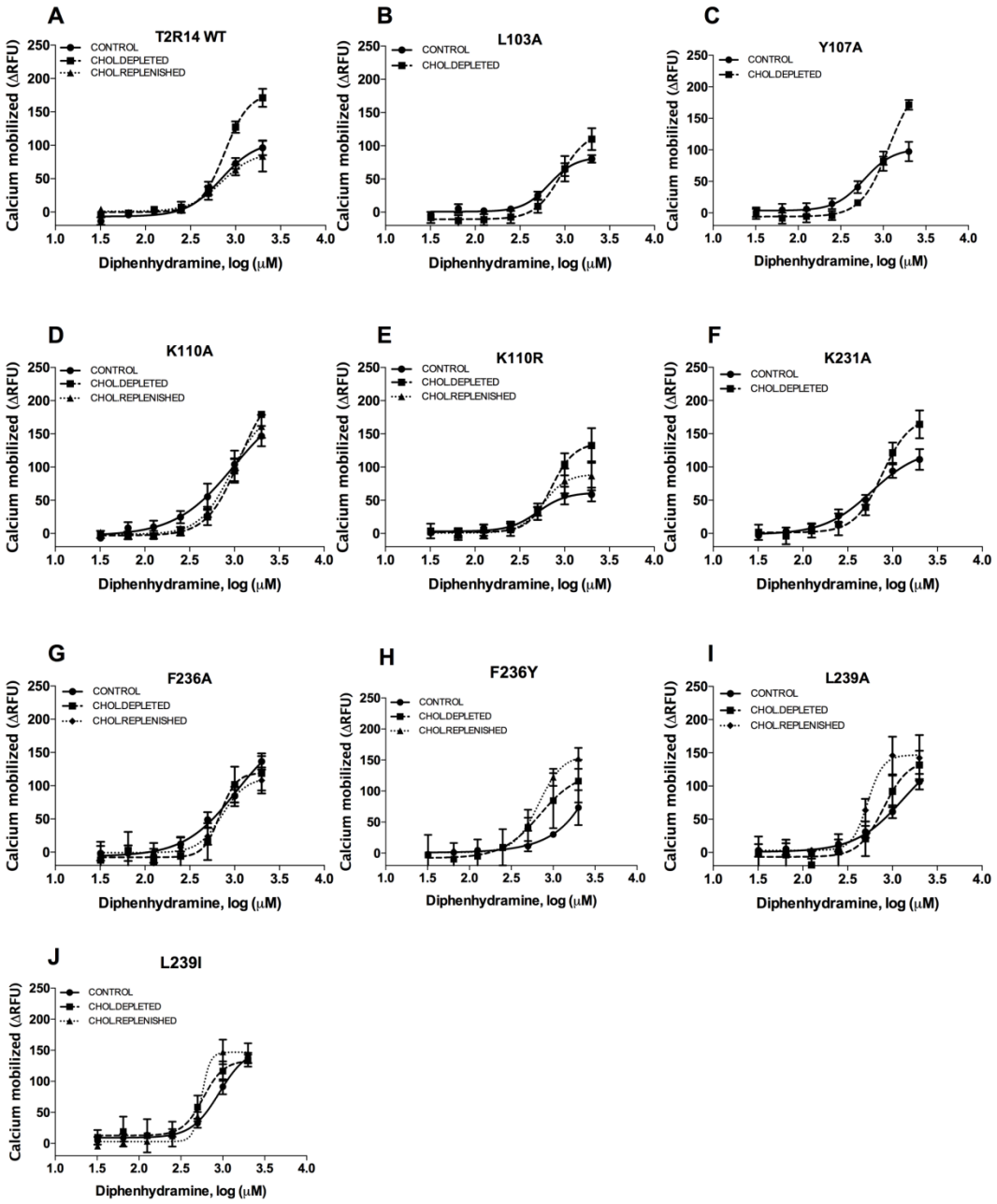

Figure 5.4.6 Mutational analysis of the cholesterol binding motifs CRAC and CARC in T2R14. T2R14 WT and mutants were transiently transfected in HEK293T cells and treated with diphenhydramine at a concentration range from 31.25 – 2000 μM. Control cells, cholesterol depleted cells and cholesterol replenished cells are loaded with calcium binding dye Fluo-4 NW and calcium mobilized (ΔRFU) was calculated by baseline subtraction of pcDNA mock transfected cells. Nonlinear dose response cure fitting was done using GraphPad Prism version 6.0 (San Diego, CA). The data represent SEM from four independent experiments performed in triplicate.

Table 5.4.1 Pharmacological characterization of CRAC and CARC residues in T2R14. Functional characterization of the mutants was pursued by measuring intracellular calcium mobilization in response to different concentrations of T2R14 agonist diphenhydramine. Cholesterol depletion and replenishment assays were pursued as described in methods.

Mutant	**Control**		**Cholesterol depleted**		**Cholesterol replenished**	
	EC_{50} (μM)	**E_{max} (ΔRFU)**	**EC_{50} (μM)**	**E_{max} (ΔRFU)**	**EC_{50} (μM)**	**E_{max} (ΔRFU)**
T2R14	696±2.1 #	96±5.7	758±2.8	171±13	702±2.8	83±23
L103A	669±2.9	87±8.6	899±2.7	109±16		
Y107A	594±2.7	97±15	1158±3.0	171±7		
K110A	979±2.8 *	146±15	1132±3.0	161±21	920±2.9	99±29
K110R	503±2.6	58±10	712±2.8	132±26	575±2.7	60±2
K231A	588±2.7	111±15	762±2.8	164±20		
F236A	1029±2.8 *	117±22	683±2.7	118±25	723±2.8	107±19
F236Y	ND	98±22	689±2.7	115±34	672±2.8	152±16
L239A	1326±2.9 *	106±11	793±2.8	131±21	528±2.7	142±39
L239I	908±2.9	137±8	584±2.7	150±19	558±2.7	145±15

* corresponds to a $p<0.05$ vs. T2R14 (denoted with an #).

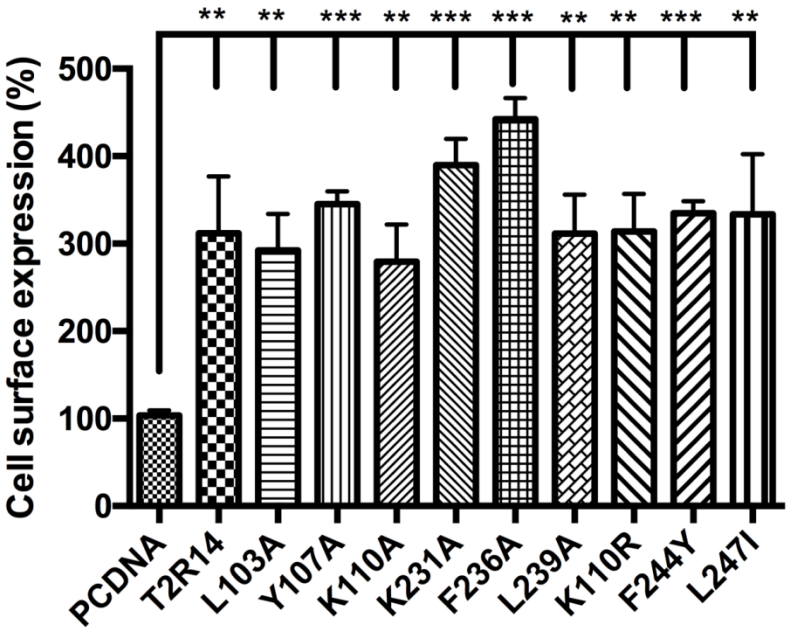

Figure 5.4.7 Analysis of cells surface expression of FLAG-T2R14 WT and mutants. HEK cells transfected with T2R14 WT and mutants were incubated with APC conjugated FLAG antibody (1:500 dilution) and the cell surface expression is normalized to mock transfected cells and presented as percentage cell surface expression compared to mock. Data represents from two independent experiments performed in duplicates. One-way ANOVA analysis was used and statistical significance was calculated between the groups using Tukey's multiple comparison test (*$p<0.05$, **$p<0.01$, ***$p<0.001$).

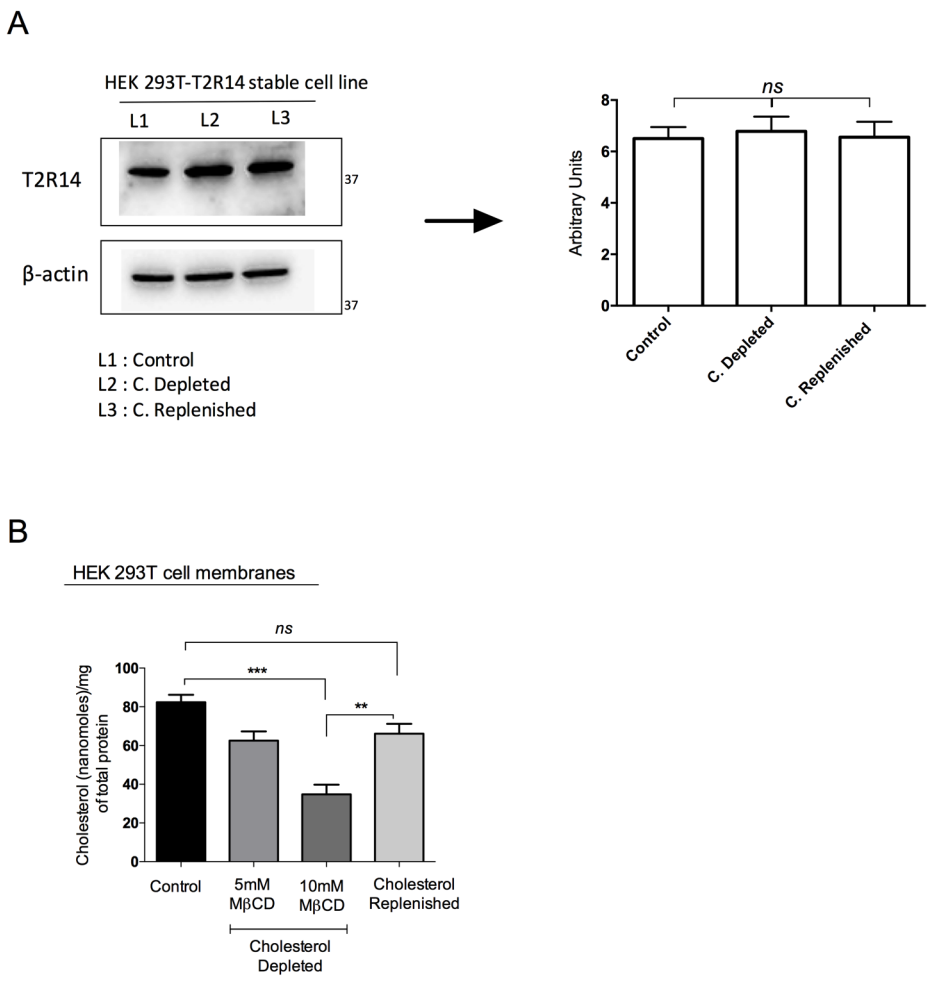

Figure 5.4.8 T2R14 expression in membrane cholesterol altered HEK293T-T2R14 cells. **A)** Immunoblot analysis of T2R14 in HEK-T2R14 cells in cholesterol altered conditions. Representative immunoblot is shown. The treatments, antibody dilutions and blot analysis are similar to figure legend 5.4.1D. **B)** Membrane cholesterol estimation in HEK-T2R14 cell membranes were similar to the conditions mentioned earlier in figure legend 5.4.1E.

5.5 DISCUSSION

Cholesterol is one of the main lipid and structural component of the cell membranes and is involved in maintaining airway function. For example, airway surfactant dysfunction in cystic fibrosis was suggested to involve excess cholesterol and its interaction with oxidized lipids (Gunasekara et al., 2017). Treatment with MβCD was suggested to improve airway surfactant function in cystic fibrosis patients (Gunasekara et al., 2017). The present work is aimed at understanding the role of membrane cholesterol in T2R14 signaling, and the underlying mechanism governing the T2R14-cholesterol interaction. Taking into consideration, the high expression levels and well known physiologically relevant responses mediated by T2R14 in the airways, we chose HASM cells and NuLi-1 as model cell systems to study the potential regulatory role of the native plasma membrane cholesterol on endogenous T2R14 signaling. Additionally, to delineate the receptor specific effects, we used heterologous expression systems to examine the role of membrane cholesterol in T2R14 signaling. Using T2R14 specific ligands (DPH and FFA), we performed pharmacological characterization of T2R14 in control and cholesterol altered states. In HASM cells, we observed a decrease in potency (increase in EC_{50}) for the agonist at the receptor in cholesterol depleted states. Similar decrease in potency for the agonist at T2R14 was observed in NuLi-1 cells, which indicates that membrane cholesterol influences T2R14 signaling in a receptor specific manner and is not cell-type dependent. An underlying cause of this sensitivity could be due to a decrease in ligand-receptor binding affinity. Due to the unavailability of radiolabelled T2R ligands, saturation experiments to measure the differences in the ligand-receptor affinities could not be pursued. However, caution should be exercised before correlating the EC_{50} shift to affinity changes, since there is precedence for cholesterol alteration resulting in an increase or decrease in agonist induced GPCR signaling

without affecting the ligand binding affinity to the receptor (Bari et al., 2005;Harikumar et al., 2005;Oddi et al., 2011).

Our findings suggest that cholesterol depleted conditions, may affect the transition of T2R14 affinity states i.e., could move into intermediate to low affinity states that might explain the decrease in agonist efficacy. As mentioned earlier, cholesterol depletion resulted in a decrease in potency (increased EC_{50}) for agonists tested, however the E_{max} values were higher in cholesterol depleted states compared to the control. This is little puzzling, as one would expect decreased potency leading to decreased efficacy for the same agonist. It is possible that depletion of membrane cholesterol might have had unintended effects on other members of the T2R signaling cascade, such as the membrane bound heterotrimeric G-protein or PLC subunits, leading to altered calcium responses (Strange, 2008). A similar decrease in potency for the agonists at T2R14 was observed with alteration of cholesterol by an alternate approach, involving enzymatic modulation of membrane cholesterol by COase treatment, instead of its physical depletion. Additional inferences that can be drawn from these results is that the lone hydroxyl group present on the steroid ring of the cholesterol molecule may be critical in its interaction with T2R14. Since, the only structural difference between cholesterol and 4-cholesten-3-one is the absence of a steroid ring hydroxyl group in the latter; instead a keto group is present as a result of oxidation at the hydroxyl group position **(Figure 5.4.3B)**. These results suggest that, it is the unavailability of the cholesterol which hampers T2R14 signaling rather than the methodology used to alter cholesterol availability to the receptor.

We demonstrate the specificity of cholesterol depletion on T2R14 signaling by pursuing competitive inhibition assays using our recently discovered novel peptide inhibitor of T2R14 (Jaggupilli et al., 2018a). Our results suggest that DPH induced T2R14 signaling is blocked by

the peptide ETSARHL with an IC_{50} of 90 to 200 μM depending on the cell type. These results suggest that the cholesterol modulation induced effects observed are predominantly T2R14 related, and not related to other GPCRs natively expressed in the cell systems used. As mentioned earlier, few class A GPCRs signaling and function have been reported to be influenced by membrane cholesterol in HASM cells, however, to our knowledge in airway epithelium, T2R14 is the first GPCR whose interplay with membrane cholesterol has been studied. Immunoblot analysis of T2R14 expressed in cholesterol-altered environments, showed no differences in membrane receptor levels. This suggests that the altered signaling by T2R14 in cholesterol-depleted conditions is not due to decreased expression of the receptors in the membrane.

Recent high-resolution structural studies have identified a strong structural association between membrane cholesterol and GPCRs such as β_2AR, A_2AR, $5HT_2$B and μ-opioid receptors (Cherezov et al., 2007;Liu et al., 2012;Manglik et al., 2012;Wacker et al., 2013). These studies have shown membrane cholesterol to be an important component in regulating GPCR activation. Unfortunately, there is no high-resolution structural information available on any T2R. In our recent structure-function study we have shown T2R4 to be sensitive to membrane cholesterol modulation, and CRAC motif might play a role (Pydi et al., 2016). In this study, we have identified K110 to play an important role in cholesterol sensitivity in T2R14. This data corroborates with previous studies on membrane proteins, where Lysine (K) in the CRAC motif was shown to interact with sterol hydroxyl group of cholesterol in T2R4 and in Peripheral Type Benzodiazepine receptors (Jamin et al., 2005;Pydi et al., 2016). Alanine mutations of the amino acids F236A and L239A in the CARC motif caused decreased ligand potency, as EC_{50} values in control cells were higher compared to WT receptor. However, upon cholesterol depletion we

observed decreased EC_{50} values and this was not recovered to control levels upon replenishment with cholesterol. The complementary mutants F236Y and L239I also exhibited similar activity as that of alanine mutants indicating these amino acids might play an important role in defining the structural stability or inherent activity of the receptor upon ligand binding. Studies have shown phenylalanine (F) and leucine (L) amino acid residues in the CARC motif to be involved in cholesterol binding (Fantini et al., 2016). Interestingly, we observed a decrease in EC_{50} upon cholesterol depletion in F236A and L239A mutants in CARC motif as opposed to an increase in EC_{50} in K110A of the CRAC motif. This difference in ligand potency between CRAC and CARC motifs can be partially described by the way cholesterol interacts with these motifs and the orientation of the motif. Studies on opioid, 5-HT and type 3 somatostatin receptors have shown Tyr or Y residue to form CH-π or –OH bond interactions with cholesterol. However, in CARC motif the aromatic amino acid F is known to exclusively form CH-π interactions and L/V are known to form van der wall interactions with cholesterol (Fantini and Barrantes, 2009;Epand et al., 2010;Fantini and Barrantes, 2013). From these results, we can infer that CRAC and CARC motifs play a significant role in cholesterol binding. This might be a reason for these CRAC and CARC motifs to be highly conserved across T2Rs and higher order vertebrates. More importantly CRAC motif is present in the TM3 of T2R14 and in recently published crystal structure of β2AR, cholesterol has been shown to interact with the cholesterol consensus residues in TM1-4 (Hanson et al., 2008). However, it is important to note that the presence of a CRAC or CARC motif should only be referred as predictive of cholesterol binding sites in GPCRs. Since a Class A GPCR, Cannabinoid receptor which contain these motifs are known to exhibit cholesterol independent activity (Oates et al., 2012).

Our findings suggest that physical interaction with the cholesterol molecule is important for T2R14 function. Interestingly, a previous study suggested the association of T2Rs and SREBP-2 (a crucial transcription factor in cholesterol metabolism) in intestinal T2R signaling and its potential implications arising from cholesterol rich dietary intake (Jeon et al., 2008). Additionally, dietary cholesterol induced stress on lipid bilayer and its detrimental effects on transmembrane receptor signaling leading to metabolic disorders have been reviewed elsewhere (Gianfrancesco et al., 2018). We speculate that, in metabolic disorders (like hyperlipidemia and obesity), whose etiology is related to dietary cholesterol intake, abnormalities in T2R signaling may arise, which may have some pathophysiological implication. Moreover, from a structural standpoint, membrane cholesterol, being an integral constituent of membrane microdomains like caveolae and lipid rafts plays a crucial role in regulating airway physiology. A recent study in airway epithelial cells has shown that CFTR molecules are predominantly confined into cholesterol enriched lipid rafts in response to microbial infections and this confinement of CFTR is membrane cholesterol dependent (Abu-Arish et al., 2015). Additionally, the importance of caveolae and lipid rafts in regulating ASM phenotypic plasticity and ASM cell membrane receptor mediated signaling is well known (Gosens et al., 2006;Hunter and Nixon, 2006;Halayko et al., 2008;Schlenz et al., 2010). Thus, it would be interesting to examine the role (if any) of lipid rafts or caveolae in airway T2R signaling.

In conclusion, this study foregrounds a novel regulatory role of membrane cholesterol in T2R14 signaling. A better understanding of various factors governing T2R function in airways could be beneficial in developing novel therapeutic avenues for different airway diseases including cystic fibrosis. Indeed, understanding of the T2R function and its concomitant

pathophysiological implications is still in its nascent stages and to this end, further studies are required.

BRIDGE TO CHAPTER 6

In chapter 5, the role of membrane cholesterol in airway T2R14 signaling was elucidated. Another, important membrane lipid which is known to regulate the structure and function of transmembrane proteins is sphingomyelin. The role of sphingomyelin in T2R function is not reported thus far. In the following chapter (Ch.6) I examined the role of membrane sphingomyelin in T2R14 signaling in airway cells and in heterologous expression system.

CHAPTER 6

6.0 The role of membrane sphingomyelin and cholesterol in bitter taste receptor T2R14 signaling

Feroz Ahmed Shaik and Prashen Chelikani

6.1 ABSTRACT

Membrane lipids regulate the structure and function of G protein-coupled receptors (GPCRs). Previously we have shown that membrane cholesterol regulates the signaling of two human bitter taste receptors (T2Rs), T2R4 and T2R14. Another major plasma membrane lipid known to influence the function of membrane proteins including GPCRs is sphingomyelin. The role of sphingomyelin in T2R function is unexplored thus far. In this work, we examined the significance of sphingomyelin in T2R14 signaling. Results suggest that unavailability of membrane sphingomyelin did not affect the agonist-promoted T2R14 Ca^{2+} signaling in heterologous expression system and also in primary human airway smooth muscle (HASM) cells. In addition, T2R14 mediated downstream AMPK activation was also unaffected in sphingomyelin depleted condition, however cholesterol depletion impaired the T2R14-mediated AMPK activation. Angiotensin II type1A receptor (AT_1R) expressed in HASM cells, and signals through Ca^{2+} and AMPK was used as a control. Results suggest that similar to T2R14, membrane sphingomyelin depletion did not affect AT_1R signaling. However, membrane cholesterol depletion impaired AT_1R mediated Ca^{2+} signaling and AMPK activation. Interestingly, amino acid sequence analysis revealed the presence of putative sphingolipid binding motif in both T2R14 and AT_1R suggesting that the presence of a motif alone might not be suggestive of sphingomyelin sensitivity. In conclusion, these results demonstrate that in contrast to membrane cholesterol, sphingomyelin does not affect the agonist-induced T2R14 signaling, however it may play a role in other aspects of T2R14 function.

6.2 INTRODUCTION

Currently humans are known to recognize five basic tastes which are sweet, umami, bitter, salt and sour (Chandrashekar et al., 2006). The bitter, sweet and umami tastes are initiated by interaction of taste molecules with integral cell membrane proteins known as G protein-coupled receptors (GPCRs) (Adler et al., 2000;Gilbertson et al., 2000;Sainz et al., 2001). Sweet taste is detected by a heterodimer of T1R2 and T1R3, and umami taste is detected by a heterodimer of T1R1 and T1R3. Bitter taste is detected by 25 GPCRs referred to as T2Rs (Adler et al., 2000;Chandrashekar et al., 2000). T1Rs belong to Class C of the GPCR family represented by the well characterized metabotropic glutamate receptors; while T2Rs were grouped with either Class F or T represented by the frizzled receptors (Munk et al., 2016). GPCRs contain a number of highly conserved motifs, such as D/ERY, NPxxY that are well studied, and non-conserved motifs like cholesterol-binding motifs (CRAC) and sphingolipid binding motifs (SBMs) that are poorly characterized (Baier et al., 2011;Jafurulla et al., 2011;Oddi et al., 2011;Bjorkholm et al., 2014;Pydi et al., 2016). Nevertheless, from a structural standpoint, the presence of these lipid-binding motifs across GPCR family underscores the importance of membrane lipids in the organization and function of GPCRs. In addition to being an integral structural constituent of the membrane, lipids contribute to a range of other cell physiological processes including acting as a substrate for post-translational modification of proteins, and recruitment of proteins through specialized signaling platforms (Simons and Ikonen, 1997;Foster et al., 2003;Sezgin et al., 2017). The main lipid composition of plasma membrane include cholesterol, sphingolipids and glycerophospholipids. However, the abundance of these lipids vary in different cell types (Harayama and Riezman, 2018).

In the context of membrane lipids allosterically regulating the function of GPCRs, cholesterol's role is widely recognized, however the role of sphingolipids still remains to be fully understood (Gimpl, 2016). Sphingolipids provide structural fluidity and permeability to the membrane, are also involved in signaling, with bioactive sphingolipid mediators controlling critical biological functions (Huwiler et al., 2000;Lonnfors et al., 2011;Hla and Dannenberg, 2012). The current work is specifically focused on sphingomyelin, a sphingolipid derivative predominantly localized in the outer membrane (Goni and Alonso, 2002). The role of sphingomyelin in regulating GPCR function has been demonstrated in a few class A GPCRs including Serotonin$_{1A}$, Serotonin$_{7}$, and cholecystokinin receptor (Harikumar et al., 2005;Sjogren and Svenningsson, 2007;Jafurulla et al., 2008;Jafurulla and Chattopadhyay, 2015;Jafurulla et al., 2017a). In these studies it was shown that in membrane sphingolipid depleted states, GPCR functions such as ligand binding, receptor trafficking and G-protein coupling were perturbed. Furthermore, it has been proposed that consensus sphingolipid binding signature sequences in Sertonin$_{1A}$ receptors may be involved in forming interactions with sphingomyelin, however the motifs were not functionally characterized (Chattopadhyay et al., 2012;Shrivastava et al., 2018). In metabotropic glutamate receptor 2 (GRM2), a specific interaction between sphingomyelin and putative sphingolipid binding motif of GRM2 has been functionally characterized (Bjorkholm et al., 2014). The role of sphingolipids in taste receptor (T1R and T2R) signaling has not been elucidated thus far. Considering the emerging role of the 25 T2Rs in various extra-oral tissues, it could be beneficial to identify additional factors like membrane lipids that could allosterically regulate T2Rs function.

We have previously demonstrated the role of cholesterol in regulating T2R14 signaling in primary human airway smooth muscle (HASM) cells and airway bronchial epithelial cell line (NuLi-1) (Shaik et al., 2018). Agonist potency in eliciting T2R14 signaling was perturbed in cholesterol-altered state. Furthermore, the role of CRAC motifs present in T2R4 and T2R14 forming functional interactions with membrane cholesterol was also reported (Pydi et al., 2016;Shaik et al., 2018). In this study, we hypothesize that similar to cholesterol, sphingomyelin could play a role in regulating T2R14 signaling. As a control, we selected a highly studied Class A GPCR, Angiotensin II type1A receptor (AT_1R) that is significantly expressed in HASM cells and upon activation causes increase in Ca^{2+} mobilization just as T2Rs (Veerappan et al., 2008;Li et al., 2012;Zhang et al., 2015a). Furthermore, both T2R14 and AT_1R have a putative SBM. The role of sphingomyelin in T2R14 signaling was studied using both, a heterologous T2R14 overexpressing system and T2R14 natively expressed in HASM cells. A combination of bioinformatics analysis, live-cell functional assays, and second messenger induced protein phosphorylation studies were utilized to characterize the role of sphingomyelin and cholesterol in T2R14 signaling.

6.3 METHODS

6.3.1 Reagents

Diphenhydramine (DPH), Flufenamic acid (FFA), Angiotensin II human and Sphingomyelinase (SMase, Cat. #S8633), Phosphatase inhibitor cocktail 3 (Cat. #539131) were acquired from Sigma Aldrich. DMEM/F12, Fetal bovine serum, Penicillin-streptomycin, Hygromycin B (Cat. #10687010), Fluo-4 NW Calcium assay kit, Amplex Red Sphingomyelinase Assay Kit (Cat. #A12220) were acquired from ThermoFisher Scientific. N-dodecyl-D-maltopyranoside (Cat. #D310S) was obtained from Anatrace. Protease inhibitor cocktail (Cat.

#539131) was obtained from Millipore Sigma and Bovine serum albumin (Cat. #0332) was acquired from VWR life sciences. Antibodies used were obtained from the following sources: Phospho-AMPKα (Thr172) antibody (Cat. #2535, Cell Signaling Technology), T2R14 antibody (Cat. #C120957, LSBio), AT_1R antibody (Cat. #SC1173, Santa Cruz Biotechnology), ß-actin antibody (Cat. #A5441, Sigma-Aldrich), Anti-rabbit secondary antibody (Cat. #170-6515, Bio-Rad), Anti-mouse secondary antibody (Cat. #31430, ThermoFisher Scientific).

6.3.2 Cell Culture

HEK293T-T2R14 stable cell line generation was done as per our earlier published protocol (Chakraborty et al., 2015;Jaggupilli et al., 2018a). The HEK-T2R14 and human airway smooth muscle (HASM) cells were cultured in DMEM/F12 media supplemented with 10% FBS and 1% penicillin (100 units/ml) –streptomycin (100 µg/ml). The HASM cells used were from passage 2-4 and the source of HASM cells is as previously described (Shaik et al., 2018). Cell culture and treatments were carried out in a humidified atmosphere with 5% CO_2 at 37°C.

6.3.3 Membrane Sphingomyelin Depletion and Cell Membrane Preparation

HEK293T-T2R14 cell lines were grown to confluency and treated with SMase at different concentrations of 0, 25, 50 and 100 mu/ml (milliunits/millilitre). SMase was dissolved in basal media and added to the cells and incubated for 90 min at 37°C. Then the cells were washed with PBS and harvested for cell membrane isolation. Cell membrane isolation was performed as previously described (Pydi et al., 2016;Shaik et al., 2018). In brief, control and SMase treated cells were harvested in a hypotonic lysis buffer (10mM Tris, 5mM EDTA, 1x protease inhibitor cocktail; pH 7.4) and homogenized mechanically with a dounce homogenizer followed by centrifugation at 500xg for 10min (4°C). The post-nuclear supernatant was collected

and subjected to ultracentrifugation at 45,000xg for 30 min (4°C). The membrane pellet was resuspended in storage buffer (50mM Tris, 1x protease inhibitor cocktail; pH 7.4). The total protein concentration in the membrane extracts was determined using a modified Lowry method (Lowry et al., 1951).

6.3.4 Membrane sphingomyelin quantification

Membrane sphingomyelin quantification of control and sphingomyelin-altered cells was done using Amplex red sphingomyelinase assay kit as per the manufacturer's instructions with some modifications as described before (Viswanathan et al., 2018). HEK293T-T2R14 membrane protein extracts of 50 µg were used to quantitate the sphingomyelin content. Standard curve of known concentrations of sphingomyelin (in the range of 0-50 nanomoles), each treated with a constant 25 mu/ml SMase were plotted. The unknown sphingomyelin content in the untreated and SMase treated HEK293T-T2R14 membrane samples was determined by comparing their corresponding fluorescence values with that of the standards. Fluorescence microplate reader with excitation at 530 nm and emission at 590 nm was used for detection, and fluorescence values were corrected for background and normalized to protein concentration.

6.3.5 Membrane cholesterol alterations

Membrane cholesterol depletion in HASM cells was performed as per our published protocols (Shaik et al., 2018). The membrane cholesterol-altered HASM cells were used for immunoblot analysis and functional assays. For immunoblot analysis, HASM cell monolayers were treated with 10 mM MßCD for 30 min at 37°C followed by agonist stimulation with 500 µM DPH or 10 µM AngII for 5 min at 37°C. The agonist-treated, control and MßCD pretreated cells were washed with PBS followed by harvesting of cells for cell lysate preparation.

6.3.6 Calcium mobilization assay

HEK293T-T2R14 stable cells and HASM cells were seeded at a density of $1x10^5$ cells/well and $4x10^4$ cells/well of 96 well plates, respectively, and cultured overnight in growth media. Then, cells were serum starved for 3 h followed by a 90 min treatment with 100 mu/ml SMase (dissolved in basal media). Next the T2R14 or AT_1R function in HEK293T-T2R14 and HASM cells was characterized by measuring their respective cognate agonist promoted mobilization of intracellular calcium ($[Ca^{2+}]_i$) as previously described (Shaik et al., 2018).

6.3.7 Immunoblot analysis

Cells were lysed in lysis buffer (20mM Tris, 500mM NaCl, 10% Glycerol and 20mM N-dodecyl-D-maltopyranoside) with 1x protease and 1x phosphatase inhibitors. 20µg of total protein equivalent samples were resolved on a 12% SDS-PAGE gel followed by transfer of proteins onto a nitrocellulose membrane. Blots were blocked in TBST with 5% BSA for 1h at 4°C. Primary antibody incubation was done overnight at 4°C and the antibody dilutions were prepared in TBST with 3% BSA. The antibody dilutions used are as follows: Phospho-AMPKα, AMPKα, T2R14 at 1:1000; beta-actin and secondary antibodies at 1:5000. Chemiluminescence based detection was used for band detection and for imaging Vibrant Lourmat Fusion FX7 imager was used. Densitometric band analysis was performed using ImageJ software (NIH) (Schneider et al., 2012).

6.3.8 Amino acid sequence analysis

The occurrence of putative SBM in T2Rs and other select GPCRs, metabotropic glutamate receptors (GRM) was determined by scanning the amino acid sequences for SBM motif using ScanProsite program (ExPASy, SIB) (Sigrist et al., 2013). The motif submitted for

scanning is as follows, [VITL]-X(2)-[VITL]-[VITL]-X(2)-[VITL]-[FWY], where X corresponds to any amino acid residue. Transmembrane prediction of the GPCRs was performed using online servers, HMMTOP2.0 (Krogh et al., 2001) and TMpred (Ikeda et al., 2003).

6.3.9 Statistical analysis

Statistical analysis of the data was performed using either an unpaired students t-test or one-way ANOVA with Tukey's post-hoc multiple comparison tests. A p-value of <0.05 was considered statistically significant and all analyses were performed using GraphPad Prism 6.0 (San Diego, CA).

6.4 RESULTS

6.4.1 Identifying putative SBMs in taste receptors

Prediction of putative SBMs in taste receptors (T1Rs and T2Rs) and other select GPCRs was pursued as described in the methods. The putative SBM which is purported to be predominantly present in the TM6 region of GPCRs (Bjorkholm et al., 2014) was not conserved in T2Rs **(Figure 6.4.1A)**. Only 3 out of the 25 human T2Rs, namely T2R9, T2R14, and T2R16 had the SBM in TM6 region **(Figure 6.4.1A)**. Next, we did sequence alignment of GRMs (1-8) with T1Rs both of which belong to class C GPCRs. In all the GRMs and in T1R1, the putative SBM is present in the TM6 region **(Figure 6.4.1B)**. In addition, a few well-characterized class A GPCRs including AT_1R were also analysed for the presence of SBM (data not shown), and no consistent pattern of SBM occurrence was observed. More specifically, in AT_1R, the SBM was not present in the TM6 region.

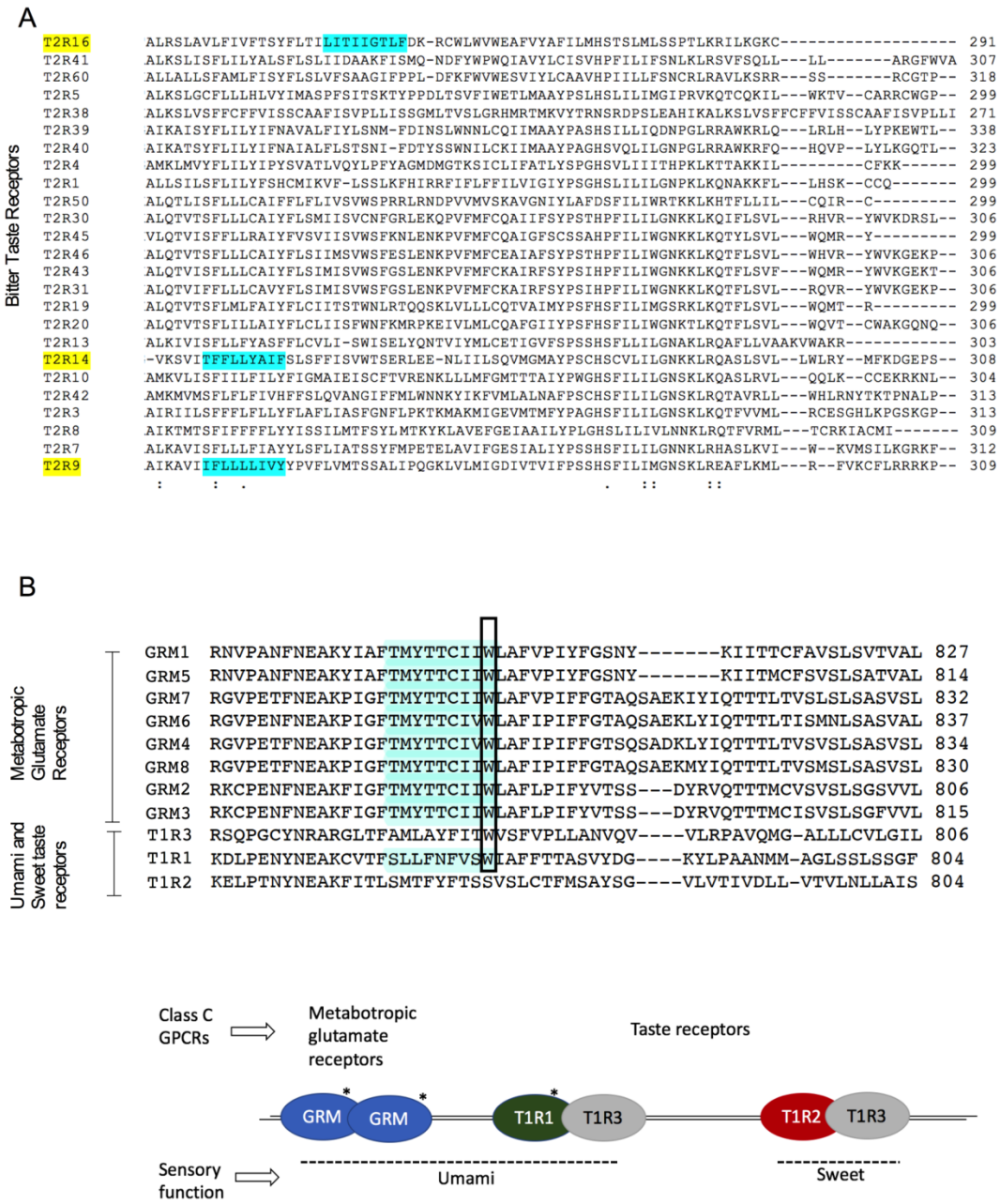

Figure 6.4.1. Analysis of sphingolipid binding motifs (SBM) in taste receptors (T1Rs and T2Rs) and metabotropic glutamate receptors (GRMs). **A)** Multiple sequence alignment of T2R regions. The analysis was carried out as described in methods for the complete T2R sequences. For clarity only the relevant portion of T2Rs are shown. The putative SBMs are only present in TM6 of 3T2Rs and highlighted in teal. **B)** Multiple sequence alignment of specific regions of T1Rs and GRMs (Class C GPCRs). Putative SBMs are highlighted in teal and the conserved Tryptophan (W) is shown in a box. In the lower panel, an illustration of heterodimers belonging

to Class C GPCRs involved in detection of umami and sweet tastes are shown. (* corresponds to presence of SBM).

6.4.2 Characterization of T2R14 signaling in sphingomyelin modulated membrane environment

To determine if T2R14 signaling is sensitive to sphingomyelin, we modulated the membrane sphingomyelin levels by exogenous addition of SMase. As shown in **figure 6.4.2A**, SMase treatment hydrolyses sphingomyelin to ceramide and phosphorylcholine and thereby decreasing the membrane sphingomyelin content. SMase at concentration of 100 mu/ml resulted in a 62.7 % reduction in sphingomyelin levels in the membrane extracts isolated from HEK293T-T2R14 cells **(Figure 6.4.2B)**. Therefore, SMase at a concentration of 100 mu/ml was used to deplete the membrane sphingomyelin content in live cells, which were used to characterize the function of T2R14. Pharmacological characterization of T2R14 in sphingomyelin-depleted condition was done using T2R14-specific agonist DPH **(Figure 6.4.2C)**. No significant effect of membrane sphingomyelin depletion on agonist-induced T2R14 signaling was observed. The T2R14 specificity of DPH was confirmed using a peptide (ETSARHL) inhibitor (Jaggupilli et al., 2018a;Shaik et al., 2018). The half-maximal inhibitory concentration (IC_{50}) for ETSARHL against T2R14 heterologously expressed in HEK293T was 91.9 ± 1.2μM **(Figure 6.4.2D)**.

6.4.3 Characterization of sensitivity of T2R14 and AT_1R signaling to membrane sphingomyelin and cholesterol in HASM cells

Similar to results obtained in the heterologous expression, the T2R14 signaling in primary HASM cells was unaffected by sphingomyelin depletion **(Figure 6.4.3A)**. Of note, we recently reported the T2R14 expression, its specificity to DPH and its signaling sensitivity to membrane cholesterol in HASM cells (Shaik et al., 2018). Next, we analyzed the sensitivity of AT_1R signaling in HASM cells to membrane sphingomyelin and cholesterol depletion. As shown

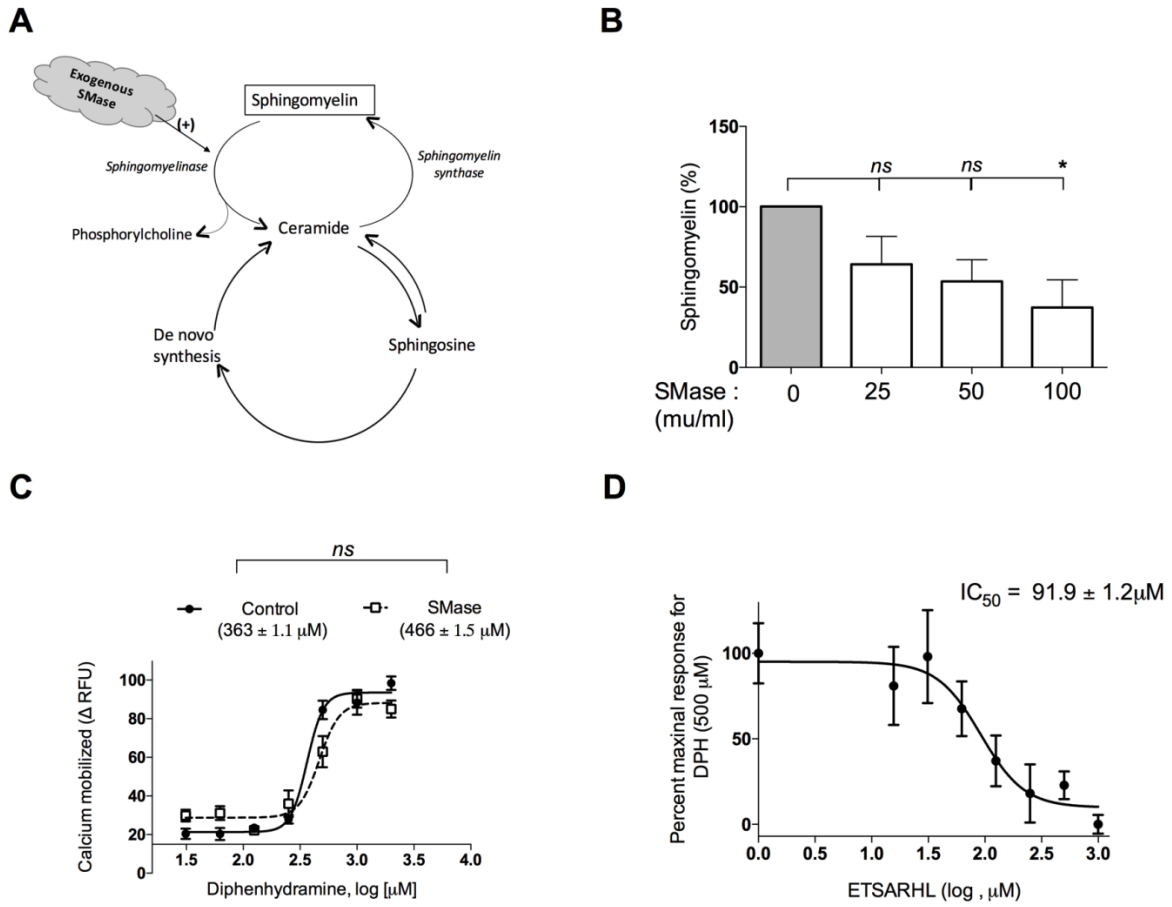

Figure 6.4.2 Analysis of T2R14 signaling in sphingomyelin modulated membrane environment. **A)** Schematic of key steps in sphingomyelin metabolism. **B)** Quantification of sphingomyelin levels in HEK293T-T2R14 cell membrane extracts. Percent decrease in sphingomyelin in SMase treated groups relative to control is shown. Data represented as mean ± S.E for 3 independent experiments performed in triplicate (ns, non-significant; *$p<0.05$). **C)** Dose-response curve for Ca^{2+} mobilized by agonist Diphenhydramine (DPH) in HEK293T-T2R14 stable cells. Control and SMase (100 mu/ml) treated cells were stimulated with indicated concentrations of DPH. Dose dependent changes in the fluorescence values in HEK293T cells stimulated with DPH are taken as baseline. The baseline values are subtracted from the dose-response values of HEK293T-T2R14 and plotted as ΔRFU. EC_{50} values are calculated from the non-linear regression of the dose-response data and is shown in brackets. Each data point corresponds to mean ± S.E form 3 independent experiments performed in triplicate (ns, non-significant). **D)** Characterization of peptide ETSARHL as an inhibitor of DPH-induced T2R14 signaling in HEK293T-T2R14 cells. Competition Ca^{2+} mobilization assay was performed with a single concentration (500 μM) of DPH in the presence of increasing concentration of ETSARHL (15.6-

1,000 μM) in HEK293T-T2R14 stable cell line. Competition Ca^{2+} mobilization assay performed in HEK293T cells was taken as baseline. Shown are the HEK293T-T2R14 values subtracted from the baseline and plotted as ΔRFU. The IC_{50} value was calculated by nonlinear regression analysis of the dose-response data. Data shown are from at least 3 independent experiments performed in triplicate.

in **figure 6.4.3B-C**, AT_1R-mediated calcium signaling is unaffected in SMase pretreated cells, however cholesterol depletion, using MßCD pretreatment impaired the Angiotensin II induced AT_1R signaling.

6.4.4 Characterizing the effect of HASM cell membrane lipid modulation on T2R14 and AT_1R induced AMPK activation

Since AMPK is one of the major regulatory element linked to stress or stimuli induced intracellular Ca^{2+} flux, we analyzed whether T2R14 stimulation, activates (phosphorylates) downstream AMPK in HASM cells and the role of membrane lipids in this process. AT_1R is known to phosphorylate AMPK through Ca^{2+}/calmodulin pathway (Kim et al., 2017b). As shown in **figure 6.4.4A**, DPH (500µM) activated T2R14 causing an increase in p-AMPK and it is attenuated in cholesterol depleted condition ($p<0.01$ vs. control). However, SMase treatment did not affect the T2R14 signaling **(Figure 6.4.4A)**. Similar to T2R14, AT_1R activation-mediated AMPK phosphorylation was impaired in membrane cholesterol depleted conditions ($p<0.05$ vs. control), but not in SMase treated cells **(Figure 6.4.4A)**.

To further confirm the receptor specificity of T2R14-induced activation of downstream AMPK, we used HEK293T-T2R14 stable cell lines. Compared to the buffer, T2R14 agonists DPH (500µM) and FFA (100µM) caused a statistically significant increase in p-AMPK **(Figure 6.4.4B)**. AT_1R natively expressed in HEK293T cell lines was stimulated with AngII (10µM) and its effect on p-AMPK is shown as a positive control **(Figure 6.4.4B)**.

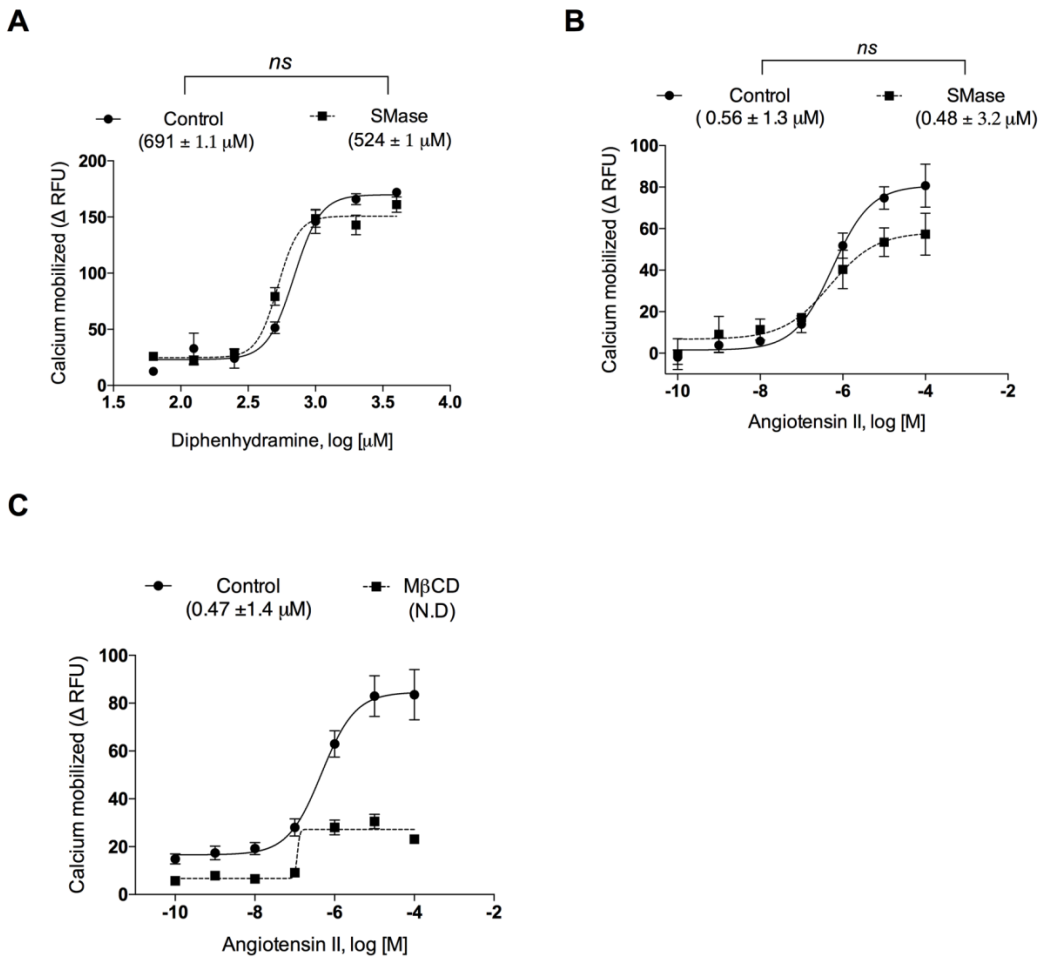

Figure 6.4.3 Effect of HASM cell membrane lipid modulation on T2R14 and AT_1R signaling. **A, B)** Dose-response curves for Ca^{2+} mobilization by DPH and AngII in HASM cells. Control and SMase (100 mu/ml) treated HASM cells were stimulated with indicated concentrations of DPH (panel A) and AngII (panel B). **C)** Dose-response curves for Ca^{2+} mobilization by Ang II in control and cholesterol-depleted (10 mM MßCD treated) HASM cells. The EC_{50} values of respective agonists are shown brackets. Data are mean± S.E of at least 3 independent experiments done in triplicate (ns, non-significant; N.D, not determined due to ambiguous EC_{50} value).

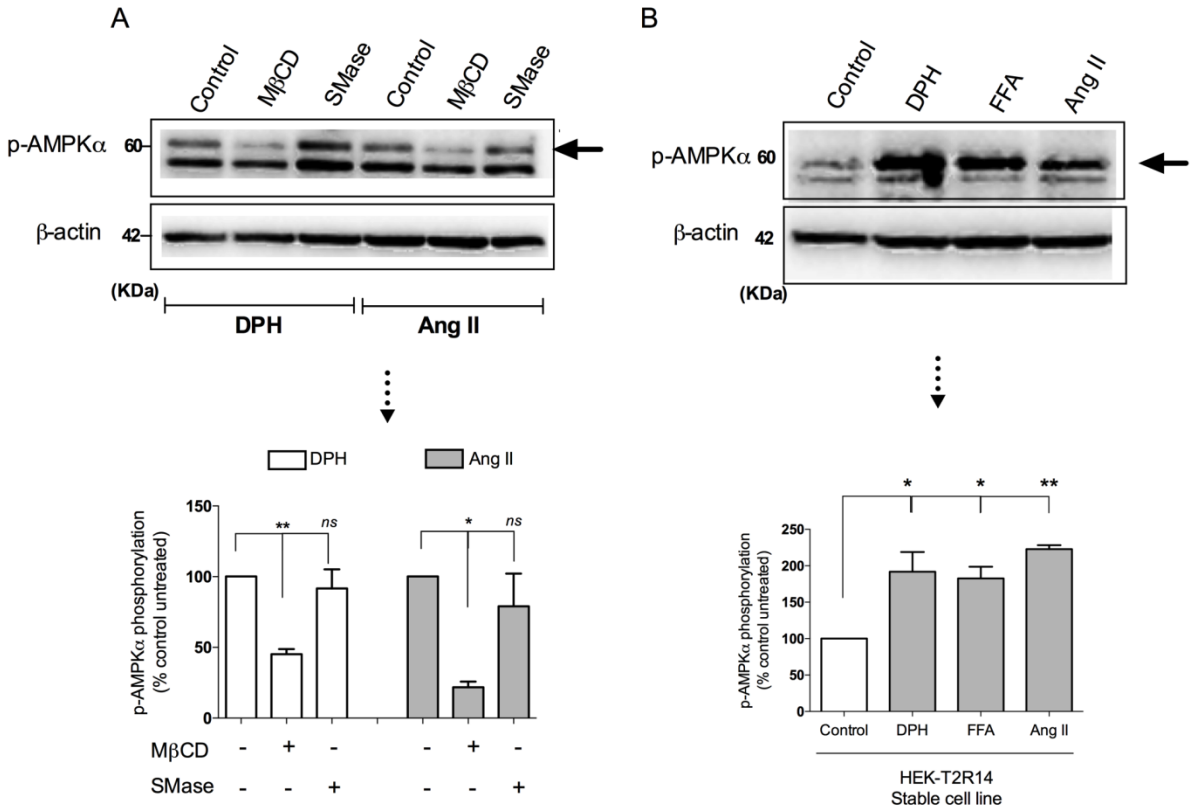

Figure 6.4.4 Analysis of T2R14 and AT_1R induced AMPK activation in membrane sphingomyelin and cholesterol modulated environments. **A)** Membrane cholesterol and sphingolipid sensitivity of T2R14 and AT_1R mediated AMPK activation. HASM cell monolayers were pretreated for 90 min at 37ºC with either 10 mM MßCD or 100 mu/ml SMase, or buffer (control) followed by an agonist stimulation (500 µM DPH, 10 µM AngII) for 5 min. DPH and AngII stimulation induced AMPK phosphorylation (p-AMPK) is shown in the blots. Pixel density analysis corresponds to data from 3 independent blots and data are expressed as percentage of p-AMPK in cholesterol-depleted (10 mM MßCD treated) and sphingomyelin depleted (100 mu/ml SMase treated) relative to their respective control groups. ß-actin was used as a loading control. Shown is a representative blot from 3 independent blots. (**p<0.01, *p<0.05, ns non-significant). **B)** HEK293T-T2R14 stable cells were treated with either buffer or T2R14 agonists (500 µM DPH, 100 µM FFA) or AT_1R agonist (10 µM Ang II) for 5 min followed by immunoblot analysis for AMPK phosphorylation. Shown is a representative blot from at least 3 independent experiments. Densitometric analysis represents the pixel density of the bands from 3 independent blots. The agonist induced AMPK phosphorylation is expressed as percentage increase over buffer induced p-AMPK. ß-actin was used as a loading control (**p<0.01, *p<0.05, ns non-significant).

CRAC motif

L/V-X(1-5)-Y-X(1-5)-R/K

Metabotropic Glutamate Receptors

Umami and Sweet taste receptors

```
GRM1  VAIQVQNLLQLFDIPQIAYSATSIDLSDKTLYKYFLRVVPSDTLQARAMLDIVKRYNWTY 226
GRM5  VAIQVQNLLQLFNIPQIAYSATSMDLSDKTLFKYFMRVVPSDAQQARAMVDIVKRYNWTY 213
GRM6  VSIMVANVLRLFAIPQISYASTAPELSDSTRYDFFSRVVPPDSYQAQAMVDIVRALGWNY 215
GRM7  VSIMVANILRLFQIPQISYASTAPELSDDRRYDFFSRVVPPDSFQAQAMVDIVKALGWNY 220
GRM4  VSIMVANILRLFKIPQISYASTAPDLSDNSRYDFFSRVVPSDTYQAQAMVDIVRALKWNY 220
GRM8  VSIMVANILRLFKIPQISYASTAPELSDNTRYDFFSRVVPPDSYQAQAMVDIVTALGWNY 217
GRM2  VSIQVANLLRLFQIPQISYASTSAKLSDKSRYDYFARTVPPDFFQAKAMAEILRFFNWTY 206
GRM3  VSIQVANLLRLFQIPQISYASTSAKLSDKSRYDYFARTVPPDFYQAKAMAEILRFFNWTY 212
T1R3  LAMVTGKFFSFFLMPQVSYGASMELLSARETFPSFFRTVPSDRVQLTAAAELLQEFGWNW 208
T1R1  RAATTAALLSPFLVPMISYAASSETLSVKRQYPSFLRTIPNDKYQVETMVLLLQKFGWTW 210
T1R2  SVMTVANFLSLFLLPQITYSAISDELRDKVRFPALLRTTPSADHHIEAMVQLMLHFRWNW 205
          .  .:  * :* ::*.:    *     :  : *. *    :  :   ::    *.:
```

Figure 6.4.5 Conserved CRAC motif in class C GPCRs (GRMs and T1Rs) is highlighted in teal.

6.5 Discussion

In the current study, we examined the role of membrane sphingomyelin in T2R14 signaling using an HEK293T heterologous expression system and primary HASM cells. To this end, we enzymatically hydrolysed sphingomyelin by exogenous addition of SMase, which depletes sphingomyelin content. SMase (EC # 3.1.4.12) is a membrane-associated enzyme, commonly used to modulate membrane sphingomyelin and to characterize sphingolipid-membrane protein interactions (Slotte and Bierman, 1988;Jafurulla et al., 2008;Gulshan et al., 2013;Eich et al., 2016). Sphingomyelin depletion did not affect T2R14 signaling in the well characterized T2R14 over-expressing HEK293T stable cell system. Here we observed that agonist-promoted T2R14 signaling is not dependent on the availability of membrane sphingomyelin but is membrane cholesterol dependent. This is in agreement with previous studies on Cholecystokinin (CCK) receptor, where it was reported that CCK signaling is not dependent on the availability of sphingomyelin but was dependent on the availability of cholesterol (Harikumar et al., 2005). Therefore, it can be inferred that different membrane lipids may distinctly modulate the T2R14 function.

Next, we characterized T2R14 function in SMase (100 mu/ml) pretreated, primary airway smooth muscle cells. We chose primary airway cells to study the native sphingolipid-T2R14 interaction in view of the significance of membrane sphingolipids in regulating the function of several other airway cell membrane proteins like CFTR and TGF-ß (Aureli et al., 2016;Liu et al., 2016a;Pan et al., 2018). Similar to the heterologous system, T2R14 signaling was unperturbed by SMase treated primary HASM cells. Additionally, we examined sphingomyelin sensitivity of AT_1R natively expressed in primary HASM cells. AT_1R signals through a similar cascade as

T2Rs in HASM cells, and also localizes within the caveolae (cholesterol and sphingomyelin enriched membrane assemblies) (Burger et al., 2000;Ushio-Fukai et al., 2001;Veerappan et al., 2008;Lu et al., 2010;Oh et al., 2011;Zhang et al., 2014). AngII induced Ca^{2+} signaling was unperturbed by SMase treatment, however, cholesterol depletion by MßCD treatment impaired the AT_1R signaling as demonstrated by the EC_{50} values for AngII. This suggests that cholesterol may allosterically regulate the interaction of AT_1R and T2R14 with their cognate ligands whereas sphingolipids may not be important in this context. However, there are few caveats; we have only examined the agonist-induced receptor mediated Ca^{2+} signaling in live cells, and other aspects of GPCR function including trafficking, signaling in micro-domains, and G-protein independent signaling, are not characterized in this study. Sphingomyelin being an integral constituent of membrane micro-domains may affect optimal T2R14 and AT_1R signaling and function.

We then examined if the lipid sensitivity (or lack thereof, as in the case of sphingomyelin) in T2R14 calcium signaling in airways translates into its downstream Ca^{2+} / CaMKKß linked AMPK activation. Recently, it was shown that T2R10 activates AMPK in enteroendocrine L- cells (Kim et al., 2018b). Moreover, AMPK activation plays a major role in airway smooth muscle physiology (Liu et al., 2016a;Pan et al., 2018). Agonist (DPH) activated T2R14 resulted in an activation or increase in pAMPK that decreased in cholesterol depleted condition, and sphingomyelin depletion did not affect it. A similar result was observed for AT_1R signaling. Therefore, alteration in membrane cholesterol influences T2R14 and AT_1R signaling.

Furthermore, to understand the potential structural basis for discrepancies in cholesterol and sphingomyelin sensitivity to T2R14 signaling, we did amino acid sequence analysis of T2Rs to identify the occurrence of putative sphingolipid binding signature sequences. Previously we

have demonstrated the occurrence of cholesterol binding motifs (CRAC and CARC); which were conserved across T2R family (Shaik et al., 2018). In contrast to cholesterol binding motifs, SBMs were not conserved across T2R family. Moreover, the SBM interaction with GRM2 (a Class C GPCR) has been experimentally shown, and sweet and umami taste receptors (T1RS) also belong to same Class C GPCRs (Munk et al., 2016). T1Rs share similarities with GRMs in structure and activation mechanisms; therefore, we pursued the amino acid alignment of T1Rs with GRMs. Only one T1R subtype, T1R1 out of the three T1R subfamily (T1R 1-3) contained the putative SBM **(Figure 6.4.1)**. Interestingly, heterodimer T1R1+T1R3 is involved in umami taste recognition, and GRMs have previously been suggested to be involved in umami taste recognition (Kusuhara et al., 2013). Therefore, we speculate that there may be a link between SBM and umami recognition. Moreover, a cholesterol binding motif (CRAC) is also conserved in T1Rs and GRM2, which further highlights the significance of membrane cholesterol in the function of GPCRs.

In conclusion, our results demonstrate that in contrast to membrane cholesterol, sphingomyelin does not directly regulate the agonist-promoted calcium signaling of T2R14 and AT_1R receptors. It suggests that different membrane lipids may distinctly modulate the taste receptor signaling. However, studies involving different approaches to modulate the membrane sphingomyelin like metabolic depletion of sphingolipids or sphingolipid-deficient cell systems would provide more conclusive evidence on the role of sphingolipids in T2R signaling. Moreover, mass spectrometric-based lipidomics techniques could be used to unequivocally characterize the specific sphingolipid species modulated post sphingolipid alteration. These results demonstrate the functional relevance of lipid-GPCR interactions for both T2R14 and AT_1R and how membrane lipid compositions could affect the receptor signaling.

BRIDGE TO CHAPTER 7

Chapters 4, 5 and 6 focussed on T2R14 signaling in native, pathophysiological and membrane altered conditions. In addition to its high expression in a number of tissues, T2R14 exhibits broad tuning breadth (i.e., activated by structurally diverse ligands) and high threshold for agonist activation. In the following chapter (Ch.7), I characterize some of the molecular and structural determinants which could influence its agonist specificity and efficacy.

CHAPTER 7

7.0 Intracellular H208 residue influences agonist selectivity in bitter taste receptor T2R14

Feroz Ahmed Shaik, Appalaraju Jaggupilli and Prashen Chelikani

7.1 ABSTRACT

Bitter taste receptors (T2Rs) are a specialized class of cell membrane receptors of the G protein-coupled receptor family and perform a crucial role in chemosensation. The 25 T2Rs in humans are activated by structurally diverse ligands of plant, animal and microbial origin. The mechanisms of activation of these receptors are poorly understood. Therefore, identification of structural determinants of T2Rs that regulate its efficacy could be beneficial in understanding the molecular mechanisms of T2R activation. In this work, we characterized a highly conserved histidine (H208), present at TM5-ICL3 region of T2R14 and its role in agonist-induced T2R14 function. Surprisingly, mutation of the conserved H208 (H208A) did not result in increased basal activity of T2R14, in contrast to similar H214A mutation in T2R4 that showed constitutive or basal activity. However, H208A mutation in T2R14 resulted in an increase in agonist-induced efficacy for Flufenamic acid (FFA). Interestingly, H208A did not affect the potency of another T2R14 agonist Diphenhydramine (DPH). The H208R compensatory mutation showed FFA response similar to wild-type T2R14. Molecular modeling suggests a FFA-induced shift in TM3 and TM5 helices of H208A, which changes the network of interactions connecting TM5-ICL3-TM6. This report identifies a crucial residue on the intracellular surface of T2Rs that is involved in bitter ligand selectivity. It also highlights the varied roles carried out by some conserved residues in different T2Rs.

7.2 INTRODUCTION

Bitter taste receptors (T2R) are cell membrane receptors that belong to the G protein-coupled receptor (GPCR) family and primarily perform a chemosensory role. T2Rs are expressed in a wide variety of cell types across various organs of the human body and are recognized as potential pharmacological targets in various pathological conditions (Robinett et al., 2014;Prakash, 2016;Shaik et al., 2016;Jaggupilli et al., 2017;Liszt et al., 2017). For instance, in bronchial and uterine smooth muscles, activation of natively expressed T2Rs evokes smooth muscle relaxation (Deshpande et al., 2010;Zheng et al., 2017). Interestingly, in vascular smooth muscles, T2Rs elicit pro-contractile effects (Upadhyaya et al., 2014). Activation of T2Rs expressed in airway epithelial cells with corresponding bitter ligands like flavones and quinolones evoked anti-bacterial responses (Hariri et al., 2017;Freund et al., 2018). Thus, pharmacological targeting of T2R-mediated signal transduction could be beneficial therapeutically in disease states.

In humans, there are 25 T2Rs and a significant number of these receptors have broad-tuning breadth i.e., receptors are activated by structurally diverse compounds to a different degree. Therefore, identifying structural elements like consensus motifs or conserved residues involved in ligand interaction and subsequent signal transduction would be beneficial. Previously, we have shown the crucial structure-function role played by the LxxSL motif in TM5 of T2R1 and T2R4, and by residues present in the intracellular loop 3 (ICL 3) of T2R4 (Singh et al., 2011a;Pydi et al., 2014b). Interestingly, the LxxSL motif in TM5 is conserved in 96% of human T2Rs with T2R14 being the only exception with an LxxSM sequence. It was proposed that LxxSL motif forms a network of hydrogen-bond interactions connecting TM5-ICL3-TM6, including the highly conserved H214 in T2R4. The H214 is located near the cytoplasmic end of

TM5 and ICL3 and is 96% conserved across human T2Rs. The H214 was suggested to be crucial in stabilizing the T2R4 in an inactive conformation, as mutation of H214 to A214 leads to a constitutive active form of T2R4 (Pydi et al., 2014b). Moreover, the importance of this TM5-ICL3-TM6 region in receptor stabilization and forming conserved inter-helical contacts is demonstrated for several GPCRs (Cvicek et al., 2016). The ICL3 has previously been shown to play a structural determinant in ligand-GPCR interaction through regulation of receptor conformation as shown in Class A GPCRs (Chee et al., 2008). Additionally, ICL3 serves as a contact site for G-protein coupling and GPCR phosphorylation (Cai et al., 2001;Butcher et al., 2011;Bouzo-Lorenzo et al., 2016).

T2R14 is highly expressed in a number of extraoral tissues compared to other T2R sub-types, and is unique in its broad ligand-recognition or tuning breadth. While a number of structure-function studies have targeted the extracellular and ligand-binding pocket in T2R14 (Levit et al., 2014;Jaggupilli et al., 2018a;Jaggupilli et al., 2018b;Nowak et al., 2018;Thawabteh et al., 2019), none have addressed the role of the crucial TM5-ICL3-TM6 region that might be involved in T2R14 activation. We hypothesize that the conserved amino acid residues near the TM5-ICL3 region of T2R14 could play a structure-function role in T2R14 agonist-induced efficacy. With previous work on T2Rs suggesting a crucial role for the highly conserved H208 in T2R14, we investigated the structure-function role of this histidine. In this study, using site-directed mutagenesis and pharmacological approaches, we characterized the role of conserved H208 residue in agonist-induced T2R14 efficacy.

7.3 MATERIALS AND METHODS

7.3.1 Reagents

Diphenhydramine, Flufenamic acid, U73122 were purchased from Sigma-Aldrich. DMEM/F12, Fetal bovine serum, Penicillin-streptomycin, Lipofectamine 2000, Opti-MEM, Hygromycin B and Fluo 4-NW Calcium assay kit were acquired from ThermoFisher Scientific. APC anti-Flag tag antibody (Cat. #637308) was obtained from BioLegend. Gallein (Cat. #3090) was acquired from Tocris.

7.3.2 Cell Culture and Transfections

The culture of HEK293T cells and transient transfection were performed as described earlier (Jaggupilli et al., 2018a;Liu et al., 2018). The recombinant plasmids encoding T2R14, $T2R14^{H208A}$, $T2R14^{H208R}$, and $T2R14^{H208F}$ cloned into mammalian expression vector pcDNA3.1-Hygro(+) were synthesized and acquired from GenScript (Piscataway, NJ). Hereafter, the mutant variants of T2R14 will be referred to as H208A, H208R and H208F and the wild-type receptor will be referred to as either WT or T2R14. Generation of stable cell lines was performed as previously described (Chakraborty et al., 2015). Briefly, T2R14 or H208A encoding plasmids were transfected into HEK293T cells using Lipofectamine 2000 as per the manufacturer's instructions. The cells were cultured in growth media supplemented with Hygromycin B (200µg/ml) for selection of clones with high expression of the protein of interest. Diphenhydramine (T2R14 agonist) induced Ca^{2+} mobilization and FACS approaches were used for stable cell line screening and the best stable cell line was selected on the basis of high cell surface expression and optimal function of the protein of interest. For experiments that involved transient transfection, functional assay or cell surface expression characterization was performed 24 h post transfection of plasmid DNA.

7.3.3 Calcium mobilization assay

Pharmacological characterization of WT and mutants was pursued by measuring the agonist-induced mobilization of intracellular calcium ($[Ca^{2+}]_i$) using Fluo-4 NW Calcium assay kit and Flex station-3 microplate reader (Molecular Devices) as previously described (Jaggupilli et al., 2018a).

7.3.4 Flow cytometry

Analysis of cell surface expression of the recombinant proteins was performed by probing the FLAG epitope of the proteins expressed using a fluorochrome (APC) conjugated anti-FLAG antibody as described in (Shaik et al., 2018). In brief, $5x10^4$ cells (either stable cell lines or transiently transfected cells) were collected and washed twice with ice-cold FACS buffer (1X PBS with 0.5% BSA) followed by a 1 h antibody incubation in dark at 4°C. Then, the cells were washed thrice with FACS buffer and finally re-suspended in 300µl of FACS buffer for analysis. BD-FACS Canto-II Flow cytometry analyser was used for detection of the proteins and data analysis was performed using FlowJo software.

7.3.5 Molecular Modeling

In silico, molecular modeling and small molecule docking protocols were performed as per our earlier published protocols (Jaggupilli et al., 2018a;Jaggupilli et al., 2018b;Liu et al., 2018). Homology models of T2R14 and H208A were generated using the I-TASSER server and selection of the best predictive models was done based on the C-score (Yang et al., 2015). Protein loop refinement and side chain optimization of the homology models were performed using Prime application [Schrödinger molecular modeling suite (v 11.0)]. Stereo chemical quality of the protein structure was validated using PROCHEK and Ramachandran plot analyses,

which shows that >98% of the residues were within the allowed regions. Further optimization of the protein structure for the downstream application like ligand docking and energy minimization of the ligand-receptor complex was done using the protein preparation wizard program. 2D Chemical structures of ligands used Diphenhydramine (DPH) and Flufenamic acid (FFA) were obtained from PubChem database and conversion of 2D structures into energy-minimized 3D structures was done using LigPrep program (Schrödinger). Ligand docking into the receptor and scoring based on the ligand-receptor affinities was performed using Glide module (SP and XP). The best receptor docked ligand pose was selected on the basis of the Glide score, which was further energy minimized. The analysis of the molecular interaction between receptors (T2R14 and H208) and ligands was done using tools available in Schrödinger suite and PyMol visualizer was used to generate images (DeLano, 2002).

7.3.6 Statistical Analysis

Unpaired students t-test and one-way ANOVA coupled with post-hoc multiple comparison tests were used to determine the statistical differences in studies involving two and >2 groups respectively. *p*-value of less than 0.05 was considered statistically significant and analyses were performed using GraphPad Prism 6.0 program (San Diego, CA).

7.4 RESULTS

7.4.1 Functional characterization of T2R14 and H208A

To examine the functional significance of the highly conserved H208 residue in T2R14, we mutated H208 residue to Ala (H208A). We examined whether H208 mutation elicits the same effects as observed for H214 in T2R4 i.e., alanine mutation resulting in a constitutive active mutant (CAM). HEK293T cells were transfected with three different concentrations of

plasmid DNA either WT or H208A mutant (2, 4 and 6μg) to obtain cells expressing varying receptor densities followed by analysing their basal $[Ca^{2+}]_i$ mobilization as described before (Pydi et al., 2014a). Results confirm an increase in receptor expression among cells transfected with different concentrations of DNA (T2R14 or H208A), however, there was no significant difference in basal $[Ca^{2+}]_i$ mobilization **(Figure 7.4.1)**.

We then analysed the effect of agonist stimulation on WT and H208A efficacy **(Figure 7.4.2)**. We generated stable cell lines of HEK293T with high expression of either T2R14 or H208A. The protein expression of T2R14 and H208A in the stable cell lines was confirmed using flow cytometry **(Figure 7.4.2A)**. There is no significant difference in protein expression between H208A and WT. To pursue agonist induced functional assays, we selected two well-characterized T2R14 agonists, FFA and DPH **(Figure 7.4.2B)**. As shown in **figure 7.4.2C**, a ~5-fold decrease (left shift of dose response) in EC_{50} for FFA in H208A expressing cells was observed compared to WT. However, in the case of DPH, there were no significant differences in EC_{50} values between WT and H208A **(Figure 7.4.2D)**. Additionally, we confirmed that FFA and DPH induced signaling is through canonical T2R signaling pathway. Prior to agonist-stimulation, the cells loaded with Ca^{2+} sensitive dye were pre-treated with small molecule inhibitors of downstream effectors PLC and Gβγ (U73122 and gallein respectively) for 30 min. As shown in **Figure 7.4.2E-F**, DPH, and FFA induced activity in WT and H208A expressing cells was ablated by U73122 and gallein treatment.

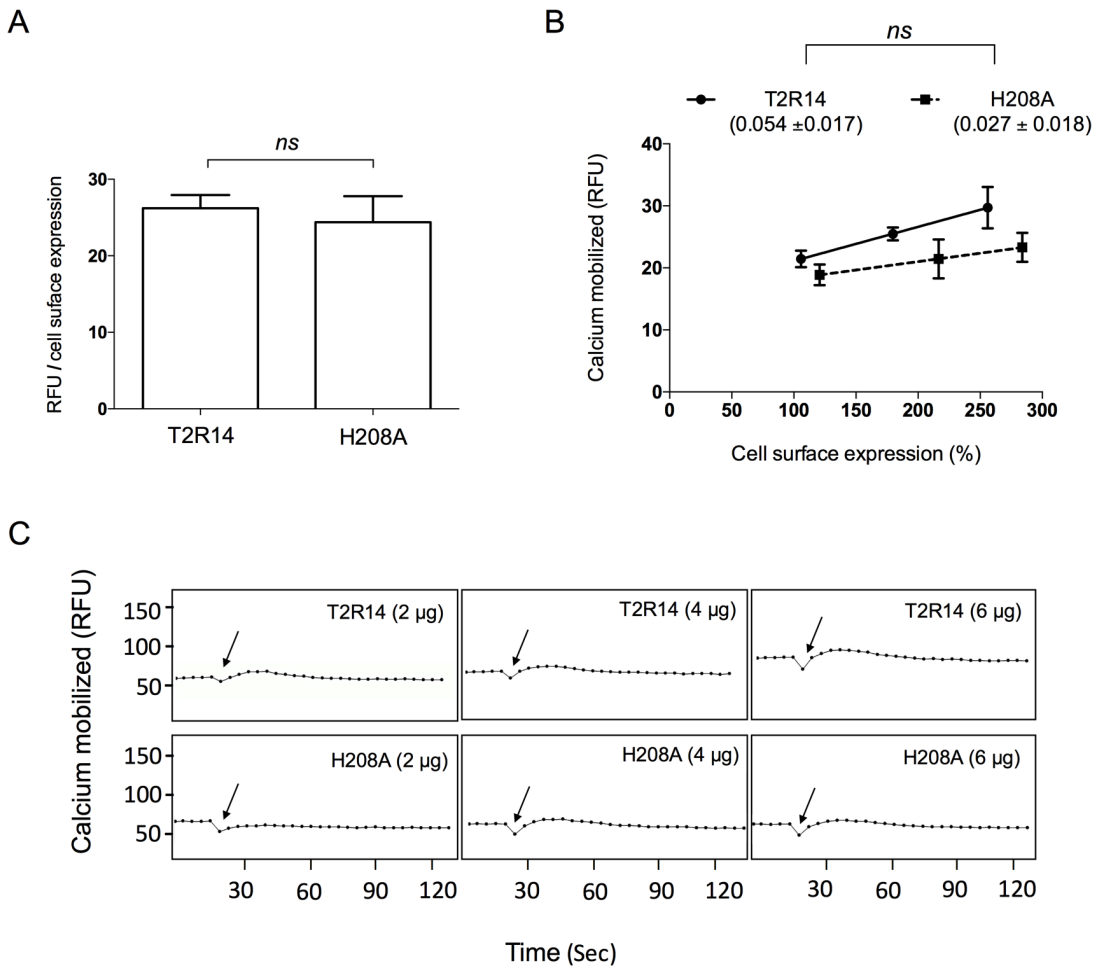

Figure 7.4.1 Pharmacological characterization of basal activity of T2R14 and H208A mutant. ***A)*** Shown is the agonist-independent or basal Ca^{2+} mobilized by T2R14 and H208A. The y-axis corresponds to the basal Ca^{2+} responses (RFU) of T2R14 and H208A normalized to the cell surface expression of WT-T2R14, as determined by FACS. Data shown is mean ± S.E.M from 3 independent experiments done in triplicate. ***B)*** Analysis of the effect of receptor density on basal activity. Cell surface expression of T2R14 and H208A is plotted against their corresponding basal Ca^{2+} responses. Three data points correspond to three different quantities of plasmid DNA (2, 4 and 6 µg) per $1x10^6$ cells used. The slopes of the best-fitting regression lines for the data corresponding T2R14 and H208A is shown. Data shown as mean ± S.E.M from 3 independent experiments done in triplicate. (ns, non-significant *p*-value; RFU, Relative fluorescence units). ***C)*** Representative calcium traces corresponding to each concentration in panel B are shown. The buffer was added at 20 sec time point, which is indicated with an arrow.

7.4.2 Functional characterization of T2R14 mutants

To further elucidate the role of H208, we pursued additional site-directed mutagenesis. We replaced H208 with a bulky phenylalanine (H208F) and with a compensatory amino acid, arginine (H208R). As shown in **Figure 7.4.3A**, transient transfection of WT and mutant genes resulted in a significant increase in expression of respective proteins over control (pcDNA). The mutations did not influence the protein folding or cell surface expression of receptor variants compared to WT. We next examined the FFA and DPH induced $[Ca^{2+}]_i$ mobilization for all the three mutants (H208A, H208R and H208F) in a transient expression system. Consistent with results described in the previous section, the EC_{50} of FFA at H208A decreased compared to WT **(Figure 7.4.3B and Table 7.4.1)**. The compensatory mutant H208R showed FFA induced $[Ca^{2+}]_i$ mobilization almost similar to WT **(Table 7.4.1)**. No change was observed for any of the mutants with DPH induced $[Ca^{2+}]_i$ response **(Figure 7.4.3C)**.

The EC_{50} (mutant/WT ratio), which is an indicator for "gain/loss-in-function" phenotype is listed in **table 7.4.1**. A ratio of <1 could be an indicator of gain-in-function and a ratio of >1 is an indicator of loss-of-function phenotype for a particular agonist at the receptor (Pydi et al., 2014b;Jaggupilli et al., 2018a;Liu et al., 2018). The EC_{50} (mutant/WT) ratio for FFA in H208A and H208F mutants was around 0.5, which indicates that an absence of a positively charged residue is critical for the observed increase in ligand-specific potency. Interestingly, the differential intrinsic effects observed between WT and H208A was only for FFA, but not for DPH. Therefore, we assessed whether there are any structural changes in active structures of T2R14 post stimulation with FFA and DPH that resulted in the ligand specific-bias for H208A activation. We utilized our previous experimentally validated computational T2R14 molecular

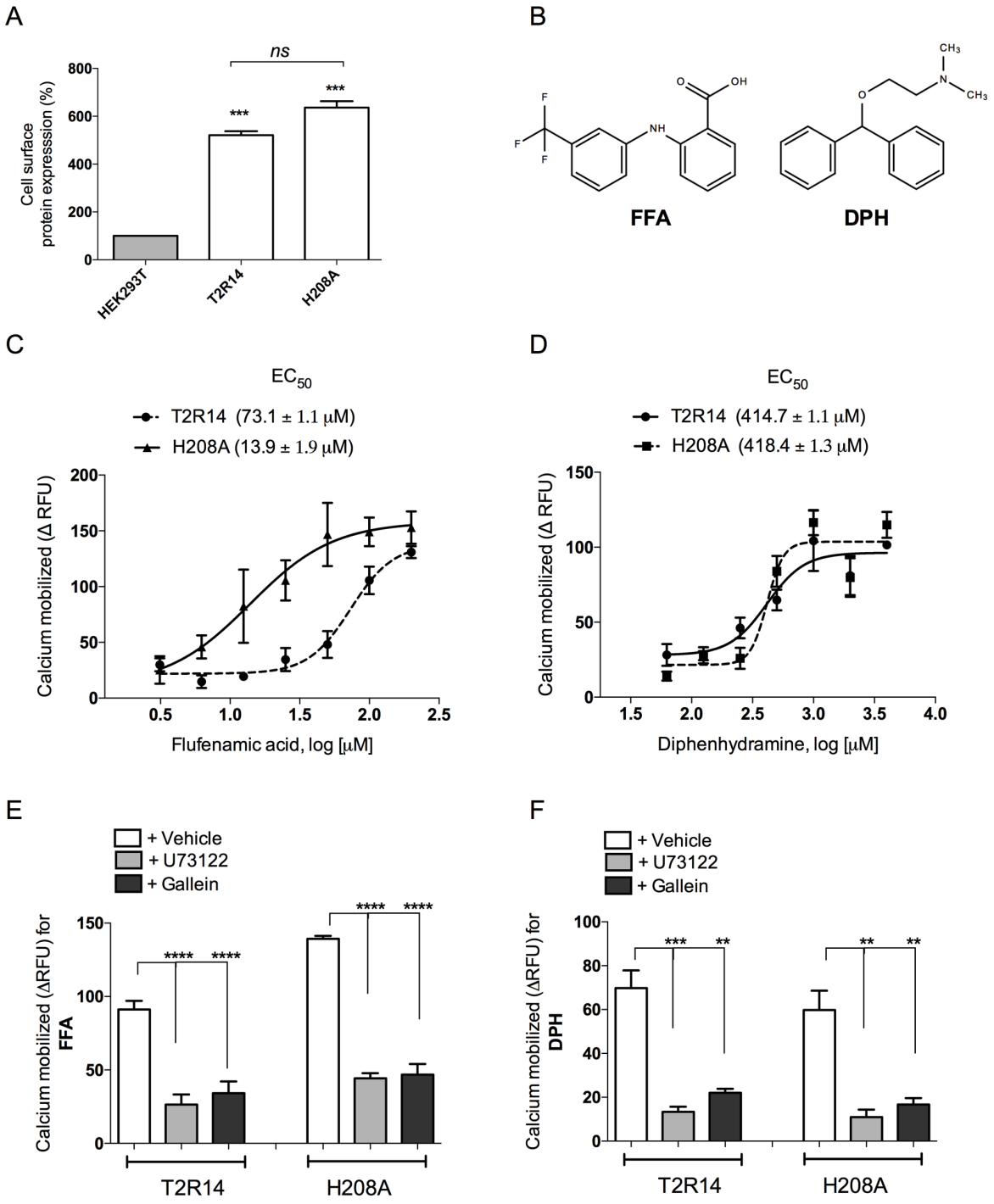

Figure 7.4.2 Pharmacological characterization of T2R14 and H208A mutant signaling. ***A)*** Cell surface expression analysis of T2R14 and H208A in stable cell lines was performed as described in the methods section. The APC anti-Flag antibody used at a dilution of 1:300 and receptor expression in stable cell lines is represented in terms of percentage mean fluorescence intensity

(MFI) relative to the base cell line (HEK293T). Data shown as mean ± S.E.M from 3 independent experiments done in duplicate. (*** $p < 0.001$ vs. HEK293T; ns, non-significant). ***B)*** Chemical structures of FFA and DPH. ***C, D)*** Agonist-induced Ca^{2+} mobilization in HEK293T-T2R14 and HEK293T-H208A stable cell lines are shown. Dose-response curves for FFA (3.12-200 μM) and DPH (62.5-4000 μM) are plotted in terms of ΔRFU, which represents the agonist-induced intracellular Ca^{2+} mobilization values post subtracting the baseline values (i.e. corresponding RFU values obtained in HEK293T). EC_{50} values for the agonists were calculated by non-linear regression analysis of the dose-response date using GraphPad Prism V6.0. Data shown as mean ± S.E from 3-4 independent experiments done in triplicate. ***E, F)*** Characterization T2R14 and H208A intrinsic activity after pretreatment with PLC inhibitor (U73122) and Gβγ antagonist (Gallein). A single concentration of either DPH (500μm) or FFA (100μM) induced Ca^{2+} mobilized in the vehicle, U73122 (10μm) and Gallein (10μM) pretreatment groups are demonstrated. Agonist-specific responses in stable cell lines is subtracted from the response in HEK293T cells (baseline) and plotted as ΔRFU. Data are shown in mean ± S.E.M from 3 independent experiments performed in triplicate. (**$p<0.01$; ***$p<0.001$)

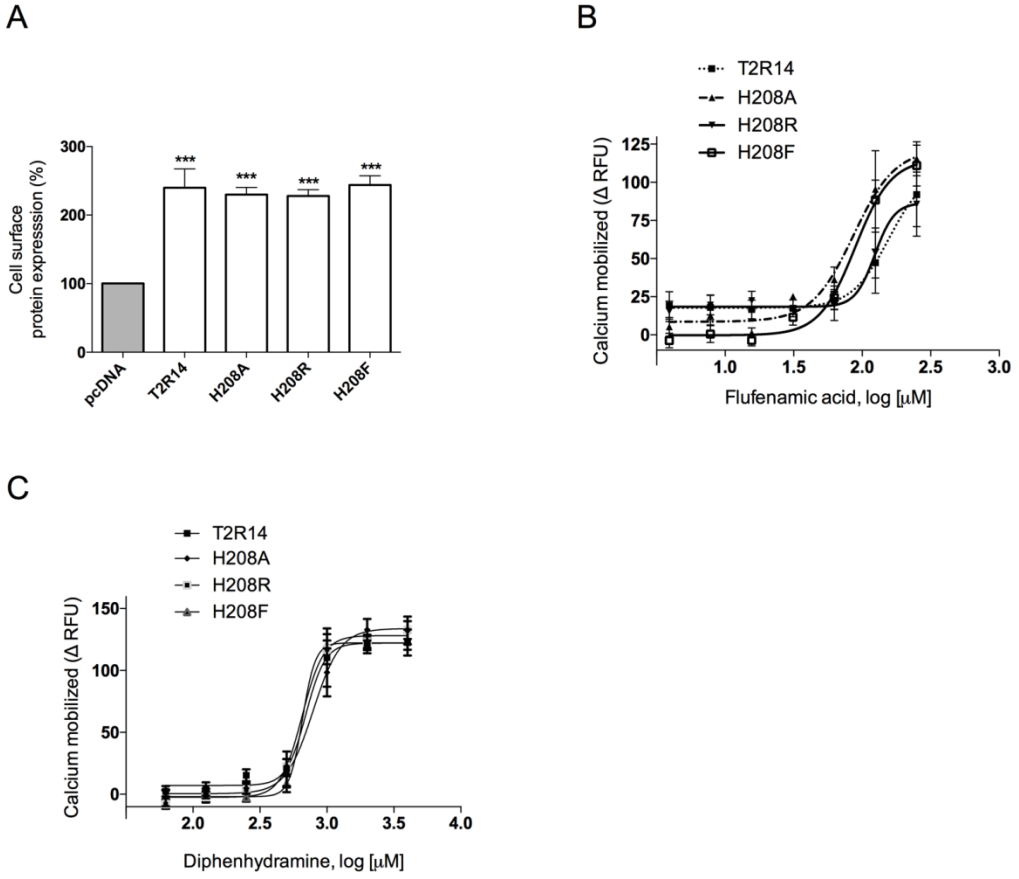

Figure 7.4.3 Pharmacological characterization of T2R14 and its mutants. ***A)*** Cell surface expression of T2R14 and mutants relative to mock transfected cells as determined by FACS. Data shown is mean± S.E.M from 3 independent experiments done in duplicate. (*** $p<0.001$ vs. pcDNA). ***B, C)*** Functional characterization of H208 mutants. Dose-response relationship of HEK293T cells transfected with T2R14, H208A, H208R, H208F to DPH (62.5-4000 μM) and FFA (3.9-250 μM) is shown. Dose-response relationships are plotted after subtracting the mock (pcDNA transfected cells) responses. Data shown is mean ± S.E from 3 independent experiments performed in triplicate.

Table 7.4.1 Pharmacological characterization of T2R14 and H208 mutants. The EC_{50} values for FFA and DPH at T2R14, H208A, H208R, and H208F as determined in figure 7.4.3 are listed. The potency of the agonist at the receptor is demonstrated by the EC_{50} ratio of mutant to WT. Data are mean ± S.E.M from 3 independent experiments done in triplicate.

	FFA		**DPH**	
	EC_{50} (μM)	[Mutant EC_{50}]/ [WT EC_{50}]	EC_{50} (μM)	[Mutant EC_{50}]/ [WT EC_{50}]
T2R14	156.8± 1.11	1	696.7 ± 1.07	1
H208A	86.3 ± 1.14	0.55[a]	787.4 ± 1.02	1.1
H208R	123.6 ± 1.04	0.78	651.9 ± 1.06	0.93
H208F	89.1 ± 1.09	0.57[a]	655 ± 1.02	0.94

[a]A Mutant EC_{50} /Wildtype EC_{50} of <1 represents an increase in potency for the agonist at the receptor level.

modeling approaches to delineate the structural basis of the aforementioned activity discrepancies.

7.4.3 Prediction of ligand induced structural changes in T2R14 and H208A

Molecular modeling analysis was performed to understand the structural changes in both WT and mutant. Initially, inactive (ligand-free) 3D models of WT and H208A were superimposed. We did not see a notable deviation between the two aligned structures. This in contrast to what has been observed for T2R4 and its CAM H214A, with a significant rearrangement in the transmembrane helices TM5 and TM6, computed to an RMSD of 2Å (Pydi et al., 2014b). In that work, the rhodopsin inactive (PDB ID: 1U19) and CAM (PDB ID: 2X72) were used as templates to build inactive WT-T2R14 and constitutive active H214A.

Next, we examined the structural differences between the active models (ligand docked) of T2R14 and H208A. Consistent with our previous T2R14 models, DPH bound T2R14 resulted in similar interactions as previously described (Jaggupilli et al., 2018a). DPH docked H208A model did not show significant variations in interactions either in the binding pocket or helix movement compared to WT **(Figure 7.4.4A)**. We analysed structural changes in the active models of FFA docked T2R14 and H208A. The results suggest FFA engages in an additional interaction with T89 and F247 in the H208A model, which was not observed in the case of WT **(Figure 7.4.4B)**. In addition, in H208A model, an FFA-induced shift in the TM3 and TM5 helices were observed. As shown in the intracellular view of the superimposed FFA bound models of WT and H208A, an outward shift of the TM3 and TM5 was present in the H208A model, with an RMSD of ~2.13 Å relative to WT **(Figure 7.4.5A)**. The effect of this on interactions with the LxxSM motif in T2R14 was analysed in our model. As previously mentioned, T2R14 is the only T2R that has an LxxSM sequence instead of the LxxSL present in

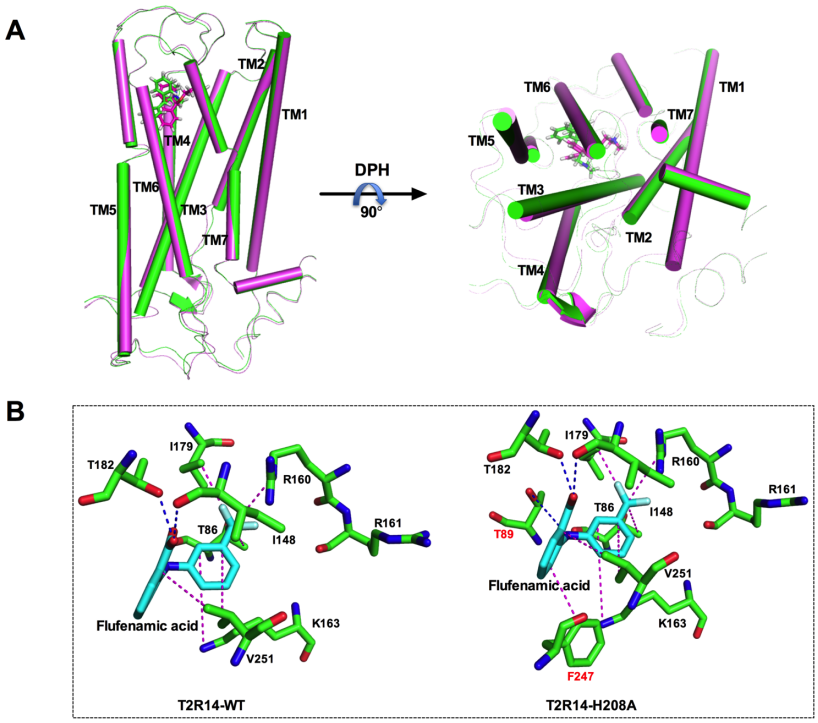

Figure 7.4.4 Molecular models of T2R14 and H208A. ***A)*** Superimposed active (DPH docked) models of T2R14 (green) and H208A (magenta). The left panel corresponds to membrane view of superimposed models and the right panel represents the intracellular view (from the cytoplasmic side). ***B)*** Predicted binding site interactions of FFA with T2R14-WT and H208A models. The additional amino acids T89 and F247 (labelled red) in H208A model are involved in interactions with FFA. All the interactions are indicated with dashed lines of different colours (blue, polar bonds; pink, pi-cation).

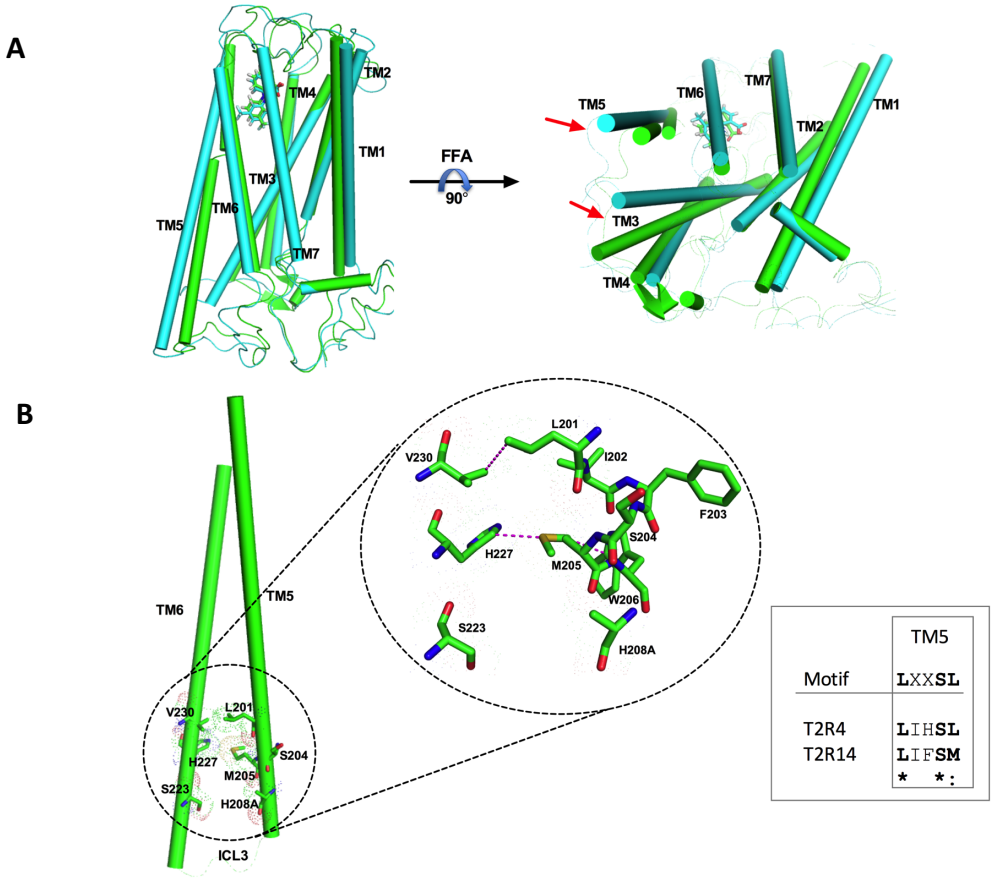

Figure 7.4.5 In silico modeling of T2R14 and H208A. ***A)*** Superimposed active models (FFA docked) of T2R14 is indicated in green and H208A is indicated in cyan. The changes in the helical movement of TM3 and TM5 are indicated with an arrow sign. ***B)*** The membrane view of TM helices (TM5 and TM6) of FFA docked H208A model is shown with key residues near the TM5-ICL3-TM6 interface highlighted. The packing interaction of H208A with the LxxSL signature motif is shown in the inset. The amino acid sequence alignment of LxxSL motif in T2R4 and T2R14 performed using Clustal Omega software (EMPL-EPI) is shown in a box.

the rest 24 T2Rs **(Figure 7.4.5B)**. An interesting property of methionine is the propensity of its sulphur to interact with aromatic residues (Valley et al., 2012). In our model, the inter-helical backbone interaction between M205 (LxxSM) and 208 residue is lost in H208A **(Figure 7.4.5B)**.

7.5 DISCUSSION

In view of the recent developments, uncovering the potential for T2Rs as novel pharmacological targets in a multitude of pathological conditions ranging from metabolic, neurological disorders, infectious diseases and cancers, it is of utmost importance to identify key structural aspects of T2Rs influencing signaling and function. In contrast to many other GPCRs, T2Rs are evolved to accommodate structurally diverse ligands derived from various sources including plants (natural and synthetic derivatives), animals (progesterone and helminth secretions) and microbes (bacterial metabolites) (Lu et al., 2017;Luo et al., 2019). T2R14 is one such example to be activated by a plethora of ligands, each with a varying degree of activation threshold (Lossow et al., 2016). Studies characterizing the ligand-binding pocket of T2Rs have provided some insights into the structural basis of T2R activation (Brockhoff et al., 2010;Singh et al., 2011a;Pydi et al., 2014c;Thomas et al., 2017). In this work, we examined the structural determinants near TM5-ICL3-TM6 interface, with a focus on the highly conserved H208 of T2R14. Using site-directed mutagenesis and functional assays we demonstrate that mutation of H208 to A208 resulted in a marked increase in efficacy only for FFA, and no change was observed for DPH. This is interesting taking into account a recent study demonstrating that, different ligands stabilize T2R14 in distinct conformations and each favouring distinct functional outcomes (Kim et al., 2019). In this study, we showed the significance of H208 residue in maintaining an FFA-bound active conformation to elicit a functional response and with alanine mutation resulting in a ~2-5 fold increase in functional response (Gain-of-function). The

decreased threshold for activation or increase in potency for FFA at H208A vs. WT is reflected in both stable and transient transfection experimental models used. However, the observed increase in potency for the FFA in H208A vs. WT in the transient system was not to the same degree as was observed in the case of stable cell system. This could be due to differences in the receptor expression in the two cell systems used. The expression of T2R14 or H208A over controls was significantly higher in the stable system compared to the transient system ($p<0.001$; (comparing **Figures 7.4.2A and 7.4.3A)**. This discrepancy is not uncommon, as shown previously that increase in GPCR expression is correlated with increase in potency for the agonists used i.e., a leftward shift in the dose-response curve (Hermans et al., 1999).

Due to the unavailability of high-resolution T2R14 structure, computational molecular modeling based approaches provide an opportunity to predict the key structural elements in agonist-promoted receptor activation. Comparison of DPH bound H208A mutant with that of DPH bound WT-T2R14 did not show any differences in ligand-receptor interactions. However, comparison of FFA-bound WT and H208A models showed marked differences in helical movements and some crucial inter-helical contacts. These FFA-induced helical rearrangements observed in H208A compared to wild-type might lead to variances in receptor engagement with $G_{\alpha\beta\gamma}$ protein and this could be the reason for enhanced intrinsic efficacy observed for H208A. Moreover, it is widely recognized that $G_{\alpha\beta\gamma}$-protein binding takes place at the TM5-ICL3-TM6 interface. The importance of residues in ICL3, not only in G-protein binding but also in forming inter-helical contacts in maintaining optimal GPCR conformation is well established (Chee et al., 2008;Butcher et al., 2011).

Previously, in T2R1 and T2R4 we have shown the structural and functional role played by LxxSL motif (TM5) in forming crucial inter-helical contacts with residues in ICL3 and TM6

(Singh et al., 2011a;Pydi et al., 2014b;Jaggupilli et al., 2016). The H214 residue of T2R4 forms crucial interactions with LxxSL motif and Ala mutation of H214 resulted in the loss of inter-helical contacts between TM5 and TM6, leading to movement of TM6 away towards the helical core. This relaxation was proposed to be the mechanistic reason behind its constitutive activity. Interestingly, in T2R14 the presence of a unique LxxSM sequence with the amino acid M205 causes new interactions in this area. Recently, it was shown that a third of the known protein structures contain an energetically stabilizing Met-aromatic motif (Valley et al., 2012). It was suggested that Met-aromatic motif is necessary for high affinity ligand binding and function in TNF ligand-receptor complexes (Valley et al., 2012). Analysis of our model reveals, three aromatic residues F203, W206, H227 present in the 5Å proximity of M205 in T2R14. Interestingly, the methyl side chain of M205 is stacked between the aromatic rings of adjacent W206 (TM5) and H227 (TM6) forming hydrophobic interactions and a Met-aromatic motif. Whether this Met-aromatic motif causes the stabilizing effect and maintains the basal state of T2R14, thereby not leading to constitutive activity remains speculative at this point. Since in our H208A model **(Figure 7.4.5B)**, the inter-helical backbone interaction between M205 (LxxSM) and 208 residue is lost and there was a significant movement of TM5 upon FFA binding, it does suggest a role of H208 in receptor activation.

The existence of naturally occurring mutations in T2Rs that may lead to gain-of-function phenotype manifesting into a pathologically relevant physiological responses are very likely. For example, a correlation between a single gain-of-function amino acid mutation (W493R) in Epithelial sodium channel (ENaC) and its increased activity has been demonstrated (Shobair et al., 2016). This malfunction of ENaC activity is directly associated with the pathology of cystic fibrosis and Liddle syndrome (Azad et al., 2009). Moreover, a W493R polymorphism and its

association in patients suffering from chronic bronchitis have been shown (Azad et al., 2009). In addition, a single disease-causing amino acid mutation in the cytosolic regions of three transmembrane proteins GLUT1, ITPR1, and CACNA1H affected the protein function through increased clathrin-dependent trafficking (Meyer et al., 2018). Disease linked gain-of-function mutations manifesting into broader ligand specificity has been demonstrated in some GPCRs. L125P of CasR and K183R or K183N in the case of TSHR are some of the examples in which the gain-of-function mutations lead to broadening the ligand specificity and consequently adversely affecting the GPCR function (Rodien et al., 1998;Vargas-Poussou et al., 2002;Coulon et al., 2016;Fukami et al., 2018). It will be interesting to explore if H208 (T2R14) or any of the conserved residues in T2Rs are mutated in disease states. T2R polymorphisms and their association with susceptibility to disease conditions like chronic rhinosinusitis, colorectal cancer and caries have previously been demonstrated (Shaik et al., 2016;Lu et al., 2017). Given the important roles played by T2Rs in extraoral tissues, naturally occurring mutations could potentially have an important role in the pathophysiological conditions.

In conclusion, our findings provide insights into the role of conserved H208 in the TM5-ICL3 region of T2R14 in influencing agonist-selectivity. This study highlights how an amino acid conserved across all the 25 T2Rs is performing varied roles in different T2Rs; affecting the basal equilibrium (in T2R4) or agonist-specific receptor activation (in T2R14). While it is the first report in the T2R field, it is not uncommon in GPCR structure-function studies that a mutation of single residue induces a rearrangement in the ligand binding pocket and consequently affecting either binding affinity (and concomitant structural rearrangements) or basal equilibrium of the receptor (Katritch et al., 2013). Further studies, examining both conserved and non-conserved T2R specific structural elements such as the LxxSM motif in

T2R14, could provide a better understanding of T2R activation mechanisms and how it influences bitter ligand specificities.

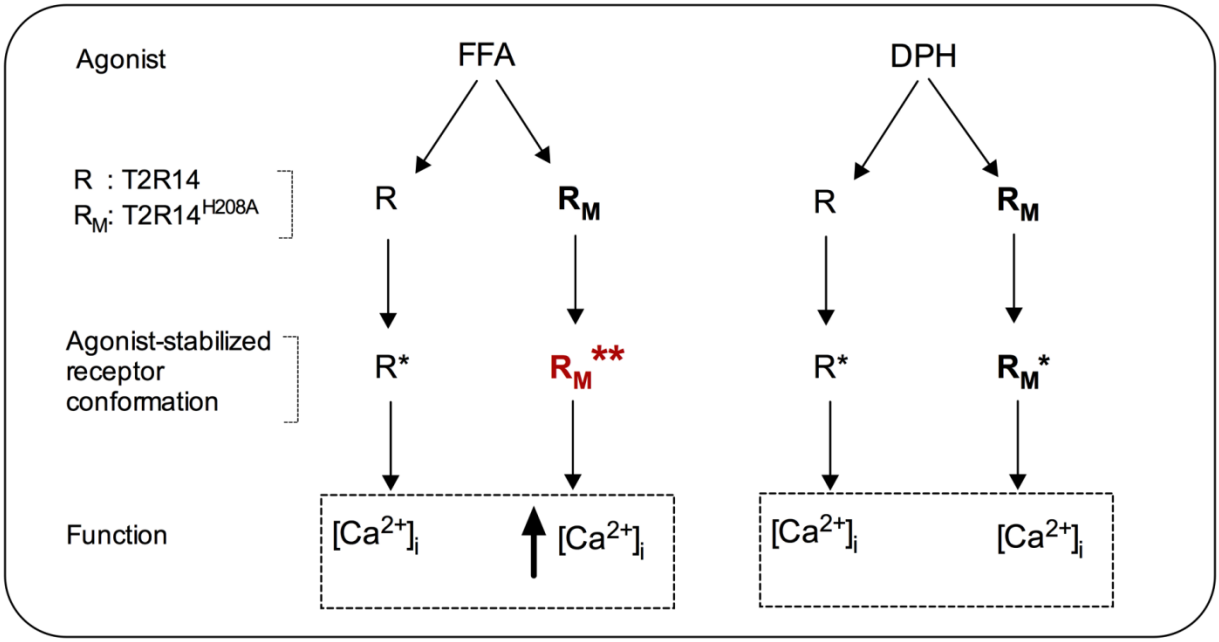

Figure 7.5.1 Schematic representation of how intracellular H208 residue affects agonist selectivity in T2R14.

CHAPTER 8

8.0 CONCLUSION AND FUTURE DIRECTIONS

8.1 Conclusion

The emerging significance of the bitter taste receptors (T2Rs) role in the extraoral tissues alludes to their potential role in many pathophysiological conditions. The dysregulation of T2R expression and function in disease has now been demonstrated in airways diseases, neurological disorders and in some cancers. However, the role of T2Rs in the pathophysiology of breast cancer is unexplored thus far. Using approaches which involve receptor knockdown, pharmacological activation and biochemical assays we found that; i) T2R4 and T2R14 expression patterns are dissimilar, with decreased levels of T2R4 and increased levels of T2R14 in BC clinical samples compared to non-cancerous controls. ii) Activation of T2Rs with their respective agonist elicited physiological responses in metastatic breast cancer cells, and no responses were seen in non-tumorigenic breast epithelial cells. iii) Intrinsic activation of T2Rs (irrespective of T2R subtype) induced anti-proliferative, pro-apoptotic and anti-migratory responses in highly metastatic breast cancer cells. Taken together, our findings demonstrate that the chemosensory T2R signaling network is involved in evoking beneficial physiological responses in breast cancer.

The next study in my thesis involved elucidating the mechanism(s) regulating the structure and function of T2R14 in airways. I examined if, membrane lipids like cholesterol play a regulatory role in T2R14 signaling in airway cells. First, the expression and signaling of T2R14 in primary HASM cells, and NuLi-1 cells was confirmed using immunoblot analysis and $[Ca^{2+}]_i$ mobilization experiments respectively. Next, T2R14 signaling was examined in membrane

cholesterol altered environments by MβCD or cholesterol oxidase treatments. In the cells analyzed, cholesterol depletion affected the agonist induced T2R14 signaling, and cholesterol replenishment rescued its efficacy. An alternative approach for cholesterol depletion (with cholesterol oxidase pretreatment) also negatively affected the agonist potency at T2R14 in HASM cells. To understand the molecular mechanism of interaction between cholesterol and T2R14, site-directed mutagenesis was utilized, and the role of putative cholesterol binding motif's (CRAC and CARC) in T2R14 was examined. Functional characterization of wild-type and mutant T2R14 receptors suggest that amino acid residues K110, F236 and L239 to be crucial in T2R14-cholesterol functional interaction. In conclusion, my results show that cholesterol influences the T2R14 signaling efficacy by forming direct interactions with the receptor and consequently plays a regulatory role in T2R14 mediated signaling in human airway cells.

A major plasma membrane lipid known to influence the function of membrane proteins including GPCRs is sphingomyelin. The role of sphingomyelin in T2R function is unexplored thus far. My results-suggest that unavailability of membrane sphingomyelin did not affect the agonist-promoted T2R14 Ca^{2+} signaling in heterologous expression system and also in primary HASM cells. In addition, T2R14 mediated downstream AMPK activation was also unaffected in sphingomyelin depleted conditions; however, cholesterol depletion impaired the T2R14-mediated AMPK activation. AT_1R expressed in HASM cells, and signals through Ca^{2+} and AMPK was used as a control. Results suggest that similar to T2R14, membrane sphingomyelin depletion did not affect AT_1R signaling. However, membrane cholesterol depletion impaired AT_1R mediated Ca^{2+} signaling and AMPK activation. Interestingly, amino acid sequence analysis revealed the presence of putative sphingolipid binding motif in both T2R14 and AT_1R suggesting that the presence of a motif alone might not be suggestive of sphingomyelin

sensitivity. These results demonstrate that in contrast to membrane cholesterol, sphingomyelin does not affect the agonist-induced T2R14 signaling, however, it may play a role in other aspects of T2R14 function.

The final part of my thesis involved studies aimed at understanding the structural basis of T2R14 activation. As the mechanisms of T2R activation is poorly understood, the identification of structural determinants of T2Rs that regulate its activation and efficacy could be beneficial in designing ligands with high potency and specificity. I characterized a highly conserved histidine, present at TM5-ICL3 region of T2R14 (H208) and its role in agonist-induced T2R14 function. Surprisingly, mutation of the conserved H208 (H208A) did not result in increased basal activity of T2R14, in contrast to similar H214A mutation in T2R4 that showed constitutive activity. The H208A mutation in T2R14 resulted in an increase in agonist-induced efficacy for FFA. Interestingly, H208A did not affect the potency of another T2R14 agonist DPH. The H208R compensatory mutation showed FFA response similar to wild-type T2R14. Molecular modeling suggests an FFA-induced shift in the TM helices of H208A that change the network of interactions connecting TM5-ICL3-TM6. These studies identify a crucial residue on the intracellular surface of T2Rs that is involved in bitter ligand selectivity. It also highlights the varied roles carried out by some conserved residues in different T2Rs.

8.2 Future directions

In view of the increasing extraoral relevance of the 25 human T2Rs, there is an urgent need for more in-depth studies focused on elucidating their roles in different pathophysiological states. Our findings demonstrate a role for chemosensory T2R signaling network in evoking beneficial physiological responses in breast cancer. Nevertheless, more studies directed at identifying the downstream signaling cascades activated via basal or intrinsic T2R activation are needed, as they will provide deeper insights into T2R roles in the pathophysiology of breast cancer. Furthermore, considering T2Rs proposed predisposition as inadvertent targets for therapeutic drugs it will be noteworthy to study if T2Rs play a role in unintended adverse effects of drugs used in cancer chemotherapy. Another area where T2Rs could play a beneficial role is in the adjuvant breast cancer therapy, where co-administration of T2R activators may lead to improving the chemosensitivity of the breast cancer cells to anticancer drugs. It has been previously shown that celecoxib, a non-steroidal anti-inflammatory drug, improves the chemosensitivity of breast cancer cells to anticancer agents by inhibiting pathways promoting drug resistance (Xu et al., 2016). Interestingly T2R agonists including chloroquine and noscapine's role in improving the chemo-sensitivity of cancers have been shown, however, T2Rs involvement has not been demonstrated (Shen et al., 2015;Zhang et al., 2015b).

My studies also demonstrate a novel regulatory role of membrane cholesterol in T2R signaling. Moreover, in contrast to membrane cholesterol, sphingomyelin does not directly regulate the agonist-promoted calcium signaling of T2R14 and AT_1R. It suggests that different membrane lipids may distinctly modulate the taste receptor signaling. However, considering the emerging role of membrane-bound signaling hubs where different signaling proteins form scaffolding complexes and each protein's function within the complex is dependent on its

confinement within the hub, therefore, it will be worthwhile to study if T2Rs are involved in forming such scaffolding complexes (Kunzelmann and Mehta, 2013;Feigin et al., 2014;Abu-Arish et al., 2015). Localization of membrane proteins within the specialized cholesterol and sphingolipid-enriched membrane microdomains such as lipid rafts for their functions has been well studied and characterized. Considering cholesterol's role in T2R function, it would be interesting to examine if compartmentalization of T2R within lipid rafts is necessary for its function. Moreover, considering membrane cholesterol's role in regulating T2R function, it would be worthwhile, examining if, T2R signaling gets affected in hypercholesterolemia. For example, low-density lipoprotein receptor deficient mouse ($LDLR^{-/-}$) model which is widely used as a model for hypercholesterolemic atherosclerosis can be used in this regard.

A major limitation in T2R research is the dearth of specific and efficacious T2R ligands. Structure-function studies aimed at understanding the agonist-induced effect on helical rearrangements and its correlation to agonist efficacy may provide novel insights into the key T2R structural determinants defining its agonist specificity and efficacy. Moreover, the role of activation microswitches (rotamer changes in amino acid side chain) in stabilizing the helices or affecting G-protein coupling is known for class A GPCRs (Nygaard et al., 2009;Katritch et al., 2013). Therefore, it would be interesting to examine the presence of such microswitches in T2Rs, which could define its G-protein dependent or independent signaling. Additionally, TAS2R14 genetic variants frequently found in the human patients could be reproduced in heterologous cell system and structure-function studies could be performed.

A better understanding of various factors governing T2R function in pathophysiological conditions could be beneficial in developing novel therapeutic avenues, especially in airway

diseases. Indeed, understanding of the T2R function and its concomitant pathophysiological implications is still in its nascent stages and to this end, further studies are required.

CHAPTER 9

9.0 REFERENCES

ScanProsite (https://prosite.expasy.org/scanprosite/).

Abu-Arish, A., Pandzic, E., Goepp, J., Matthes, E., Hanrahan, J.W., and Wiseman, P.W. (2015). Cholesterol modulates CFTR confinement in the plasma membrane of primary epithelial cells. *Biophys J* 109**,** 85-94.

Adappa, N.D., Workman, A.D., Hadjiliadis, D., Dorgan, D.J., Frame, D., Brooks, S., Doghramji, L., Palmer, J.N., Mansfield, C., Reed, D.R., and Cohen, N.A. (2015). T2R38 genotype is correlated with sinonasal quality of life in homozygous DeltaF508 cystic fibrosis patients. *Int Forum Allergy Rhinol*.

Adappa, N.D., Zhang, Z., Palmer, J.N., Kennedy, D.W., Doghramji, L., Lysenko, A., Reed, D.R., Scott, T., Zhao, N.W., Owens, D., Lee, R.J., and Cohen, N.A. (2014). The bitter taste receptor T2R38 is an independent risk factor for chronic rhinosinusitis requiring sinus surgery. *Int Forum Allergy Rhinol* 4**,** 3-7.

Adler, E., Hoon, M.A., Mueller, K.L., Chandrashekar, J., Ryba, N.J., and Zuker, C.S. (2000). A novel family of mammalian taste receptors. *Cell* 100**,** 693-702.

Alcohol. Available: http://www.who.int/substance_abuse/facts/alcohol/en/ [Accessed 28 January 2016].

Allen, L.F., Lefkowitz, R.J., Caron, M.G., and Cotecchia, S. (1991). G-protein-coupled receptor genes as protooncogenes: constitutively activating mutation of the alpha 1B-adrenergic receptor enhances mitogenesis and tumorigenicity. *Proc Natl Acad Sci U S A* 88**,** 11354-11358.

Amundson, D.M., and Zhou, M. (1999). Fluorometric method for the enzymatic determination of cholesterol. *J Biochem Biophys Methods* 38**,** 43-52.

Ansoleaga, B., Garcia-Esparcia, P., Pinacho, R., Haro, J.M., Ramos, B., and Ferrer, I. (2015). Decrease in olfactory and taste receptor expression in the dorsolateral prefrontal cortex in chronic schizophrenia. *J Psychiatr Res* 60**,** 109-116.

Aureli, M., Schiumarini, D., Loberto, N., Bassi, R., Tamanini, A., Mancini, G., Tironi, M., Munari, S., Cabrini, G., Dechecchi, M.C., and Sonnino, S. (2016). Unravelling the role of sphingolipids in cystic fibrosis lung disease. *Chem Phys Lipids* 200**,** 94-103.

Avau, B., Rotondo, A., Thijs, T., Andrews, C.N., Janssen, P., Tack, J., and Depoortere, I. (2015). Targeting extra-oral bitter taste receptors modulates gastrointestinal motility with effects on satiation. *Sci Rep* 5**,** 15985.

Azad, A.K., Rauh, R., Vermeulen, F., Jaspers, M., Korbmacher, J., Boissier, B., Bassinet, L., Fichou, Y., Des Georges, M., Stanke, F., De Boeck, K., Dupont, L., Balascakova, M., Hjelte, L., Lebecque, P., Radojkovic, D., Castellani, C., Schwartz, M., Stuhrmann, M., Schwarz, M., Skalicka, V., De Monestrol, I., Girodon, E., Ferec, C., Claustres, M., Tummler, B., Cassiman, J.J., Korbmacher, C., and Cuppens, H. (2009). Mutations in the amiloride-sensitive epithelial sodium channel in patients with cystic fibrosis-like disease. *Hum Mutat* 30**,** 1093-1103.

Baier, C.J., Fantini, J., and Barrantes, F.J. (2011). Disclosure of cholesterol recognition motifs in transmembrane domains of the human nicotinic acetylcholine receptor. *Sci Rep* 1**,** 69.

Bari, M., Paradisi, A., Pasquariello, N., and Maccarrone, M. (2005). Cholesterol-dependent modulation of type 1 cannabinoid receptors in nerve cells. *J Neurosci Res* 81**,** 275-283.

Barnes, P.J. (2008). Immunology of asthma and chronic obstructive pulmonary disease. *Nat Rev Immunol* 8**,** 183-192.

Barnett-Norris, J., Lynch, D., and Reggio, P.H. (2005). Lipids, lipid rafts and caveolae: their importance for GPCR signaling and their centrality to the endocannabinoid system. *Life Sci* 77**,** 1625-1639.

Bauer, D., Redmon, N., Mazzio, E., and Soliman, K.F. (2017). Apigenin inhibits TNFalpha/IL-1alpha-induced CCL2 release through IKBK-epsilon signaling in MDA-MB-231 human breast cancer cells. *PLoS One* 12**,** e0175558.

Behrens, M., and Meyerhof, W. (2006). Bitter taste receptors and human bitter taste perception. *Cell Mol Life Sci* 63**,** 1501-1509.

Besnard, P., Passilly-Degrace, P., and Khan, N.A. (2016). Taste of Fat: A Sixth Taste Modality? *Physiol Rev* 96**,** 151-176.

Bjorkholm, P., Ernst, A.M., Hacke, M., Wieland, F., Brugger, B., and Von Heijne, G. (2014). Identification of novel sphingolipid-binding motifs in mammalian membrane proteins. *Biochim Biophys Acta* 1838**,** 2066-2070.

Blanchard, A.A., Skliris, G.P., Watson, P.H., Murphy, L.C., Penner, C., Tomes, L., Young, T.L., Leygue, E., and Myal, Y. (2009). Claudins 1, 3, and 4 protein expression in ER negative breast cancer correlates with markers of the basal phenotype. *Virchows Arch* 454**,** 647-656.

Bouzo-Lorenzo, M., Santo-Zas, I., Lodeiro, M., Nogueiras, R., Casanueva, F.F., Castro, M., Pazos, Y., Tobin, A.B., Butcher, A.J., and Camina, J.P. (2016). Distinct phosphorylation sites on the ghrelin receptor, GHSR1a, establish a code that determines the functions of ss-arrestins. *Sci Rep* 6**,** 22495.

Braun, T., Mack, B., and Kramer, M.F. (2011). Solitary chemosensory cells in the respiratory and vomeronasal epithelium of the human nose: a pilot study. *Rhinology* 49**,** 507-512.

Brockhoff, A., Behrens, M., Niv, M.Y., and Meyerhof, W. (2010). Structural requirements of bitter taste receptor activation. *Proc Natl Acad Sci U S A* 107**,** 11110-11115.

Brown, D.A., and London, E. (2000). Structure and function of sphingolipid- and cholesterol-rich membrane rafts. *J Biol Chem* 275**,** 17221-17224.

Bufe, B., Breslin, P.A., Kuhn, C., Reed, D.R., Tharp, C.D., Slack, J.P., Kim, U.K., Drayna, D., and Meyerhof, W. (2005). The molecular basis of individual differences in phenylthiocarbamide and propylthiouracil bitterness perception. *Curr Biol* 15**,** 322-327.

Burger, K., Gimpl, G., and Fahrenholz, F. (2000). Regulation of receptor function by cholesterol. *Cell Mol Life Sci* 57**,** 1577-1592.

Butcher, A.J., Prihandoko, R., Kong, K.C., Mcwilliams, P., Edwards, J.M., Bottrill, A., Mistry, S., and Tobin, A.B. (2011). Differential G-protein-coupled receptor phosphorylation provides evidence for a signaling bar code. *J Biol Chem* 286**,** 11506-11518.

Cai, K., Itoh, Y., and Khorana, H.G. (2001). Mapping of contact sites in complex formation between transducin and light-activated rhodopsin by covalent crosslinking: use of a photoactivatable reagent. *Proc Natl Acad Sci U S A* 98**,** 4877-4882.

Caicedo, A., Pereira, E., Margolskee, R.F., and Roper, S.D. (2003). Role of the G-protein subunit alpha-gustducin in taste cell responses to bitter stimuli. *J Neurosci* 23**,** 9947-9952.

Camoretti-Mercado, B., Pauer, S.H., Yong, H.M., Smith, D.C., Deshpande, D.A., An, S.S., and Liggett, S.B. (2015). Pleiotropic Effects of Bitter Taste Receptors on [Ca2+]i Mobilization, Hyperpolarization, and Relaxation of Human Airway Smooth Muscle Cells. *PLoS One* 10**,** e0131582.

Campa, D., De Rango, F., Carrai, M., Crocco, P., Montesanto, A., Canzian, F., Rose, G., Rizzato, C., Passarino, G., and Barale, R. (2012). Bitter taste receptor polymorphisms and human aging. *PLoS One* 7**,** e45232.

Campa, D., Vodicka, P., Pardini, B., Naccarati, A., Carrai, M., Vodickova, L., Novotny, J., Hemminki, K., Forsti, A., Barale, R., and Canzian, F. (2010). A gene-wide investigation on polymorphisms in the taste receptor 2R14 (TAS2R14) and susceptibility to colorectal cancer. *BMC Med Genet* 11**,** 88.

Caramori, G., and Adcock, I. (2003). Pharmacology of airway inflammation in asthma and COPD. *Pulm Pharmacol Ther* 16**,** 247-277.

Cargiulo, T. (2007). Understanding the health impact of alcohol dependence. *Am J Health Syst Pharm* 64**,** S5-11.

Carrai, M., Steinke, V., Vodicka, P., Pardini, B., Rahner, N., Holinski-Feder, E., Morak, M., Schackert, H.K., Gorgens, H., Stemmler, S., Betz, B., Kloor, M., Engel, C., Buttner, R., Naccarati, A., Vodickova, L., Novotny, J., Stein, A., Hemminki, K., Propping, P., Forsti, A., Canzian, F., Barale, R., and Campa, D. (2011). Association between TAS2R38 gene polymorphisms and colorectal cancer risk: a case-control study in two independent populations of Caucasian origin. *PLoS One* 6**,** e20464.

Catapano, L.A., and Manji, H.K. (2007). G protein-coupled receptors in major psychiatric disorders. *Biochim Biophys Acta* 1768**,** 976-993.

Cattaneo, C., Gargari, G., Koirala, R., Laureati, M., Riso, P., Guglielmetti, S., and Pagliarini, E. (2019). New insights into the relationship between taste perception and oral microbiota composition. *Sci Rep* 9**,** 3549.

Chakraborty, R., Xu, B., Bhullar, R.P., and Chelikani, P. (2015). Expression of g protein-coupled receptors in Mammalian cells. *Methods Enzymol* 556**,** 267-281.

Chandrashekar, J., Hoon, M.A., Ryba, N.J., and Zuker, C.S. (2006). The receptors and cells for mammalian taste. *Nature* 444**,** 288-294.

Chandrashekar, J., Mueller, K.L., Hoon, M.A., Adler, E., Feng, L., Guo, W., Zuker, C.S., and Ryba, N.J. (2000). T2Rs function as bitter taste receptors. *Cell* 100**,** 703-711.

Chattopadhyay, A., Paila, Y.D., Shrivastava, S., Tiwari, S., Singh, P., and Fantini, J. (2012). Sphingolipid-binding domain in the serotonin(1A) receptor. *Adv Exp Med Biol* 749**,** 279-293.

Chaudhari, N., and Roper, S.D. (2010). The cell biology of taste. *J Cell Biol* 190**,** 285-296.

Chee, M.J., Morl, K., Lindner, D., Merten, N., Zamponi, G.W., Light, P.E., Beck-Sickinger, A.G., and Colmers, W.F. (2008). The third intracellular loop stabilizes the inactive state of the neuropeptide Y1 receptor. *J Biol Chem* 283**,** 33337-33346.

Chen, M.C., Wu, S.V., Reeve, J.R., Jr., and Rozengurt, E. (2006). Bitter stimuli induce Ca2+ signaling and CCK release in enteroendocrine STC-1 cells: role of L-type voltage-sensitive Ca2+ channels. *Am J Physiol Cell Physiol* 291**,** C726-739.

Cheng, H., Lear-Rooney, C.M., Johansen, L., Varhegyi, E., Chen, Z.W., Olinger, G.G., and Rong, L. (2015). Inhibition of Ebola and Marburg Virus Entry by G Protein-Coupled Receptor Antagonists. *J Virol* 89**,** 9932-9938.

Cherezov, V., Rosenbaum, D.M., Hanson, M.A., Rasmussen, S.G., Thian, F.S., Kobilka, T.S., Choi, H.J., Kuhn, P., Weis, W.I., Kobilka, B.K., and Stevens, R.C. (2007). High-resolution crystal structure of an engineered human beta2-adrenergic G protein-coupled receptor. *Science* 318**,** 1258-1265.

Choi, J.H., Lee, J., Yang, S., Lee, E.K., Hwangbo, Y., and Kim, J. (2018). Genetic variations in TAS2R3 and TAS2R4 bitterness receptors modify papillary carcinoma risk and thyroid function in Korean females. *Sci Rep* 8**,** 15004.

Clapp, T.R., Stone, L.M., Margolskee, R.F., and Kinnamon, S.C. (2001). Immunocytochemical evidence for co-expression of Type III IP3 receptor with signaling components of bitter taste transduction. *BMC Neurosci* 2**,** 6.

Clapp, T.R., Trubey, K.R., Vandenbeuch, A., Stone, L.M., Margolskee, R.F., Chaudhari, N., and Kinnamon, S.C. (2008). Tonic activity of Galpha-gustducin regulates taste cell responsivity. *FEBS Lett* 582**,** 3783-3787.

Clark, A.A., Dotson, C.D., Elson, A.E., Voigt, A., Boehm, U., Meyerhof, W., Steinle, N.I., and Munger, S.D. (2015). TAS2R bitter taste receptors regulate thyroid function. *FASEB J* 29**,** 164-172.

Cohen, T.S., and Prince, A. (2012). Cystic fibrosis: a mucosal immunodeficiency syndrome. *Nat Med* 18**,** 509-519.

Coulon, A.L., Savagner, F., Briet, C., Vernin, M., Munier, M., Chabre, O., and Rodien, P. (2016). Prolonged and Severe Gestational Thyrotoxicosis Due to Enhanced hCG Sensitivity of a Mutant Thyrotropin Receptor. *J Clin Endocrinol Metab* 101**,** 10-11.

Craig, W.J. (1997). Phytochemicals: guardians of our health. *J Am Diet Assoc* 97**,** S199-204.

Cross, B.M., Breitwieser, G.E., Reinhardt, T.A., and Rao, R. (2014). Cellular calcium dynamics in lactation and breast cancer: from physiology to pathology. *Am J Physiol Cell Physiol* 306**,** C515-526.

Cvicek, V., Goddard, W.A., 3rd, and Abrol, R. (2016). Structure-Based Sequence Alignment of the Transmembrane Domains of All Human GPCRs: Phylogenetic, Structural and Functional Implications. *PLoS Comput Biol* 12**,** e1004805.

Damak, S., Rong, M., Yasumatsu, K., Kokrashvili, Z., Perez, C.A., Shigemura, N., Yoshida, R., Mosinger, B., Jr., Glendinning, J.I., Ninomiya, Y., and Margolskee, R.F. (2006). Trpm5 null mice respond to bitter, sweet, and umami compounds. *Chem Senses* 31**,** 253-264.

Delano, W.L. (2002). PyMOL: An open-source molecular graphics tool. *CCP4 Newsletter on Protein Crystallography***,** 82-92.

Deshpande, D.A., Robinett, K.S., Wang, W.C., Sham, J.S., An, S.S., and Liggett, S.B. (2011). Bronchodilator activity of bitter tastants in human tissue. *Nat Med* 17**,** 776-778.

Deshpande, D.A., Wang, W.C., Mcilmoyle, E.L., Robinett, K.S., Schillinger, R.M., An, S.S., Sham, J.S., and Liggett, S.B. (2010). Bitter taste receptors on airway smooth muscle bronchodilate by localized calcium signaling and reverse obstruction. *Nat Med* 16**,** 1299-1304.

Di Scala, C., Baier, C.J., Evans, L.S., Williamson, P.T.F., Fantini, J., and Barrantes, F.J. (2017). Relevance of CARC and CRAC Cholesterol-Recognition Motifs in the Nicotinic Acetylcholine Receptor and Other Membrane-Bound Receptors. *Curr Top Membr* 80**,** 3-23.

Dorsam, R.T., and Gutkind, J.S. (2007). G-protein-coupled receptors and cancer. *Nat Rev Cancer* 7**,** 79-94.

Dotson, C.D., Shaw, H.L., Mitchell, B.D., Munger, S.D., and Steinle, N.I. (2010). Variation in the gene TAS2R38 is associated with the eating behavior disinhibition in Old Order Amish women. *Appetite* 54**,** 93-99.

Dotson, C.D., Wallace, M.R., Bartoshuk, L.M., and Logan, H.L. (2012). Variation in the gene TAS2R13 is associated with differences in alcohol consumption in patients with head and neck cancer. *Chem Senses* 37**,** 737-744.

Drewnowski, A., Henderson, S.A., and Shore, A.B. (1997a). Genetic sensitivity to 6-n-propylthiouracil (PROP) and hedonic responses to bitter and sweet tastes. *Chem Senses* 22**,** 27-37.

Drewnowski, A., Henderson, S.A., and Shore, A.B. (1997b). Taste responses to naringin, a flavonoid, and the acceptance of grapefruit juice are related to genetic sensitivity to 6-n-propylthiouracil. *Am J Clin Nutr* 66**,** 391-397.

Duffy, V.B., Davidson, A.C., Kidd, J.R., Kidd, K.K., Speed, W.C., Pakstis, A.J., Reed, D.R., Snyder, D.J., and Bartoshuk, L.M. (2004). Bitter receptor gene (TAS2R38), 6-n-propylthiouracil (PROP) bitterness and alcohol intake. *Alcohol Clin Exp Res* 28**,** 1629-1637.

Durig, J., Schmucker, U., and Duhrsen, U. (2001). Differential expression of chemokine receptors in B cell malignancies. *Leukemia* 15**,** 752-756.

Eich, C., Manzo, C., De Keijzer, S., Bakker, G.J., Reinieren-Beeren, I., Garcia-Parajo, M.F., and Cambi, A. (2016). Changes in membrane sphingolipid composition modulate dynamics and adhesion of integrin nanoclusters. *Sci Rep* 6**,** 20693.

Ekoff, M., Choi, J.H., James, A., Dahlen, B., Nilsson, G., and Dahlen, S.E. (2014). Bitter taste receptor (TAS2R) agonists inhibit IgE-dependent mast cell activation. *J Allergy Clin Immunol* 134**,** 475-478.

Epand, R.M., Thomas, A., Brasseur, R., and Epand, R.F. (2010). Cholesterol interaction with proteins that partition into membrane domains: an overview. *Subcell Biochem* 51**,** 253-278.

Fanta, C.H. (2009). Asthma. *New England Journal of Medicine* 360**,** 1002-1014.

Fantini, J., and Barrantes, F.J. (2009). Sphingolipid/cholesterol regulation of neurotransmitter receptor conformation and function. *Biochim Biophys Acta* 1788**,** 2345-2361.

Fantini, J., and Barrantes, F.J. (2013). How cholesterol interacts with membrane proteins: an exploration of cholesterol-binding sites including CRAC, CARC, and tilted domains. *Front Physiol* 4**,** 31.

Fantini, J., Di Scala, C., Evans, L.S., Williamson, P.T., and Barrantes, F.J. (2016). A mirror code for protein-cholesterol interactions in the two leaflets of biological membranes. *Sci Rep* 6**,** 21907.

Feigin, M.E., Xue, B., Hammell, M.C., and Muthuswamy, S.K. (2014). G-protein-coupled receptor GPR161 is overexpressed in breast cancer and is a promoter of cell proliferation and invasion. *Proc Natl Acad Sci U S A* 111**,** 4191-4196.

Feldman, D.S., Carnes, C.A., Abraham, W.T., and Bristow, M.R. (2005). Mechanisms of disease: beta-adrenergic receptors--alterations in signal transduction and pharmacogenomics in heart failure. *Nat Clin Pract Cardiovasc Med* 2**,** 475-483.

Foster, L.J., De Hoog, C.L., and Mann, M. (2003). Unbiased quantitative proteomics of lipid rafts reveals high specificity for signaling factors. *Proc Natl Acad Sci U S A* 100**,** 5813-5818.

Foster, S.R., Porrello, E.R., Purdue, B., Chan, H.W., Voigt, A., Frenzel, S., Hannan, R.D., Moritz, K.M., Simmons, D.G., Molenaar, P., Roura, E., Boehm, U., Meyerhof, W., and Thomas, W.G. (2013). Expression, regulation and putative nutrient-sensing function of taste GPCRs in the heart. *PLoS One* 8**,** e64579.

Foulkes, W.D., Smith, I.E., and Reis-Filho, J.S. (2010). Triple-negative breast cancer. *N Engl J Med* 363**,** 1938-1948.

Freund, J.R., Mansfield, C.J., Doghramji, L.J., Adappa, N.D., Palmer, J.N., Kennedy, D.W., Reed, D.R., Jiang, P., and Lee, R.J. (2018). Activation of airway epithelial bitter taste receptors by Pseudomonas aeruginosa quinolones modulates calcium, cyclic-AMP, and nitric oxide signaling. *J Biol Chem* 293**,** 9824-9840.

Fukami, M., Suzuki, E., Igarashi, M., Miyado, M., and Ogata, T. (2018). Gain-of-function mutations in G-protein-coupled receptor genes associated with human endocrine disorders. *Clin Endocrinol (Oxf)* 88**,** 351-359.

Gache, C., Berthois, Y., Cvitkovic, E., Martin, P.M., and Saez, S. (1999). Differential regulation of normal and tumoral breast epithelial cell growth by fibroblasts and 1,25-dihydroxyvitamin D3. *Breast Cancer Res Treat* 55**,** 29-39.

Gaida, M.M., Mayer, C., Dapunt, U., Stegmaier, S., Schirmacher, P., Wabnitz, G.H., and Hansch, G.M. (2016a). Expression of the bitter receptor T2R38 in pancreatic cancer: localization in lipid droplets and activation by a bacteria-derived quorum-sensing molecule. *Oncotarget* 7**,** 12623-12632.

Gaida, M.M., Mayer, C., Dapunt, U., Stegmaier, S., Schirmacher, P., Wabnitz, G.H., and Hansch, G.M. (2016b). Expression of the bitter receptor T2R38 in pancreatic cancer: localization in lipid droplets and activation by a bacteria-derived quorum-sensing molecule. *Oncotarget*.

Ghio, A., Lehmann, J., Winsett, D., Richards, J., and Costa, D. (2005). Colchicine decreases airway hyperreactivity after phosgene exposure. *Inhal Toxicol* 17**,** 277-285.

Gianfrancesco, M.A., Paquot, N., Piette, J., and Legrand-Poels, S. (2018). Lipid bilayer stress in obesity-linked inflammatory and metabolic disorders. *Biochem Pharmacol*.

Gilbertson, T.A., Damak, S., and Margolskee, R.F. (2000). The molecular physiology of taste transduction. *Curr Opin Neurobiol* 10**,** 519-527.

Gimpl, G. (2016). Interaction of G protein coupled receptors and cholesterol. *Chem Phys Lipids* 199**,** 61-73.

Gimpl, G., Burger, K., and Fahrenholz, F. (1997). Cholesterol as modulator of receptor function. *Biochemistry* 36**,** 10959-10974.

Goni, F.M., and Alonso, A. (2002). Sphingomyelinases: enzymology and membrane activity. *FEBS Lett* 531**,** 38-46.

Gosens, R., Stelmack, G.L., Dueck, G., Mcneill, K.D., Yamasaki, A., Gerthoffer, W.T., Unruh, H., Gounni, A.S., Zaagsma, J., and Halayko, A.J. (2006). Role of caveolin-1 in p42/p44 MAP kinase activation and proliferation of human airway smooth muscle. *Am J Physiol Lung Cell Mol Physiol* 291**,** L523-534.

Grassin-Delyle, S., Abrial, C., Fayad-Kobeissi, S., Brollo, M., Faisy, C., Alvarez, J.C., Naline, E., and Devillier, P. (2013). The expression and relaxant effect of bitter taste receptors in human bronchi. *Respir Res* 14**,** 134.

Gray, K.A., Yates, B., Seal, R.L., Wright, M.W., and Bruford, E.A. (2015). Genenames.org: the HGNC resources in 2015. *Nucleic Acids Res* 43**,** D1079-1085.

Green, S.A., Turki, J., Bejarano, P., Hall, I.P., and Liggett, S.B. (1995). Influence of beta 2-adrenergic receptor genotypes on signal transduction in human airway smooth muscle cells. *Am J Respir Cell Mol Biol* 13**,** 25-33.

Gu, Q.D., Joe, D.S., and Gilbert, C.A. (2017). Activation of bitter taste receptors in pulmonary nociceptors sensitizes TRPV1 channels through the PLC and PKC signaling pathway. *Am J Physiol Lung Cell Mol Physiol* 312**,** L326-L333.

Gulshan, K., Brubaker, G., Wang, S., Hazen, S.L., and Smith, J.D. (2013). Sphingomyelin depletion impairs anionic phospholipid inward translocation and induces cholesterol efflux. *J Biol Chem* 288**,** 37166-37179.

Gunasekara, L., Al-Saiedy, M., Green, F., Pratt, R., Bjornson, C., Yang, A., Michael Schoel, W., Mitchell, I., Brindle, M., Montgomery, M., Keys, E., Dennis, J., Shrestha, G., and Amrein, M. (2017). Pulmonary surfactant dysfunction in pediatric cystic fibrosis: Mechanisms and reversal with a lipid-sequestering drug. *J Cyst Fibros* 16**,** 565-572.

Halayko, A.J., Tran, T., and Gosens, R. (2008). Phenotype and functional plasticity of airway smooth muscle: role of caveolae and caveolins. *Proc Am Thorac Soc* 5**,** 80-88.

Hanson, M.A., Cherezov, V., Griffith, M.T., Roth, C.B., Jaakola, V.P., Chien, E.Y., Velasquez, J., Kuhn, P., and Stevens, R.C. (2008). A specific cholesterol binding site is established by the 2.8 A structure of the human beta2-adrenergic receptor. *Structure* 16**,** 897-905.

Harayama, T., and Riezman, H. (2018). Understanding the diversity of membrane lipid composition. *Nat Rev Mol Cell Biol* 19**,** 281-296.

Harikumar, K.G., Puri, V., Singh, R.D., Hanada, K., Pagano, R.E., and Miller, L.J. (2005). Differential effects of modification of membrane cholesterol and sphingolipids on the conformation, function, and trafficking of the G protein-coupled cholecystokinin receptor. *J Biol Chem* 280**,** 2176-2185.

Hariri, B.M., Mcmahon, D.B., Chen, B., Freund, J.R., Mansfield, C.J., Doghramji, L.J., Adappa, N.D., Palmer, J.N., Kennedy, D.W., Reed, D.R., Jiang, P., and Lee, R.J. (2017). Flavones modulate respiratory epithelial innate immunity: Anti-inflammatory effects and activation of the T2R14 receptor. *J Biol Chem* 292**,** 8484-8497.

Heng, B.C., Aubel, D., and Fussenegger, M. (2013). An overview of the diverse roles of G-protein coupled receptors (GPCRs) in the pathophysiology of various human diseases. *Biotechnol Adv* 31**,** 1676-1694.

Hermans, E., Challiss, R.A., and Nahorski, S.R. (1999). Effects of varying the expression level of recombinant human mGlu1alpha receptors on the pharmacological properties of agonists and antagonists. *Br J Pharmacol* 126**,** 873-882.

Hinrichs, A.L., Wang, J.C., Bufe, B., Kwon, J.M., Budde, J., Allen, R., Bertelsen, S., Evans, W., Dick, D., Rice, J., Foroud, T., Nurnberger, J., Tischfield, J.A., Kuperman, S., Crowe, R., Hesselbrock, V., Schuckit, M., Almasy, L., Porjesz, B., Edenberg, H.J., Begleiter, H., Meyerhof, W., Bierut, L.J., and Goate, A.M. (2006). Functional variant in a bitter-taste receptor (hTAS2R16) influences risk of alcohol dependence. *Am J Hum Genet* 78**,** 103-111.

Hla, T., and Dannenberg, A.J. (2012). Sphingolipid signaling in metabolic disorders. *Cell Metab* 16**,** 420-434.

Hoon, M.A., Adler, E., Lindemeier, J., Battey, J.F., Ryba, N.J., and Zuker, C.S. (1999). Putative mammalian taste receptors: a class of taste-specific GPCRs with distinct topographic selectivity. *Cell* 96**,** 541-551.

Howitt, M.R., Lavoie, S., Michaud, M., Blum, A.M., Tran, S.V., Weinstock, J.V., Gallini, C.A., Redding, K., Margolskee, R.F., Osborne, L.C., Artis, D., and Garrett, W.S. (2016). Tuft cells, taste-chemosensory cells, orchestrate parasite type 2 immunity in the gut. *Science* 351**,** 1329-1333.

Huang, L., Shanker, Y.G., Dubauskaite, J., Zheng, J.Z., Yan, W., Rosenzweig, S., Spielman, A.I., Max, M., and Margolskee, R.F. (1999). Ggamma13 colocalizes with gustducin in taste receptor cells and mediates IP3 responses to bitter denatonium. *Nat Neurosci* 2**,** 1055-1062.

Hunter, I., and Nixon, G.F. (2006). Spatial compartmentalization of tumor necrosis factor (TNF) receptor 1-dependent signaling pathways in human airway smooth muscle cells. Lipid rafts are essential for TNF-alpha-mediated activation of RhoA but dispensable for the activation of the NF-kappaB and MAPK pathways. *J Biol Chem* 281**,** 34705-34715.

Huwiler, A., Kolter, T., Pfeilschifter, J., and Sandhoff, K. (2000). Physiology and pathophysiology of sphingolipid metabolism and signaling. *Biochim Biophys Acta* 1485**,** 63-99.

Ikeda, M., Arai, M., Okuno, T., and Shimizu, T. (2003). TMPDB: a database of experimentally-characterized transmembrane topologies. *Nucleic Acids Res* 31**,** 406-409.

Illinger, D., Duportail, G., Mely, Y., Poirel-Morales, N., Gerard, D., and Kuhry, J.G. (1995). A comparison of the fluorescence properties of TMA-DPH as a probe for plasma membrane and for endocytic membrane. *Biochim Biophys Acta* 1239**,** 58-66.

Inoue, H., Nojima, H., and Okayama, H. (1990). High efficiency transformation of Escherichia coli with plasmids. *Gene* 96**,** 23-28.

Insel, P.A., Head, B.P., Ostrom, R.S., Patel, H.H., Swaney, J.S., Tang, C.M., and Roth, D.M. (2005). Caveolae and lipid rafts: G protein-coupled receptor signaling microdomains in cardiac myocytes. *Ann N Y Acad Sci* 1047**,** 166-172.

Jafurulla, M., Bandari, S., Pucadyil, T.J., and Chattopadhyay, A. (2017a). Sphingolipids modulate the function of human serotonin1A receptors: Insights from sphingolipid-deficient cells. *Biochim Biophys Acta* 1859**,** 598-604.

Jafurulla, M., and Chattopadhyay, A. (2015). Sphingolipids in the function of G protein-coupled receptors. *Eur J Pharmacol* 763**,** 241-246.

Jafurulla, M., and Chattopadhyay, A. (2017). Structural Stringency of Cholesterol for Membrane Protein Function Utilizing Stereoisomers as Novel Tools: A Review. *Methods Mol Biol* 1583**,** 21-39.

Jafurulla, M., Nalli, A., and Chattopadhyay, A. (2017b). Membrane cholesterol oxidation in live cells enhances the function of serotonin1A receptors. *Chem Phys Lipids* 203**,** 71-77.

Jafurulla, M., Pucadyil, T.J., and Chattopadhyay, A. (2008). Effect of sphingomyelinase treatment on ligand binding activity of human serotonin1A receptors. *Biochim Biophys Acta* 1778**,** 2022-2025.

Jafurulla, M., Tiwari, S., and Chattopadhyay, A. (2011). Identification of cholesterol recognition amino acid consensus (CRAC) motif in G-protein coupled receptors. *Biochem Biophys Res Commun* 404**,** 569-573.

Jaggupilli, A., Howard, R., Upadhyaya, J.D., Bhullar, R.P., and Chelikani, P. (2016). Bitter taste receptors: Novel insights into the biochemistry and pharmacology. *Int J Biochem Cell Biol* 77**,** 184-196.

Jaggupilli, A., Singh, N., De Jesus, V.C., Gounni, M.S., Dhanaraj, P., and Chelikani, P. (2018a). Chemosensory bitter taste receptors (T2Rs) are activated by multiple antibiotics. *FASEB J***,** fj201800521RR.

Jaggupilli, A., Singh, N., Jesus, V.C., Duan, K., and Chelikani, P. (2018b). Characterization of the Binding Sites for Bacterial Acyl Homoserine Lactones (AHLs) on Human Bitter Taste Receptors (T2Rs). *ACS Infect Dis* 4**,** 1146-1156.

Jaggupilli, A., Singh, N., Upadhyaya, J., Sikarwar, A.S., Arakawa, M., Dakshinamurti, S., Bhullar, R.P., Duan, K., and Chelikani, P. (2017). Analysis of the expression of human bitter taste receptors in extraoral tissues. *Mol Cell Biochem* 426**,** 137-147.

Jamin, N., Neumann, J.M., Ostuni, M.A., Vu, T.K., Yao, Z.X., Murail, S., Robert, J.C., Giatzakis, C., Papadopoulos, V., and Lacapere, J.J. (2005). Characterization of the cholesterol recognition amino acid consensus sequence of the peripheral-type benzodiazepine receptor. *Mol Endocrinol* 19**,** 588-594.

Jang, H.J., Kokrashvili, Z., Theodorakis, M.J., Carlson, O.D., Kim, B.J., Zhou, J., Kim, H.H., Xu, X., Chan, S.L., Juhaszova, M., Bernier, M., Mosinger, B., Margolskee, R.F., and Egan, J.M. (2007). Gut-expressed gustducin and taste receptors regulate secretion of glucagon-like peptide-1. *Proc Natl Acad Sci U S A* 104**,** 15069-15074.

Jeon, T.I., Zhu, B., Larson, J.L., and Osborne, T.F. (2008). SREBP-2 regulates gut peptide secretion through intestinal bitter taste receptor signaling in mice. *J Clin Invest* 118**,** 3693-3700.

Jeong, J.H., An, J.Y., Kwon, Y.T., Rhee, J.G., and Lee, Y.J. (2009). Effects of low dose quercetin: cancer cell-specific inhibition of cell cycle progression. *J Cell Biochem* 106**,** 73-82.

Jones, L.J., Gray, M., Yue, S.T., Haugland, R.P., and Singer, V.L. (2001). Sensitive determination of cell number using the CyQUANT cell proliferation assay. *J Immunol Methods* 254**,** 85-98.

Kanoh, S., Tanabe, T., and Rubin, B.K. (2011). Dapsone inhibits IL-8 secretion from human bronchial epithelial cells stimulated with lipopolysaccharide and resolves airway inflammation in the ferret. *Chest* 140**,** 980-990.

Katdare, M., Osborne, M.P., and Telang, N.T. (1998). Inhibition of aberrant proliferation and induction of apoptosis in pre-neoplastic human mammary epithelial cells by natural phytochemicals. *Oncol Rep* 5**,** 311-315.

Katritch, V., Cherezov, V., and Stevens, R.C. (2013). Structure-function of the G protein-coupled receptor superfamily. *Annu Rev Pharmacol Toxicol* 53**,** 531-556.

Kim, D., Cho, S., Castano, M.A., Panettieri, R.A., Woo, J.A., and Liggett, S.B. (2018a). Biased TAS2R Bronchodilators Inhibit Airway Smooth Muscle Growth by Downregulating pERK1/2. *Am J Respir Cell Mol Biol*.

Kim, D., Cho, S., Castano, M.A., Panettieri, R.A., Woo, J.A., and Liggett, S.B. (2019). Biased TAS2R Bronchodilators Inhibit Airway Smooth Muscle Growth by Downregulating Phosphorylated Extracellular Signal-regulated Kinase 1/2. *Am J Respir Cell Mol Biol* 60**,** 532-540.

Kim, D., Woo, J.A., Geffken, E., An, S.S., and Liggett, S.B. (2017a). Coupling of Airway Smooth Muscle Bitter Taste Receptors to Intracellular Signaling and Relaxation Is via Galphai1,2,3. *Am J Respir Cell Mol Biol* 56**,** 762-771.

Kim, K.H., Lee, I.S., Park, J.Y., Kim, Y., An, E.J., and Jang, H.J. (2018b). Cucurbitacin B Induces Hypoglycemic Effect in Diabetic Mice by Regulation of AMP-Activated Protein Kinase Alpha and Glucagon-Like Peptide-1 via Bitter Taste Receptor Signaling. *Front Pharmacol* 9**,** 1071.

Kim, N., Jung, Y., Nam, M., Sun Kang, M., Lee, M.K., Cho, Y., Choi, E.K., Hwang, G.S., and Soo Kim, H. (2017b). Angiotensin II affects inflammation mechanisms via AMPK-related signalling pathways in HL-1 atrial myocytes. *Sci Rep* 7**,** 10328.

Kim, U., Wooding, S., Ricci, D., Jorde, L.B., and Drayna, D. (2005). Worldwide haplotype diversity and coding sequence variation at human bitter taste receptor loci. *Hum Mutat* 26**,** 199-204.

Kim, U.K., Jorgenson, E., Coon, H., Leppert, M., Risch, N., and Drayna, D. (2003). Positional cloning of the human quantitative trait locus underlying taste sensitivity to phenylthiocarbamide. *Science* 299**,** 1221-1225.

Kinnamon, S.C. (2012). Taste receptor signalling - from tongues to lungs. *Acta Physiol (Oxf)* 204**,** 158-168.

Koarai, A., Yanagisawa, S., Sugiura, H., Ichikawa, T., Kikuchi, T., Furukawa, K., Akamatsu, K., Hirano, T., Nakanishi, M., Matsunaga, K., Minakata, Y., and Ichinose, M. (2012). 25-Hydroxycholesterol enhances cytokine release and Toll-like receptor 3 response in airway epithelial cells. *Respir Res* 13**,** 63.

Krogh, A., Larsson, B., Von Heijne, G., and Sonnhammer, E.L. (2001). Predicting transmembrane protein topology with a hidden Markov model: application to complete genomes. *J Mol Biol* 305**,** 567-580.

Kunzelmann, K., and Mehta, A. (2013). CFTR: a hub for kinases and crosstalk of cAMP and Ca2+. *FEBS J* 280**,** 4417-4429.

Kusuhara, Y., Yoshida, R., Ohkuri, T., Yasumatsu, K., Voigt, A., Hubner, S., Maeda, K., Boehm, U., Meyerhof, W., and Ninomiya, Y. (2013). Taste responses in mice lacking taste receptor subunit T1R1. *J Physiol* 591**,** 1967-1985.

Kwatra, D., Venugopal, A., Standing, D., Ponnurangam, S., Dhar, A., Mitra, A., and Anant, S. (2013). Bitter melon extracts enhance the activity of chemotherapeutic agents through the modulation of multiple drug resistance. *J Pharm Sci* 102**,** 4444-4454.

Lakshmanan, I., and Batra, S.K. (2013). Protocol for Apoptosis Assay by Flow Cytometry Using Annexin V Staining Method. *Bio Protoc* 3.

Lambert, J.D., Vandusen, S.R., Cockroft, J.E., Smith, E.C., Greenwood, D.C., and Cade, J.E. (2018). Bitter taste sensitivity, food intake, and risk of malignant cancer in the UK Women's Cohort Study. *Eur J Nutr*.

Lania, A.G., Mantovani, G., and Spada, A. (2006). Mechanisms of disease: Mutations of G proteins and G-protein-coupled receptors in endocrine diseases. *Nat Clin Pract Endocrinol Metab* 2**,** 681-693.

Lee, R.J., Kofonow, J.M., Rosen, P.L., Siebert, A.P., Chen, B., Doghramji, L., Xiong, G., Adappa, N.D., Palmer, J.N., Kennedy, D.W., Kreindler, J.L., Margolskee, R.F., and Cohen, N.A. (2014). Bitter and sweet taste receptors regulate human upper respiratory innate immunity. *J Clin Invest* 124**,** 1393-1405.

Lee, R.J., Xiong, G., Kofonow, J.M., Chen, B., Lysenko, A., Jiang, P., Abraham, V., Doghramji, L., Adappa, N.D., Palmer, J.N., Kennedy, D.W., Beauchamp, G.K., Doulias, P.T., Ischiropoulos, H., Kreindler, J.L., Reed, D.R., and Cohen, N.A. (2012). T2R38 taste receptor polymorphisms underlie susceptibility to upper respiratory infection. *J Clin Invest* 122**,** 4145-4159.

Levit, A., Nowak, S., Peters, M., Wiener, A., Meyerhof, W., Behrens, M., and Niv, M.Y. (2014). The bitter pill: clinical drugs that activate the human bitter taste receptor TAS2R14. *FASEB J* 28**,** 1181-1197.

Levitsky, D.O., and Dembitsky, V.M. (2014). Anti-breast Cancer Agents Derived from Plants. *Nat Prod Bioprospect*.

Lewinska, A., Bednarz, D., Adamczyk-Grochala, J., and Wnuk, M. (2017). Phytochemical-induced nucleolar stress results in the inhibition of breast cancer cell proliferation. *Redox Biol* 12**,** 469-482.

Li, H., and Papadopoulos, V. (1998). Peripheral-type benzodiazepine receptor function in cholesterol transport. Identification of a putative cholesterol recognition/interaction amino acid sequence and consensus pattern. *Endocrinology* 139**,** 4991-4997.

Li, N., Cai, R., Niu, Y., Shen, B., Xu, J., and Cheng, Y. (2012). Inhibition of angiotensin II-induced contraction of human airway smooth muscle cells by angiotensin-(1-7) via downregulation of the RhoA/ROCK2 signaling pathway. *Int J Mol Med* 30**,** 811-818.

Li, X., Staszewski, L., Xu, H., Durick, K., Zoller, M., and Adler, E. (2002). Human receptors for sweet and umami taste. *Proc Natl Acad Sci U S A* 99**,** 4692-4696.

Limame, R., Wouters, A., Pauwels, B., Fransen, E., Peeters, M., Lardon, F., De Wever, O., and Pauwels, P. (2012). Comparative analysis of dynamic cell viability, migration and invasion assessments by novel real-time technology and classic endpoint assays. *PLoS One* 7**,** e46536.

Lin, C.H., Chang, C.Y., Lee, K.R., Lin, H.J., Chen, T.H., and Wan, L. (2015). Flavones inhibit breast cancer proliferation through the Akt/FOXO3a signaling pathway. *BMC Cancer* 15**,** 958.

Lin, C.M., Chen, H.H., Lin, C.A., Wu, H.C., Sheu, J.J., and Chen, H.J. (2017). Apigenin-induced lysosomal degradation of beta-catenin in Wnt/beta-catenin signaling. *Sci Rep* 7**,** 372.

Liszt, K.I., Ley, J.P., Lieder, B., Behrens, M., Stoger, V., Reiner, A., Hochkogler, C.M., Kock, E., Marchiori, A., Hans, J., Widder, S., Krammer, G., Sanger, G.J., Somoza, M.M., Meyerhof, W., and Somoza, V. (2017). Caffeine induces gastric acid secretion via bitter taste signaling in gastric parietal cells. *Proc Natl Acad Sci U S A* 114**,** E6260-E6269.

Liu, K., Jaggupilli, A., Premnath, D., and Chelikani, P. (2018). Plasticity of the ligand binding pocket in the bitter taste receptor T2R7. *Biochim Biophys Acta* 1860**,** 991-999.

Liu, L., Pan, Y., Song, Y., Su, X., Ke, R., Yang, L., Gao, L., and Li, M. (2016a). Activation of AMPK alpha2 inhibits airway smooth muscle cells proliferation. *Eur J Pharmacol* 791**,** 235-243.

Liu, S., Edgerton, S.M., Moore, D.H., 2nd, and Thor, A.D. (2001). Measures of cell turnover (proliferation and apoptosis) and their association with survival in breast cancer. *Clin Cancer Res* 7**,** 1716-1723.

Liu, W., Chun, E., Thompson, A.A., Chubukov, P., Xu, F., Katritch, V., Han, G.W., Roth, C.B., Heitman, L.H., Ap, I.J., Cherezov, V., and Stevens, R.C. (2012). Structural basis for allosteric regulation of GPCRs by sodium ions. *Science* 337**,** 232-236.

Liu, W., Qi, Y., Liu, L., Tang, Y., Wei, J., and Zhou, L. (2016b). Suppression of tumor cell proliferation by quinine via the inhibition of the tumor necrosis factor receptorassociated factor 6AKT interaction. *Mol Med Rep* 14**,** 2171-2179.

Liu, Y., An, S., Ward, R., Yang, Y., Guo, X.X., Li, W., and Xu, T.R. (2016c). G protein-coupled receptors as promising cancer targets. *Cancer Lett* 376**,** 226-239.

Livak, K.J., and Schmittgen, T.D. (2001). Analysis of relative gene expression data using real-time quantitative PCR and the 2(-Delta Delta C(T)) Method. *Methods* 25**,** 402-408.

Lonnfors, M., Doux, J.P., Killian, J.A., Nyholm, T.K., and Slotte, J.P. (2011). Sterols have higher affinity for sphingomyelin than for phosphatidylcholine bilayers even at equal acyl-chain order. *Biophys J* 100**,** 2633-2641.

Lossow, K., Hubner, S., Roudnitzky, N., Slack, J.P., Pollastro, F., Behrens, M., and Meyerhof, W. (2016). Comprehensive Analysis of Mouse Bitter Taste Receptors Reveals Different Molecular Receptive Ranges for Orthologous Receptors in Mice and Humans. *J Biol Chem* 291**,** 15358-15377.

Lowry, O.H., Rosebrough, N.J., Farr, A.L., and Randall, R.J. (1951). Protein measurement with the Folin phenol reagent. *J Biol Chem* 193**,** 265-275.

Lu, P., Zhang, C.H., Lifshitz, L.M., and Zhuge, R. (2017). Extraoral bitter taste receptors in health and disease. *J Gen Physiol* 149**,** 181-197.

Lu, T., Zhang, D.M., Wang, X.L., He, T., Wang, R.X., Chai, Q., Katusic, Z.S., and Lee, H.C. (2010). Regulation of coronary arterial BK channels by caveolae-mediated angiotensin II signaling in diabetes mellitus. *Circ Res* 106**,** 1164-1173.

Lund, T.C., Kobs, A.J., Kramer, A., Nyquist, M., Kuroki, M.T., Osborn, J., Lidke, D.S., Low-Nam, S.T., Blazar, B.R., and Tolar, J. (2013). Bone marrow stromal and vascular smooth muscle cells have chemosensory capacity via bitter taste receptor expression. *PLoS One* 8**,** e58945.

Luo, X.C., Chen, Z.H., Xue, J.B., Zhao, D.X., Lu, C., Li, Y.H., Li, S.M., Du, Y.W., Liu, Q., Wang, P., Liu, M., and Huang, L. (2019). Infection by the parasitic helminth Trichinella spiralis activates a Tas2r-mediated signaling pathway in intestinal tuft cells. *Proc Natl Acad Sci U S A*.

Manglik, A., Kruse, A.C., Kobilka, T.S., Thian, F.S., Mathiesen, J.M., Sunahara, R.K., Pardo, L., Weis, W.I., Kobilka, B.K., and Granier, S. (2012). Crystal structure of the micro-opioid receptor bound to a morphinan antagonist. *Nature* 485**,** 321-326.

Manson, M.L., Safholm, J., Al-Ameri, M., Bergman, P., Orre, A.C., Sward, K., James, A., Dahlen, S.E., and Adner, M. (2014). Bitter taste receptor agonists mediate relaxation of human and rodent vascular smooth muscle. *Eur J Pharmacol* 740**,** 302-311.

Martin, L.T.P., Nachtigal, M.W., Selman, T., Nguyen, E., Salsman, J., Dellaire, G., and Dupre, D.J. (2018). Bitter taste receptors are expressed in human epithelial ovarian and prostate cancers cells and noscapine stimulation impacts cell survival. *Mol Cell Biochem*.

Meyer, K., Kirchner, M., Uyar, B., Cheng, J.Y., Russo, G., Hernandez-Miranda, L.R., Szymborska, A., Zauber, H., Rudolph, I.M., Willnow, T.E., Akalin, A., Haucke, V., Gerhardt, H., Birchmeier, C., Kuhn, R., Krauss, M., Diecke, S., Pascual, J.M., and Selbach, M. (2018). Mutations in Disordered Regions Can Cause Disease by Creating Dileucine Motifs. *Cell* 175**,** 239-253 e217.

Muhammad, N., Steele, R., Isbell, T.S., Philips, N., and Ray, R.B. (2017). Bitter melon extract inhibits breast cancer growth in preclinical model by inducing autophagic cell death. *Oncotarget* 8**,** 66226-66236.

Muller, A., Homey, B., Soto, H., Ge, N., Catron, D., Buchanan, M.E., Mcclanahan, T., Murphy, E., Yuan, W., Wagner, S.N., Barrera, J.L., Mohar, A., Verastegui, E., and Zlotnik, A. (2001). Involvement of chemokine receptors in breast cancer metastasis. *Nature* 410**,** 50-56.

Munk, C., Isberg, V., Mordalski, S., Harpsoe, K., Rataj, K., Hauser, A.S., Kolb, P., Bojarski, A.J., Vriend, G., and Gloriam, D.E. (2016). GPCRdb: the G protein-coupled receptor database - an introduction. *Br J Pharmacol* 173**,** 2195-2207.

Narrandes, S., Huang, S., Murphy, L., and Xu, W. (2018). The exploration of contrasting pathways in Triple Negative Breast Cancer (TNBC). *BMC Cancer* 18**,** 22.

Navarro, G., Borroto-Escuela, D.O., Fuxe, K., and Franco, R. (2015). Purinergic signaling in Parkinson's disease. Relevance for treatment. *Neuropharmacology*.

Nieto Gutierrez, A., and Mcdonald, P.H. (2018). GPCRs: Emerging anti-cancer drug targets. *Cell Signal* 41**,** 65-74.

Nowak, S., Di Pizio, A., Levit, A., Niv, M.Y., Meyerhof, W., and Behrens, M. (2018). Reengineering the ligand sensitivity of the broadly tuned human bitter taste receptor TAS2R14. *Biochim Biophys Acta Gen Subj* 1862**,** 2162-2173.

Nygaard, R., Frimurer, T.M., Holst, B., Rosenkilde, M.M., and Schwartz, T.W. (2009). Ligand binding and micro-switches in 7TM receptor structures. *Trends Pharmacol Sci* 30**,** 249-259.

O'hayre, M., Vazquez-Prado, J., Kufareva, I., Stawiski, E.W., Handel, T.M., Seshagiri, S., and Gutkind, J.S. (2013). The emerging mutational landscape of G proteins and G-protein-coupled receptors in cancer. *Nat Rev Cancer* 13**,** 412-424.

Oates, J., Faust, B., Attrill, H., Harding, P., Orwick, M., and Watts, A. (2012). The role of cholesterol on the activity and stability of neurotensin receptor 1. *Biochim Biophys Acta* 1818**,** 2228-2233.

Oddi, S., Dainese, E., Fezza, F., Lanuti, M., Barcaroli, D., De Laurenzi, V., Centonze, D., and Maccarrone, M. (2011). Functional characterization of putative cholesterol binding sequence (CRAC) in human type-1 cannabinoid receptor. *J Neurochem* 116**,** 858-865.

Oh, Y.B., Gao, S., Lim, J.M., Kim, H.T., Park, B.H., and Kim, S.H. (2011). Caveolae are essential for angiotensin II type 1 receptor-mediated ANP secretion. *Peptides* 32**,** 1422-1430.

Orsmark-Pietras, C., James, A., Konradsen, J.R., Nordlund, B., Soderhall, C., Pulkkinen, V., Pedroletti, C., Daham, K., Kupczyk, M., Dahlen, B., Kere, J., Dahlen, S.E., Hedlin, G., and Melen, E. (2013). Transcriptome analysis reveals upregulation of bitter taste receptors in severe asthmatics. *Eur Respir J* 42**,** 65-78.

Paila, Y.D., and Chattopadhyay, A. (2009). The function of G-protein coupled receptors and membrane cholesterol: specific or general interaction? *Glycoconj J* 26**,** 711-720.

Pan, S., Sharma, P., Shah, S.D., and Deshpande, D.A. (2017). Bitter taste receptor agonists alter mitochondrial function and induce autophagy in airway smooth muscle cells. *Am J Physiol Lung Cell Mol Physiol* 313**,** L154-L165.

Pan, Y., Liu, L., Li, S., Wang, K., Ke, R., Shi, W., Wang, J., Yan, X., Zhang, Q., Wang, Q., Chai, L., Xie, X., and Li, M. (2018). Activation of AMPK inhibits TGF-beta1-induced airway smooth muscle cells proliferation and its potential mechanisms. *Sci Rep* 8**,** 3624.

Perez, C.A., Huang, L., Rong, M., Kozak, J.A., Preuss, A.K., Zhang, H., Max, M., and Margolskee, R.F. (2002). A transient receptor potential channel expressed in taste receptor cells. *Nat Neurosci* 5**,** 1169-1176.

Pierce, K.L., Premont, R.T., and Lefkowitz, R.J. (2002). Seven-transmembrane receptors. *Nat Rev Mol Cell Biol* 3**,** 639-650.

Prakash, Y.S. (2016). Emerging concepts in smooth muscle contributions to airway structure and function: implications for health and disease. *Am J Physiol Lung Cell Mol Physiol* 311**,** L1113-L1140.

Pucadyil, T.J., and Chattopadhyay, A. (2006). Role of cholesterol in the function and organization of G-protein coupled receptors. *Prog Lipid Res* 45**,** 295-333.

Pucadyil, T.J., and Chattopadhyay, A. (2007). Cholesterol depletion induces dynamic confinement of the G-protein coupled serotonin(1A) receptor in the plasma membrane of living cells. *Biochim Biophys Acta* 1768**,** 655-668.

Pydi, S.P., Bhullar, R.P., and Chelikani, P. (2014a). Constitutive activity of bitter taste receptors (T2Rs). *Adv Pharmacol* 70**,** 303-326.

Pydi, S.P., Jafurulla, M., Wai, L., Bhullar, R.P., Chelikani, P., and Chattopadhyay, A. (2016). Cholesterol modulates bitter taste receptor function. *Biochim Biophys Acta* 1858**,** 2081-2087.

Pydi, S.P., Singh, N., Upadhyaya, J., Bhullar, R.P., and Chelikani, P. (2014b). The third intracellular loop plays a critical role in bitter taste receptor activation. *Biochim Biophys Acta* 1838**,** 231-236.

Pydi, S.P., Sobotkiewicz, T., Billakanti, R., Bhullar, R.P., Loewen, M.C., and Chelikani, P. (2014c). Amino acid derivatives as bitter taste receptor (T2R) blockers. *J Biol Chem* 289**,** 25054-25066.

Pydi, S.P., Upadhyaya, J., Singh, N., Pal Bhullar, R., and Chelikani, P. (2012). Recent advances in structure and function studies on human bitter taste receptors. *Curr Protein Pept Sci* 13**,** 501-508.

Radisky, E.S., Raeeszadeh-Sarmazdeh, M., and Radisky, D.C. (2017). Therapeutic Potential of Matrix Metalloproteinase Inhibition in Breast Cancer. *J Cell Biochem* 118**,** 3531-3548.

Ray, R.B., Raychoudhuri, A., Steele, R., and Nerurkar, P. (2010). Bitter melon (Momordica charantia) extract inhibits breast cancer cell proliferation by modulating cell cycle regulatory genes and promotes apoptosis. *Cancer Res* 70**,** 1925-1931.

Riordan, J.R., Rommens, J.M., Kerem, B., Alon, N., Rozmahel, R., Grzelczak, Z., Zielenski, J., Lok, S., Plavsic, N., Chou, J.L., and Et Al. (1989). Identification of the cystic fibrosis gene: cloning and characterization of complementary DNA. *Science* 245**,** 1066-1073.

Rivera Rivera, A., Castillo-Pichardo, L., Gerena, Y., and Dharmawardhane, S. (2016). Anti-Breast Cancer Potential of Quercetin via the Akt/AMPK/Mammalian Target of Rapamycin (mTOR) Signaling Cascade. *PLoS One* 11**,** e0157251.

Robinett, K.S., Koziol-White, C.J., Akoluk, A., An, S.S., Panettieri, R.A., Jr., and Liggett, S.B. (2014). Bitter taste receptor function in asthmatic and nonasthmatic human airway smooth muscle cells. *Am J Respir Cell Mol Biol* 50**,** 678-683.

Robinson, L.E., Shridar, M., Smith, P., and Murrell-Lagnado, R.D. (2014). Plasma membrane cholesterol as a regulator of human and rodent P2X7 receptor activation and sensitization. *J Biol Chem* 289**,** 31983-31994.

Rodien, P., Bremont, C., Sanson, M.L., Parma, J., Van Sande, J., Costagliola, S., Luton, J.P., Vassart, G., and Duprez, L. (1998). Familial gestational hyperthyroidism caused by a mutant thyrotropin receptor hypersensitive to human chorionic gonadotropin. *N Engl J Med* 339**,** 1823-1826.

Roland, W.S., Van Buren, L., Gruppen, H., Driesse, M., Gouka, R.J., Smit, G., and Vincken, J.P. (2013). Bitter taste receptor activation by flavonoids and isoflavonoids: modeled structural requirements for activation of hTAS2R14 and hTAS2R39. *J Agric Food Chem* 61**,** 10454-10466.

Rose, P., Huang, Q., Ong, C.N., and Whiteman, M. (2005). Broccoli and watercress suppress matrix metalloproteinase-9 activity and invasiveness of human MDA-MB-231 breast cancer cells. *Toxicol Appl Pharmacol* 209**,** 105-113.

Rossler, P., Boekhoff, I., Tareilus, E., Beck, S., Breer, H., and Freitag, J. (2000). G protein betagamma complexes in circumvallate taste cells involved in bitter transduction. *Chem Senses* 25**,** 413-421.

Running, C.A., Craig, B.A., and Mattes, R.D. (2015). Oleogustus: The Unique Taste of Fat. *Chem Senses* 40**,** 507-516.

Sainz, E., Korley, J.N., Battey, J.F., and Sullivan, S.L. (2001). Identification of a novel member of the T1R family of putative taste receptors. *J Neurochem* 77**,** 896-903.

Sanz, M.J., Nabah, Y.N., Cerda-Nicolas, M., O'connor, J.E., Issekutz, A.C., Cortijo, J., and Morcillo, E.J. (2005). Erythromycin exerts in vivo anti-inflammatory activity downregulating cell adhesion molecule expression. *Br J Pharmacol* 144**,** 190-201.

Saunders, C.J., Christensen, M., Finger, T.E., and Tizzano, M. (2014). Cholinergic neurotransmission links solitary chemosensory cells to nasal inflammation. *Proc Natl Acad Sci U S A* 111**,** 6075-6080.

Schembre, S.M., Cheng, I., Wilkens, L.R., Albright, C.L., and Marchand Le, L. (2013). Variations in bitter-taste receptor genes, dietary intake, and colorectal adenoma risk. *Nutr Cancer* 65**,** 982-990.

Schlenz, H., Kummer, W., Jositsch, G., Wess, J., and Krasteva, G. (2010). Muscarinic receptor-mediated bronchoconstriction is coupled to caveolae in murine airways. *Am J Physiol Lung Cell Mol Physiol* 298**,** L626-636.

Schneider, C.A., Rasband, W.S., and Eliceiri, K.W. (2012). NIH Image to ImageJ: 25 years of image analysis. *Nat Methods* 9**,** 671-675.

Schoneberg, T., Schulz, A., Biebermann, H., Hermsdorf, T., Rompler, H., and Sangkuhl, K. (2004). Mutant G-protein-coupled receptors as a cause of human diseases. *Pharmacol Ther* 104**,** 173-206.

Seo, H.S., Jo, J.K., Ku, J.M., Choi, H.S., Choi, Y.K., Woo, J.K., Kim, H.I., Kang, S.Y., Lee, K.M., Nam, K.W., Park, N., Jang, B.H., Shin, Y.C., and Ko, S.G. (2015). Induction of caspase-dependent extrinsic apoptosis by apigenin through inhibition of signal transducer and activator of transcription 3 (STAT3) signalling in HER2-overexpressing BT-474 breast cancer cells. *Biosci Rep* 35.

Seo, Y., Kim, Y.S., Lee, K.E., Park, T.H., and Kim, Y. (2017). Anti-cancer stemness and anti-invasive activity of bitter taste receptors, TAS2R8 and TAS2R10, in human neuroblastoma cells. *PLoS One* 12**,** e0176851.

Sezgin, E., Levental, I., Mayor, S., and Eggeling, C. (2017). The mystery of membrane organization: composition, regulation and roles of lipid rafts. *Nat Rev Mol Cell Biol* 18**,** 361-374.

Shaik, F.A., Medapati, M.R., and Chelikani, P. (2018). Cholesterol modulates signaling of the chemosensory bitter taste receptor T2R14 in human airway cells. *Am J Physiol Lung Cell Mol Physiol*.

Shaik, F.A., Singh, N., Arakawa, M., Duan, K., Bhullar, R.P., and Chelikani, P. (2016). Bitter taste receptors: Extraoral roles in pathophysiology. *Int J Biochem Cell Biol* 77**,** 197-204.

Sharma, P., Panebra, A., Pera, T., Tiegs, B.C., Hershfeld, A., Kenyon, L.C., and Deshpande, D.A. (2015). Anti-mitogenic Effect of Bitter Taste Receptor Agonists on Airway Smooth Muscle Cells. *Am J Physiol Lung Cell Mol Physiol***,** ajplung 00373 02015.

Sharma, P., Panebra, A., Pera, T., Tiegs, B.C., Hershfeld, A., Kenyon, L.C., and Deshpande, D.A. (2016). Antimitogenic effect of bitter taste receptor agonists on airway smooth muscle cells. *Am J Physiol Lung Cell Mol Physiol* 310**,** L365-376.

Sharma, P., Yi, R., Nayak, A.P., Wang, N., Tang, F., Knight, M.J., Pan, S., Oliver, B., and Deshpande, D.A. (2017). Bitter Taste Receptor Agonists Mitigate Features of Allergic Asthma in Mice. *Sci Rep* 7**,** 46166.

Shen, W., Liang, B., Yin, J., Li, X., and Cheng, J. (2015). Noscapine Increases the Sensitivity of Drug-Resistant Ovarian Cancer Cell Line SKOV3/DDP to Cisplatin by Regulating Cell Cycle and Activating Apoptotic Pathways. *Cell Biochem Biophys* 72**,** 203-213.

Shobair, M., Dagliyan, O., Kota, P., Dang, Y.L., He, H., Stutts, M.J., and Dokholyan, N.V. (2016). Gain-of-Function Mutation W493R in the Epithelial Sodium Channel Allosterically Reconfigures Intersubunit Coupling. *J Biol Chem* 291**,** 3682-3692.

Shrivastava, S., Jafurulla, M., Tiwari, S., and Chattopadhyay, A. (2018). Identification of Sphingolipid-binding Motif in G Protein-coupled Receptors. *Adv Exp Med Biol* 1112**,** 141-149.

Sigrist, C.J., De Castro, E., Cerutti, L., Cuche, B.A., Hulo, N., Bridge, A., Bougueleret, L., and Xenarios, I. (2013). New and continuing developments at PROSITE. *Nucleic Acids Res* 41**,** D344-347.

Simons, K., and Ikonen, E. (1997). Functional rafts in cell membranes. *Nature* 387**,** 569-572.

Singh, N., Chakraborty, R., Bhullar, R.P., and Chelikani, P. (2014). Differential expression of bitter taste receptors in non-cancerous breast epithelial and breast cancer cells. *Biochem Biophys Res Commun* 446**,** 499-503.

Singh, N., Pydi, S.P., Upadhyaya, J., and Chelikani, P. (2011a). Structural Basis of Activation of Bitter Taste Receptor T2R1 and Comparison with Class A G-protein-coupled Receptors (GPCRs). *J Biol Chem* 286**,** 36032-36041.

Singh, N., Vrontakis, M., Parkinson, F., and Chelikani, P. (2011b). Functional bitter taste receptors are expressed in brain cells. *Biochem Biophys Res Commun* 406**,** 146-151.

Sjogren, B., and Svenningsson, P. (2007). Depletion of the lipid raft constituents, sphingomyelin and ganglioside, decreases serotonin binding at human 5-HT7(a) receptors in HeLa cells. *Acta Physiol (Oxf)* 190**,** 47-53.

Skliris, G.P., Hube, F., Gheorghiu, I., Mutawe, M.M., Penner, C., Watson, P.H., Murphy, L.C., Leygue, E., and Myal, Y. (2008). Expression of small breast epithelial mucin (SBEM) protein in tissue microarrays (TMAs) of primary invasive breast cancers. *Histopathology* 52**,** 355-369.

Slotte, J.P., and Bierman, E.L. (1988). Depletion of plasma-membrane sphingomyelin rapidly alters the distribution of cholesterol between plasma membranes and intracellular cholesterol pools in cultured fibroblasts. *Biochem J* 250**,** 653-658.

Stanislas Grassin, D., Charlotte, A., Marion, B., Sarah, F.-K., Emmanuel, N., and Philippe, D. (2014). "Characterization Of The Expression And The Role Of Bitter Taste Receptors In Human Lung Parenchyma And Macrophages," in *D36. SEPSIS, ACUTE RESPIRATORY DISTRESS SYNDROME, AND ACUTE LUNG INJURY*. American Thoracic Society), A5749-A5749.

Steinmetz, K.A., and Potter, J.D. (1996). Vegetables, fruit, and cancer prevention: a review. *J Am Diet Assoc* 96**,** 1027-1039.

Stern, L., Giese, N., Hackert, T., Strobel, O., Schirmacher, P., Felix, K., and Gaida, M.M. (2018). Overcoming chemoresistance in pancreatic cancer cells: role of the bitter taste receptor T2R10. *J Cancer* 9**,** 711-725.

Straat, K., De Klark, R., Gredmark-Russ, S., Eriksson, P., and Soderberg-Naucler, C. (2009). Infection with human cytomegalovirus alters the MMP-9/TIMP-1 balance in human macrophages. *J Virol* 83**,** 830-835.

Strange, P.G. (2008). Agonist binding, agonist affinity and agonist efficacy at G protein-coupled receptors. *Br J Pharmacol* 153**,** 1353-1363.

Sud, N., Sharma, R., Ray, R., Chattopadhyay, T.K., and Ralhan, R. (2006). Differential expression of G-protein coupled receptor 56 in human esophageal squamous cell carcinoma. *Cancer Lett* 233**,** 265-270.

Tao, Y.X. (2006). Inactivating mutations of G protein-coupled receptors and diseases: structure-function insights and therapeutic implications. *Pharmacol Ther* 111**,** 949-973.

Taruno, A., Matsumoto, I., Ma, Z., Marambaud, P., and Foskett, J.K. (2013a). How do taste cells lacking synapses mediate neurotransmission? CALHM1, a voltage-gated ATP channel. *Bioessays* 35**,** 1111-1118.

Taruno, A., Vingtdeux, V., Ohmoto, M., Ma, Z., Dvoryanchikov, G., Li, A., Adrien, L., Zhao, H., Leung, S., Abernethy, M., Koppel, J., Davies, P., Civan, M.M., Chaudhari, N., Matsumoto, I., Hellekant, G., Tordoff, M.G., Marambaud, P., and Foskett, J.K. (2013b). CALHM1 ion channel mediates purinergic neurotransmission of sweet, bitter and umami tastes. *Nature* 495**,** 223-226.

Tepper, B.J., Koelliker, Y., Zhao, L., Ullrich, N.V., Lanzara, C., D'adamo, P., Ferrara, A., Ulivi, S., Esposito, L., and Gasparini, P. (2008). Variation in the bitter-taste receptor gene TAS2R38, and adiposity in a genetically isolated population in Southern Italy. *Obesity (Silver Spring)* 16**,** 2289-2295.

Thathiah, A., and De Strooper, B. (2011). The role of G protein-coupled receptors in the pathology of Alzheimer's disease. *Nat Rev Neurosci* 12**,** 73-87.

Thawabteh, A., Lelario, F., Scrano, L., Bufo, S.A., Nowak, S., Behrens, M., Di Pizio, A., Niv, M.Y., and Karaman, R. (2019). Bitterless guaifenesin prodrugs-design, synthesis, characterization, in vitro kinetics, and bitterness studies. *Chem Biol Drug Des* 93**,** 262-271.

Thomas, A., Sulli, C., Davidson, E., Berdougo, E., Phillips, M., Puffer, B.A., Paes, C., Doranz, B.J., and Rucker, J.B. (2017). The Bitter Taste Receptor TAS2R16 Achieves High Specificity and Accommodates Diverse Glycoside Ligands by using a Two-faced Binding Pocket. *Sci Rep* 7**,** 7753.

Timpson, N.J., Christensen, M., Lawlor, D.A., Gaunt, T.R., Day, I.N., Ebrahim, S., and Davey Smith, G. (2005). TAS2R38 (phenylthiocarbamide) haplotypes, coronary heart disease traits, and eating behavior in the British Women's Heart and Health Study. *Am J Clin Nutr* 81**,** 1005-1011.

Tizzano, M., Cristofoletti, M., Sbarbati, A., and Finger, T.E. (2011). Expression of taste receptors in solitary chemosensory cells of rodent airways. *BMC Pulm Med* 11**,** 3.

Tizzano, M., Gulbransen, B.D., Vandenbeuch, A., Clapp, T.R., Herman, J.P., Sibhatu, H.M., Churchill, M.E., Silver, W.L., Kinnamon, S.C., and Finger, T.E. (2010). Nasal chemosensory cells use bitter taste signaling to detect irritants and bacterial signals. *Proc Natl Acad Sci U S A* 107**,** 3210-3215.

Tsutsumi, R., Goda, M., Fujimoto, C., Kanno, K., Nobe, M., Kitamura, Y., Abe, K., Kawai, M., Matsumoto, H., Sakai, T., and Takeda, N. (2015). Effects of chemotherapy on gene expression of lingual taste receptors in patients with head and neck cancer. *Laryngoscope*.

Ungefroren, H., Groth, S., Sebens, S., Lehnert, H., Gieseler, F., and Fandrich, F. (2011). Differential roles of Smad2 and Smad3 in the regulation of TGF-beta1-mediated growth inhibition and cell migration in pancreatic ductal adenocarcinoma cells: control by Rac1. *Mol Cancer* 10**,** 67.

Upadhyaya, J.D., Singh, N., Sikarwar, A.S., Chakraborty, R., Pydi, S.P., Bhullar, R.P., Dakshinamurti, S., and Chelikani, P. (2014). Dextromethorphan mediated bitter taste receptor activation in the pulmonary circuit causes vasoconstriction. *PLoS One* 9**,** e110373.

Ushio-Fukai, M., Hilenski, L., Santanam, N., Becker, P.L., Ma, Y., Griendling, K.K., and Alexander, R.W. (2001). Cholesterol depletion inhibits epidermal growth factor receptor transactivation by angiotensin II in vascular smooth muscle cells: role of cholesterol-rich microdomains and focal adhesions in angiotensin II signaling. *J Biol Chem* 276**,** 48269-48275.

Valley, C.C., Cembran, A., Perlmutter, J.D., Lewis, A.K., Labello, N.P., Gao, J., and Sachs, J.N. (2012). The methionine-aromatic motif plays a unique role in stabilizing protein structure. *J Biol Chem* 287**,** 34979-34991.

Vargas-Poussou, R., Huang, C., Hulin, P., Houillier, P., Jeunemaitre, X., Paillard, M., Planelles, G., Dechaux, M., Miller, R.T., and Antignac, C. (2002). Functional characterization of a calcium-sensing receptor mutation in severe autosomal dominant hypocalcemia with a Bartter-like syndrome. *J Am Soc Nephrol* 13**,** 2259-2266.

Veerappan, A., Reid, A.C., Estephan, R., O'connor, N., Thadani-Mulero, M., Salazar-Rodriguez, M., Levi, R., and Silver, R.B. (2008). Mast cell renin and a local renin-angiotensin system in the airway: role in bronchoconstriction. *Proc Natl Acad Sci U S A* 105**,** 1315-1320.

Venkatakrishnan, A.J., Deupi, X., Lebon, G., Tate, C.G., Schertler, G.F., and Babu, M.M. (2013). Molecular signatures of G-protein-coupled receptors. *Nature* 494**,** 185-194.

Vischer, H.F., Siderius, M., Leurs, R., and Smit, M.J. (2014). Herpesvirus-encoded GPCRs: neglected players in inflammatory and proliferative diseases? *Nat Rev Drug Discov* 13**,** 123-139.

Viswanathan, G., Jafurulla, M., Kumar, G.A., Raghunand, T.R., and Chattopadhyay, A. (2018). Macrophage sphingolipids are essential for the entry of mycobacteria. *Chem Phys Lipids* 213**,** 25-31.

Vrielink, A., and Ghisla, S. (2009). Cholesterol oxidase: biochemistry and structural features. *FEBS J* 276**,** 6826-6843.

Wacker, D., Wang, C., Katritch, V., Han, G.W., Huang, X.P., Vardy, E., Mccorvy, J.D., Jiang, Y., Chu, M., Siu, F.Y., Liu, W., Xu, H.E., Cherezov, V., Roth, B.L., and Stevens, R.C. (2013). Structural features for functional selectivity at serotonin receptors. *Science* 340**,** 615-619.

Wang, J.C., Hinrichs, A.L., Bertelsen, S., Stock, H., Budde, J.P., Dick, D.M., Bucholz, K.K., Rice, J., Saccone, N., Edenberg, H.J., Hesselbrock, V., Kuperman, S., Schuckit, M.A., Bierut, L.J., and Goate, A.M. (2007). Functional variants in TAS2R38 and TAS2R16 influence alcohol consumption in high-risk families of African-American origin. *Alcohol Clin Exp Res* 31**,** 209-215.

Weichelt, U., Cay, R., Schmitz, T., Strauss, E., Sifringer, M., Buhrer, C., and Endesfelder, S. (2013). Prevention of hyperoxia-mediated pulmonary inflammation in neonatal rats by caffeine. *Eur Respir J* 41**,** 966-973.

Wendell, S., Wang, X., Brown, M., Cooper, M.E., Desensi, R.S., Weyant, R.J., Crout, R., Mcneil, D.W., and Marazita, M.L. (2010). Taste genes associated with dental caries. *J Dent Res* 89**,** 1198-1202.

Who. Available: http://gco.iarc.fr/today/online-analysis-multi-bars?v=2018&mode=cancer&mode_population=countries&population=900&populations=900&key=total&sex=2&cancer=39&type=0&statistic=5&prevalence=0&population_group=0&ages_group%5B%5D=0&ages_group%5B%5D=17&nb_items=10&group_cancer=1&include_nmsc=1&include_nmsc_other=1&type_multiple=%257B%2522inc%2522%253Atrue%252C%2522mort%2522%253Atrue%252C%2522prev%2522%253Afalse%257D&orientation=horizontal&type_sort=0&type_nb_items=%257B%2522top%2522%253Atrue%252C%2522bottom%2522%253Afalse%257D&population_group_globocan_id= [Accessed].

Workman, A.D., Palmer, J.N., Adappa, N.D., and Cohen, N.A. (2015). The Role of Bitter and Sweet Taste Receptors in Upper Airway Immunity. *Curr Allergy Asthma Rep* 15**,** 72.

Xu, H.B., Shen, F.M., and Lv, Q.Z. (2016). Celecoxib enhanced the cytotoxic effect of cisplatin in chemo-resistant gastric cancer xenograft mouse models through a cyclooxygenase-2-dependent manner. *Eur J Pharmacol* 776**,** 1-8.

Yagi, H., Tan, W., Dillenburg-Pilla, P., Armando, S., Amornphimoltham, P., Simaan, M., Weigert, R., Molinolo, A.A., Bouvier, M., and Gutkind, J.S. (2011). A synthetic biology approach reveals a CXCR4-G13-Rho signaling axis driving transendothelial migration of metastatic breast cancer cells. *Sci Signal* 4**,** ra60.

Yamaki, M., Saito, H., Isono, K., Goto, T., Shirakawa, H., Shoji, N., Satoh-Kuriwada, S., Sasano, T., Okada, R., Kudoh, K., Motoi, F., Unno, M., and Komai, M. (2017). Genotyping Analysis of Bitter-Taste Receptor Genes TAS2R38 and TAS2R46 in Japanese Patients with Gastrointestinal Cancers. *J Nutr Sci Vitaminol (Tokyo)* 63**,** 148-154.

Yang, J., Yan, R., Roy, A., Xu, D., Poisson, J., and Zhang, Y. (2015). The I-TASSER Suite: protein structure and function prediction. *Nat Methods* 12**,** 7-8.

Zhang, C.H., Lifshitz, L.M., Uy, K.F., Ikebe, M., Fogarty, K.E., and Zhuge, R. (2013). The cellular and molecular basis of bitter tastant-induced bronchodilation. *PLoS Biol* 11**,** e1001501.

Zhang, H., Unal, H., Desnoyer, R., Han, G.W., Patel, N., Katritch, V., Karnik, S.S., Cherezov, V., and Stevens, R.C. (2015a). Structural Basis for Ligand Recognition and Functional Selectivity at Angiotensin Receptor. *J Biol Chem* 290**,** 29127-29139.

Zhang, H.Q., Fang, N., Liu, X.M., Xiong, S.P., Liao, Y.Q., Jin, W.J., Song, R.F., and Wan, Y.Y. (2015b). Antitumor activity of chloroquine in combination with Cisplatin in human gastric cancer xenografts. *Asian Pac J Cancer Prev* 16**,** 3907-3912.

Zhang, Y., Hoon, M.A., Chandrashekar, J., Mueller, K.L., Cook, B., Wu, D., Zuker, C.S., and Ryba, N.J. (2003). Coding of sweet, bitter, and umami tastes: different receptor cells sharing similar signaling pathways. *Cell* 112**,** 293-301.

Zhang, Z., Li, M., Lu, R., Alioua, A., Stefani, E., and Toro, L. (2014). The angiotensin II type 1 receptor (AT1R) closely interacts with large conductance voltage- and Ca2+-activated K+ (BK) channels and inhibits their activity independent of G-protein activation. *J Biol Chem* 289**,** 25678-25689.

Zheng, K., Lu, P., Delpapa, E., Bellve, K., Deng, R., Condon, J.C., Fogarty, K., Lifshitz, L.M., Simas, T.a.M., Shi, F., and Zhuge, R. (2017). Bitter taste receptors as targets for tocolytics in preterm labor therapy. *FASEB J* 31**,** 4037-4052.

Zhou, Q., Mccracken, M.A., and Strobl, J.S. (2002). Control of mammary tumor cell growth in vitro by novel cell differentiation and apoptosis agents. *Breast Cancer Res Treat* 75**,** 107-117.